

Quantitative Analysis of Climate Heterogeneity via an Unconditional Quantile Vector Error Correction Model

Andrey Ramos*

Universidad Carlos III de Madrid

October 31, 2024

[Click here for the latest version of the paper]

Abstract

This paper introduces a time-series methodology to quantify heterogeneity in the evolution of the unconditional temperature distribution and its association with climate drivers. By recognizing that temperature quantiles correspond to different locations—or seasons—I establish an equivalence between a One-Dimensional Energy Balance Model and a Vector Error Correction Model (VECM) for a range of distributional characteristics of temperature—mean and quantiles—and total radiative forcing, including radiative forcing from anthropogenic greenhouse gases. The VECM is estimated employing time series methods robust to the type of trends in the data, and is utilized to produce the following outcomes of practical interest for economic analyses: *i*) quantile-dependent climate sensitivities, *ii*) long-term temperature density forecasts, *iii*) identification of distributional shocks and impulse-responses, and *iv*) projections of temperature distribution under different scenarios of future greenhouse gas emissions. An empirical analysis using station-level temperature records (1880–2021) reveals strong climate heterogeneity at global, hemispheric, and continental scales, with important potential implications for damage analysis and integrated assessment modeling. A deeper understanding of global warming dynamics is crucial for better informing adaptation and mitigation policies.

JEL Classification: C32, C50, Q54

Keywords: Global warming, Climate heterogeneity, Temperature, Co-trending, Vector autorregression, Unconditional quantiles

*Email: anramosr@eco.uc3m.es. I thank Jesús Gonzalo and Lola Gadea for their valuable guidance and support throughout this project, and to Eric Hillebrand, Mikkel Bennedsen, Gustavo Canavire, Álvaro Escribano, Ignacio Garrón, and Adrià Romero for their insightful discussions and comments. My gratitude also extends to the participants of the Econometrics Reading Group at Universidad Carlos III de Madrid, as well as to the attendees at the following events: Virtual Workshop for Junior Researchers in Time Series, 2024 Annual Meeting of the European Association of Young Economists (EAYE), 2024 Jamboree of the European Network for Training in Economic Research (ENTER), 2024 Annual Meeting of the International Association for Applied Econometrics (IAAE), VIII Econometric Models of Climate Change Conference (EMCC), and 2024 European Climate and Energy Modelling Platform (ECEMP).

1 Introduction

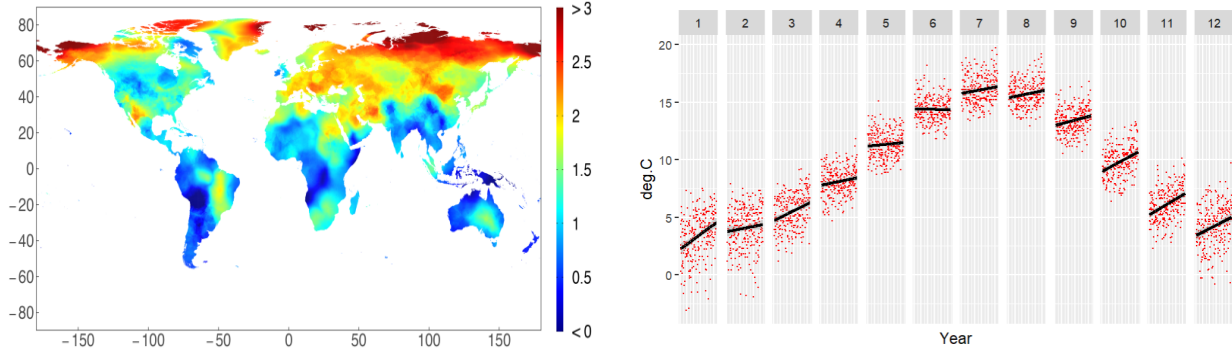
Climate observations and climate modeling provide compelling evidence of a global warming trend, primarily attributed to anthropogenic emissions of greenhouse gases (GHGs) (AR6-IPCC, 2021). It has also been well established that climate change dynamics are non-uniform across space and time (Chapman et al., 2013; Ji et al., 2014; Gadea and Gonzalo, 2023). For instance, not all regions on the globe warm at the same rate: surface air temperature over the Arctic Pole is warming at a rate almost twice as fast as the global mean, a phenomenon referred to as Arctic Amplification (AA)¹ (Serreze et al., 2009; Bekryaev et al., 2010; Screen and Simmonds, 2010; Smith et al., 2019; You et al., 2021). More generally, equatorial latitudes have on average experienced slower warming than northern latitudes. Panel (a) in Figure 1, sourced from Desmet and Rossi-Hansberg (2024), depicts the fitted linear trend change in local temperatures between 1970 and 2019. Some regions in Alaska, northern Europe, and Siberia have experienced temperature changes above 3°C, while in regions closer to the equator the change is negligible.

For a constant spatial dimension, evidence of heterogeneity in seasonal temperatures has been also extensively documented (Balling et al., 1998; Vogelsang and Franses, 2005; Cohen et al., 2012; Hillebrand and Proietti, 2017). Panel (b) in Figure 1, obtained from Hillebrand and Proietti (2017), shows the monthly plots for the Central England temperature series between 1754 and 2020. Black lines represent the least-squares fit of a constant and a linear trend to each annual month series separately. From these plots, it is evident that the upward trends are steeper in winter months than in the rest of the year, a regularity that is also observed in many other locations. A third type of heterogeneity originates from the fact that night-time temperatures are increasing more rapidly than daytime temperatures (Donat and Alexander, 2012; Davy et al., 2017).

This paper introduces a time series quantitative methodology to analyze different types of heterogeneity in the dynamics of the temperature distribution and its association with climate forcings. The proposed methodology consists of a Vector Autoregressive Model (VAR) for a range of unconditional distributional characteristics of temperature, such as mean and quantiles, alongside the radiative forcing² of GHGs, including carbon dioxide (CO₂), methane (CH₄), and nitrous

¹Several physical mechanisms are responsible for AA. Factors local to the Arctic include sea ice-albedo, cloud, and water vapor feedbacks (You et al., 2021). In addition, poleward heat and moisture transport through the atmosphere and ocean from lower latitudes influence the extent of AA (Lee et al., 2017; Luo et al., 2017).

²Radiative forcing is a concept used in climate science to quantify the energy imbalance in Earth's atmosphere caused by anthropogenic activities or natural events (Hansen et al., 2011; Andrews et al., 2021). Since the start of the industrial era until the present day, anthropogenic forcing has typically been increasing and has been the dominant component of the total forcing on the Earth system except for brief periods following large volcanic eruptions (Smith et al., 2020).



(a) Local Temperature Changes 1970-2019

(b) Monthly Temperature in Central England

Figure 1: Empirical Evidence of Climate Heterogeneity

oxide (N_2O).³ At global and hemispheric scales, the methodology is motivated by the physical mechanisms of a one-dimensional (1D) Energy Balance Model (EBM) (Held and Suarez, 1974). In a 1D-EBM, temperature is modeled as a function of latitude, and heat transport between adjacent latitudes in the direction from the Equator to the poles is permitted. Compared to the more basic zero-dimensional (0D) EBM (Budyko, 1969), the 1D-EBM allows for geographical heterogeneity in the climate sensitivity⁴ and enables the study of processes such as AA. By assuming that the unconditional quantiles of temperature represent temperatures at different latitudes, it is possible to establish an equivalence between the 1D-EBM and a restricted Vector Error Correction Model (VECM) for the unconditional distributional characteristics of temperature and radiative forcing. Using historical data, the model is estimated and tested employing time series methods that are robust to the nature of trends in the variables.⁵

The empirical analysis uses station-level temperature observations for the period 1880-2021 obtained from the latest version of the HadCRUT5 dataset, developed jointly by the Climatic Research Unit (CRU) at the University of East Anglia and the Hadley Centre at the UK Met Office (Morice et al., 2021). Temperature unconditional distributional characteristics are derived

³This methodology can be implemented in other type of econometric applications where the interest is to analyze the dynamic relationship between a p -variate vector of variables X_t and the distribution of another variable Y_t , provided that the distribution of Y_t can be estimated each period $t = 1, 2, \dots, T$. A simple example is the study of the dynamic relationship between (shocks to) fiscal policy and the income distribution.

⁴The climate sensitivity is a physical concept defined as the long-term change in temperature in response to a doubling in the CO_2 concentrations.

⁵Following Stock et al. (1990), a VAR model in levels estimated by OLS is consistent whether or not the elements contain trending components, as long as the innovations have sufficient moments and a zero mean, conditional on past values of the variables. Although this is a valid approach, estimating the VECM structure is particularly relevant in this application. First, it allows for more precise estimation with narrower confidence intervals, which is crucial for a more credible uncertainty analysis when incorporating the methodology's outcomes into climate science or economic studies. Second, the coefficients of the long-run (level) relationships are of explicit interest, as they provide information regarding the magnitude of amplification in the temperature distribution or are directly used to compute physical quantities such as the climate sensitivity.

from a balanced panel of stations with continuous observations from 1880 to 2021. Radiative forcing series are gathered from the most recent version of the dataset developed by [Hansen et al. \(2011\)](#). This dataset provides information on radiative forcing in units of watts per square meter (W/m^2) originating from various anthropogenic and natural sources, including GHGs like CO₂, CH₄, or N₂O. Following [Bennedsen et al. \(2023\)](#), total radiative forcing (TRF) is decomposed into natural forcing, from solar and volcanic activities, and anthropogenic forcing attributed to human activities.

The methodology is implemented at three geographical scales: the Globe, the Northern Hemisphere, and Europe.⁶ At these scales, the estimated quantiles represent temperatures at different latitudes, and the results obtained are comparable to the predictions of the 1D-EBM. However, the methodology is adaptable to more general settings with limited spatial variation. For instance, if high-frequency data is available for a specific location, the unconditional distributional characteristics of temperature can be estimated at a lower frequency, and the unconditional-quantile VECM model remains a valid approach to quantify climate heterogeneity. In this scenario, the results would characterize seasonal heterogeneity, as described by [Balling et al. \(1998\)](#), [Vogelsang and Franses \(2005\)](#), [Cohen et al. \(2012\)](#), and [Hillebrand and Proietti \(2017\)](#). An example analysis of Central England, using daily data, is provided to further illustrate the methodology's flexibility.

A brief summary of the results is as follows. The evidence from a simple-parsimonious model that incorporates temperature distributional characteristics solely, reveals significant interdependencies among different segments of the temperature distribution. The long-term unconditional density forecasting exercise predicts that temperatures will continue to increase during the next decades with the magnitude of the changes far from being homogeneous across the temperature distribution. By integrating the radiative forcing variable into the analysis, I study how different temperature quantiles respond to radiative forcing changes. For the Globe and the North Hemisphere, empirical results suggest that the average temperature could rise by approximately 2.4°C with a doubling of CO₂ concentrations. Substantial heterogeneity in the climate sensitivity across the temperature distribution is found, with estimates exceeding 3.6°C for the lower quantiles. Empirical results are in line with both empirical evidence from the related literature and predictions from large-scale climate models that consider climate heterogeneity.

The estimated models are used to produce several additional outcomes of practical inter-

⁶These scales of analysis are selected to ensure sufficient variation in latitude levels among the stations in the CRU dataset. In principle, the analysis can be replicated at any continent, country, or city level, provided there is enough cross-sectional or higher-frequency data to estimate the unconditional distributional characteristics over a reasonable number of periods.

est, including: *i*) unconditional long-term density forecasts of temperature based on the underlying dynamics of the data, *ii*) identification of distributional structural shocks and impulse-response analysis, and *iii*) projections of the temperature distribution under hypothetical GHG emissions/concentration scenarios derived from the Shared Socioeconomic Pathways (SSP) framework. As discussed later in this introduction, an alternative to produce this type of results is to use simulations from complex large-scale General Circulation Models. However, these models are highly non-linear, require large amounts of inputs data, are computationally expensive to solve and heavily dependent on the initial conditions of the system. In contrast, the unconditional quantile VECM achieves a desirable balance between a purely statistical multivariate approach and the theoretical/structural model of the climate system, allowing the production of estimation and forecasting/projection results and for the assessment of estimation uncertainty in a simpler reduced-form procedure. Moreover, while most of the climate models produce projections for the average temperature (considered as a sufficient statistic for the global climate), this proposal produces projections for the whole temperature distribution. It provides a wider understanding of global warming dynamics, with significant implications for modeling and policy decisions. For example, these outputs can be integrated into economic studies (e.g., damage analysis or Integrated Assessment Modeling) to quantify the economic consequences of climate change, while explicitly accounting for different forms of climate heterogeneity. This type of information is crucial to better inform adaptation and mitigation policies at global and local scales.

Incorporating climate heterogeneity into economic/econometric modeling is crucial, given its significant impact on the climate system dynamics and the implications for the economics of climate change. From a climate system perspective, climate heterogeneity triggers a series of global responses with substantial environmental and ecological consequences. For instance, AA has led to a considerable reduction in sea ice cover over the Arctic Pole ([Simmonds, 2015](#); [Kwok, 2018](#)) and has contributed to the continuous melting of the Greenland Ice Sheet that is responsible for approximately 25% of the observed global sea level rise between 1993 and 2014 ([Chen et al., 2017](#); [You et al., 2021](#)). Furthermore, AA has accelerated permafrost⁷ degradation, which is expected to cause widespread disturbances in terrestrial ecosystems, increase erosion, harm subsistence livelihoods, and damage infrastructure ([Vihma, 2014](#); [Shepherd, 2016](#)). Permafrost thawing will also release GHGs, primarily CH₄ and CO₂ stored in organic frozen soils, leading to significant global feedback effects ([Kerr, 2010](#); [Schaefer et al., 2014](#); [Schuur et al., 2015](#)). Beyond its environmental impacts for the Arctic region, AA may also influence the frequency and duration of extreme climate events in

⁷Permafrost refers to the soil at or below the freezing point of water for two or more years. Permafrost regions occupy about 24% of the exposed land surface of the Northern Hemisphere.

mid-latitudes. A growing number of studies suggest that AA has contributed to an increase in the frequency of severe cold winters, heatwaves, and precipitation/snowfall events (Tang et al., 2014; Vihma, 2014; Francis and Vavrus, 2015; Wu et al., 2016; Zhang et al., 2020).

Apart from its importance for the climate system, understanding climate heterogeneity is also crucial for the economics of climate change, and particularly, for the correct anticipation of local damages and the optimality of climate policies. Regarding local damages, a growing number of studies in Integrated Assessment Modeling propose climate heterogeneity as a potential cause of the nowhere near uniform economic impacts of climate change (Krusell and Smith, 2022; Cruz and Rossi-Hansberg, 2024; Desmet and Rossi-Hansberg, 2024). As the globe warms with varying warming trends across regions or seasons, some regions and industries suffer serious damages, while others may benefit. Empirical evidence suggests that the regions that obtain potential benefits are the cold ones (Dell et al., 2014; Burke et al., 2015; Hsiang et al., 2017; Acevedo et al., 2020; Nath et al., 2024), precisely those that are warming at a faster rate.⁸ The consequences of non-uniform seasonal local temperature changes are less studied in the empirical literature. A recent study by Nguyen (2024) for the United States finds that higher winter temperature generates short lived increases in the private sector employment growth, while higher summer temperature permanently decreases it. These type of findings may extend to other outcomes such as natality/mortality, local amenities, migration, or conflict.

Regarding climate policies, Brock and Xepapadeas (2017) introduce AA into an economic model and explore its impact on the design of a carbon tax scheme. Using a two-box model, where each box represents a region of the globe, Brock and Xepapadeas (2017) demonstrate that ignoring AA in economic modeling may lead regulators to overestimate or underestimate the tax on GHG emissions. The direction of the bias depends on the relationship between the marginal damages from temperature increases in each box (region) and the parameters characterizing the strength of AA. If marginal damages due to a temperature increase in the northern box exceed marginal damages from a corresponding increase in the southern box, as is the case in practice, then omitting the AA mechanism leads to underestimate the optimal tax. A related d'Autume et al. (2016) discusses the optimal carbon taxation when there exists a local component to the damage caused by global emissions.

The main message in this discussion is that climate heterogeneity is crucial for both climate science and climate economics, and it must be incorporated into economic studies. Econometric modeling of climate systems can contribute to this discussion by developing quantitative method-

⁸To provide a concrete example of the potential benefits of AA, Borgerson (2008) discusses that the loss of sea ice may increase the access to Arctic fish, timber, and minerals, along with the opening of new sea routes in the North.

ologies that effectively account for various forms of climate heterogeneity. This requires moving beyond using the annual average temperature as a sufficient statistic for global climate change and instead focusing on the entire temperature distribution (see [Gadea and Gonzalo \(2020\)](#) or [Gadea and Gonzalo \(2023\)](#)). Combined with economic theory and data, this approach provides a better understanding of climate dynamics and its consequences, enabling the production of more reliable information to guide the design of efficient mitigation and adaptation strategies. This is precisely what I aim to achieve in this paper with the proposal of the unconditional-quantile VECM as a methodological alternative to empirically quantify different forms of climate heterogeneity.

This paper relates to several strands of literature. First, it complements and extends the literature on the attribution and forecasting of climate change using observational data. In the last decade, there has been a growing body of literature on the application of econometric time series techniques to model the global climate system and the effects of human activity on climate change. The choice of methodology often depends on how trends are modeled, specifically whether trends are assumed to be stochastic ([Kaufmann and Stern, 2002](#); [Pretis, 2020](#); [Bruns et al., 2020](#); [Phillips et al., 2020](#); [Benati, 2023](#)) or (possibly non-linear) deterministic ([Gay-Garcia et al., 2009](#); [Estrada et al., 2013, 2021](#); [Chen et al., 2023](#); [McKittrick et al., 2023](#))—see Section 2 for a detailed review of this group of literature. The methodology proposed in this paper is robust to the type of trends in the data.

While most of the contributions in this area rely on 0D-EBMs and focus on the average temperature response to changes in CO₂ and other GHGs, recent studies like those by [Gadea and Gonzalo \(2020\)](#), [Estrada et al. \(2021\)](#), [Anderson et al. \(2023\)](#), or [Brock and Miller \(2023\)](#) have explored methodologies to study geographical heterogeneity in the climate dynamics. The current paper aligns more closely with this latter group of contributions. Unlike [Estrada et al. \(2021\)](#) or [Anderson et al. \(2023\)](#), which allow the climate sensitivity to be different across all units/locations, my approach focusing on specific distributional characteristics of temperature is more aggregated and provides a more robust forecasting framework. Compared to [Brock and Miller \(2023\)](#), the unconditional-quantile VECM model allows dividing the Earth into more than two boxes (or regions) offering a more detailed characterization of heterogeneity. The closest reference is [Gadea and Gonzalo \(2020\)](#), who study the dynamics of the distributional characteristics of temperature using individual linear trend models. In this paper I adopt a multivariate approach to jointly model the dynamics of the whole temperature distribution in a VAR framework and include the effect of the radiative forcing. Additionally, as previously discussed, the methodology extends its applicability beyond traditional EBMs to contexts with seasonal rather than geographical variability.

Second, this paper contributes to the literature on the estimation and testing of time-series models with deterministic (and possibly stochastic) co-trending. Analogous to co-integration, co-trending is a useful concept of co-movement in the presence of non-linear deterministic trends. Co-trending study was initially motivated by the empirical evidence in [Nelson and Plosser \(1982\)](#), which suggested that macroeconomic variables, initially perceived as unit root processes, are likely more aligned with a non-linear trend-stationary hypothesis. Classical references analyzing common non-linear deterministic time trends include [Bierens \(2000\)](#), [Hatanaka \(2000\)](#), [Hatanaka and Yamada \(2003\)](#), and [Guo and Shintani \(2013\)](#). The methodology I propose uses the [Guo and Shintani \(2013\)](#) procedure to determine the co-trending rank, defined as the number of co-trending vectors when both stochastic and non-linear deterministic trends are present in a multivariate system. The procedure selects the co-trending rank by minimizing the von Neumann criterion, exploiting the fact that identifying the co-trending rank is equivalent to identifying three groups of eigenvalues of the generalized von Neumann ratio.

Once the co-trending rank is established, and based on theory from climate models, the co-trending vectors are estimated using the recent approach of [Chen et al. \(2022\)](#). Building on [Phillips \(1998\)](#), [Chen et al. \(2022\)](#) propose a two-stage least squares (2SLS) procedure to estimate co-trending slopes when both stochastic and deterministic trends are present. My contribution to this literature is twofold. First, I demonstrate the existence of an error correction mechanism in the presence of deterministic co-trending. Second, I propose the estimation of the VECM in a two-step procedure (akin to the Engle-Granger approach in cointegration) and exploit the estimated dynamics of model for complementary purposes such as computing physical parameters of interest, producing conditional and unconditional forecasts, and identifying structural shocks.

Third, this paper is complementary to the climate science research that uses highly complex climate models. In climate science, much research on the historical effects of anthropogenic GHGs on global climate compares observed temperatures and other climatic variables with the outputs of General Circulation Models (GCMs) ([Barnett et al., 2005](#)). GCMs are complex computer simulation models based on mathematical equations representing various features of the Earth's climate system, including interactions between the atmosphere, oceans, land surface, and ice. These models are essential tools for studying the climate system and predicting future changes; their most widely recognized application is the projection of future climate states under various scenarios of increasing atmospheric CO₂ ([Lupo et al., 2013](#)). Due to their complexity, GCMs are computationally expensive to solve and heavily dependent on the initial conditions of the system. Moreover, simulating these models require large amount of input data and a coupling of various submodels ([Taylor et al., 2012](#)).

Observational time-series studies and GCMs are complementary in a similar way to the complementarity in economics between Structural VAR (SVAR) methods and Dynamic Stochastic General Equilibrium (DSGE) models. While DSGE models aim to provide a detailed description of all interactions in the economy, SVAR models start with a plausible time-series representation of the data and impose minimal restrictions to make meaningful inferences (Benati, 2023). Concretely, a statistical multivariate approach entailing the estimation of a system capturing the dynamics and the interaction of the relevant variables, often have a better forecasting record than theory-based models (Coulombe and Göbel, 2021). In the context of the current research, the unconditional-quantile VECM achieves a desirable balance between a purely statistical multivariate approach and the theoretical/structural modeling of the climate system. The estimated model generates estimation and forecasting outputs by iterating a complete system of different equations in multiple endogenous variables. These outputs are comparable to those from GCMs but are obtained in a simpler, less time-consuming manner.

To illustrate this point, let's consider the estimation of the climate sensitivity. In the GCMs approach, the climate sensitivity is often determined by simulating a known radiative forcing change (e.g., doubling CO₂) and computing the resultant temperature change with respect to an initial equilibrium (Knutti et al., 2017; Dong et al., 2021; Zhu et al., 2021). Recent estimates place climate sensitivity likely between 2 and 5 °C, with the uncertainty reflecting a range of possible outcomes depending on feedback strengths and interactions within the climate system. In a typical observational study, the climate sensitivity is estimated from the long-run relationship between the temperature distributional characteristics and the radiative forcing series. This involves estimating a simple co-trending slope, with confidence intervals obtained from the asymptotic distribution of the estimator.

For forecasts or scenario projections, climate scientists simulate GCMs assuming future paths of emissions or concentration scenarios (e.g., Representative Concentration Pathways or Shared Socioeconomic Pathways) and provide uncertainty measures by running the model multiple times from slightly different initial conditions (Lupo et al., 2013; AR6-IPCC, 2021). With the proposed unconditional-quantile VECM, I can perform a similar exercise using the estimated short- and long-run dynamics of the data. The measure of uncertainty comes from the residual variance of the model in the form of forecast uncertainty. An additional advantage of my methodology is that, unlike most GCMs, it can provide climate sensitivity estimates and conditional projections for the entire distribution of temperature, rather than just for the average.

Finally, this paper complements the literature on Integrated Assessment Models (IAMs), spe-

cially those models featuring certain level of geographical resolution. Two excellent recent reviews on the practice and development of IAMs are provided by Hassler et al. (2024) and Fernández-Villaverde et al. (2024). Beginning with Nordhaus (1993), IAMs combine standard economic theory with key insights from climate science, and are essential tools for policymakers and researchers to evaluate the economic impact of global warming and the optimality of different climate policies (Fernández-Villaverde et al., 2024). The economy–climate interaction typically involves three interdependent components: *i*) an economic module describing how production and consumption are determined, *ii*) a climate module linking emissions from production to changes in global and/or local temperatures, and *iii*) a damage module translating climate changes into output and productivity losses. The most recent IAMs feature a high level of spatial resolution, aiming to capture the geographical heterogeneity observed in the physical and economic effects of climate change. Relevant references from the neoclassical or the economic geography approach include Krusell and Smith (2022), Cruz and Rossi-Hansberg (2024), and Desmet and Rossi-Hansberg (2024). IAMs are predominantly quantitative, dynamic, non-statistical, with parameters set or calibrated to produce plausible outputs.

The unconditional-quantile VECM connects to the practice of IAMs through the climate science module. To model how atmospheric concentrations of CO₂ and other GHGs influence the climate, with global mean surface temperature as the primary variable of interest, IAM modelers typically rely on climate emulators—simplified climate models that provide a realistic quantitative link between CO₂ concentrations and global warming at low computational costs (Fernández-Villaverde et al., 2024). These emulators need to be calibrated and evaluated to ensure that they reproduce climate dynamics consistent with current climate science models (Folini et al., 2024). For example, the global average temperature \bar{T}_t is determined by the stock of carbon in the atmosphere S_t , $\bar{T}_t = \lambda \frac{\log(S_t/\bar{S})}{\log(2)}$, where \bar{S} is the pre-industrial stock of carbon and λ is the sensitivity of global temperature to changes in the stock of atmospheric carbon. As discussed by Pindyck (2021), there is considerable uncertainty over the true value of λ , but a typical calibrated value is 3. Rather than relying on specific predetermined values, IAM practitioners can directly use the estimated climate sensitivity for the average temperature obtained empirically through the unconditional-quantile VECM. This estimate is accompanied by confidence bands constructed based on the residual variance of the model, which are useful for quantifying the effects of uncertainty. Similar to Hassler et al. (2018), the upper and lower bounds of the confidence bands can be evaluated within the structural model to assess changes in other quantities of interest, such as optimal taxes or welfare.

In the case of IAMs with spatial resolution, knowledge of regional temperatures is required (Fernández-Villaverde et al., 2024; Desmet and Rossi-Hansberg, 2024). The regional temperatures

at a specific location i , T_{it} , are inferred from the global average temperature without the need to compute a local climate model, following a technique known as “statistical downscaling” ([Tebaldi and Arblaster, 2014](#)). This technique assumes that the average temperature is a sufficient statistic for local temperatures and proposes modeling $T_{it} = f(\bar{T}_t) + \eta_{it}$ through statistical methods. A form of “statistical downscaling” is implicit in the unconditional-quantile VECM through co-trending relationships between the global average temperature and the unconditional quantiles, which represent temperatures at different locations or latitudes. One of the outcomes of the methodology is the estimation of that co-trending relationships, which provides information about amplification in the temperature distribution, as well as quantile-dependent climate sensitivities. These estimates can be integrated into the calibration of regional IAMs. Moreover, when the analysis is applied on a specific location, the unconditional-quantile VECM can produce seasonal climate sensitivities, which are generally difficult to obtain using traditional climate model emulators.

The remainder of the paper is organized as follows. Section 2 reviews the related literature on the attribution and forecasting of global warming using historical data and discusses its key findings. Section 3 introduces the basic physics of 0D and 1D EBMs. Section 4 establishes an equivalence between a 1D-EBM and an unconditional-quantile restricted VECM. Section 5 outlines the Climate Econometrics methodology, detailing estimation and testing methods used in this study. The results of the empirical analysis, using CRU data for the Globe, Northern Hemisphere, and Europe, are presented in Section 6. Section 7 discusses the main limitations of the methodology and proposes several ideas for future research. Section 8 concludes.

2 Related Literature

This section presents a detailed revision of the literature on the attribution and forecasting of global warming using historical data, the type of literature more closely related to this paper.

Existing studies in this domain typically implement time series methods to estimate the surface temperature response to the radiative forcing from various climate drivers, including GHGs. A critical aspect is the assumption about the nature of trends, that conditions the choice of models suitable for this purpose.⁹ Starting with [Kaufmann and Stern \(2002\)](#) and [Kaufmann et al. \(2006\)](#), a group of authors argue that global temperature and radiative forcing of GHGs contain stochastic trends. These authors advocate for the use of cointegration procedures to test for basic hypotheses regarding the relationship among the variables and to estimate physical parameters such as the cli-

⁹See [McKittrick et al. \(2023\)](#) and [Gadea et al. \(2024\)](#) for a discussion.

mate sensitivity. [Kaufmann and Stern \(2002\)](#), for instance, obtain that doubling the pre-industrial concentration of CO₂ raises the long-run equilibrium temperature in the Northern Hemisphere between 2.3°C and 3.5°C, while for the Southern Hemisphere the estimated temperature sensitivity vary from 1.7°C to 2.2°C. More recently, [Pretis \(2020\)](#) estimate a cointegrated VAR model of global surface temperature anomalies, global ocean heat content anomalies, and global radiative forcing from natural and anthropogenic forces. A set of restrictions on the cointegrating slopes and the adjusting coefficients are imposed based on the underlying physics of the EBM. The resulting estimates indicate an equilibrium climate sensitivity ranging from 1.37°C to 2.16°C, and a transient climate response varying from 1.24°C to 1.38°C.

Other contributions analyzing the relationship between average temperature and radiative forcings using cointegration methods include [Bruns et al. \(2020\)](#), [Phillips et al. \(2020\)](#), and [Benati \(2023\)](#). [Bruns et al. \(2020\)](#) shows that there exists a long-run equilibrium between surface temperature and radiative forcing which represents the energy balance of the earth system. A further long-run equilibrium exists between surface temperature and the accumulated deviations from the energy balance, which represents the stock of heat of the earth system predominantly stored in the ocean. It motivates the use of a multicointegrating I(2) model to account for the role of the ocean in climate change dynamics. These authors find that the climate sensitivity is 2.8 °C and the rate of adjustment to equilibrium is realistically slow in comparison to the I(1) cointegration models. In the same direction, [Benati \(2023\)](#) argues that the I(1) cointegration models suffer from model mis-specification and proposes a forecast exercise exploiting the cointegration between global temperature anomalies for both the land and the ocean, and the radiative forcing assuming a common I(2) component.

There are other authors who believe that temperatures are trend-stationary around a (possibly non-linear) deterministic trend. [Gao and Hawthorne \(2006\)](#) and [Gay-Garcia et al. \(2009\)](#) argue that temperature series are better characterized by a trend-stationary process with a smooth non-linear time trend, or a linear trend with breaks. The assumption of deterministic trends is also common in the climate analysis as inferred from the statistical procedures implemented by the Intergovernmental Panel on Climate Change (IPCC) on its Sixth Assessment ([AR6-IPCC, 2021](#)) and previous reports. The typical approach in this case is to apply co-trending statistical tests to demonstrate that temperature and radiative forcing of GHGs in fact share a common deterministic trend, as is the case of [Estrada et al. \(2013\)](#) or [Estrada and Perron \(2017\)](#). Alternatively, [Chen et al. \(2023\)](#) consider the first differences of radiative forcing—that appear to be trend-stationary—and establish its predictive association with the levels of temperature using Granger-causality tests.

Methodological alternatives that are robust to the nature of trends have been implemented recently, for example in [Chen et al. \(2022\)](#) and [Bennedsen et al. \(2023\)](#). [Chen et al. \(2022\)](#) introduces a common features approach to test for common trends and to estimate long-run relationships without conditioning on a particular type of trends. Building on [Phillips \(1998\)](#), these authors propose an instrumental variable estimator for the co-trending slope between the radiative forcing of GHGs and the average temperature, employing Legendre polynomials of time as instruments. Their empirical analysis suggests a common trend between both series and estimates a climate sensitivity of 1.41°C . [Bennedsen et al. \(2023\)](#), on the other hand, proposes a multivariate Gaussian state-space representation of a two-component 0D-EBM, and estimate the model through maximum-likelihood methods. The model is used to generate long-term global temperature projections under different emissions/concentrations scenarios; the climate sensitivity is estimated at 3.63°C .

The discussed literature implicitly relies on 0D-EBMs that establish a relationship between global average temperature and the radiative forcing from GHGs. However, as previously discussed, an approach assuming global mean temperature as a sufficient statistic for climate change is limited because it fails to account for the non-homogeneous nature of climate dynamics across space and time. In fact, even though the phenomenon of AA is well established in climate science, only few economic and econometric studies have incorporated its impacts. This paper complements and extends the existing literature by introducing a time series methodology capable of accounting for heterogeneity in climate dynamics, particularly in the association between the unconditional distributional characteristics of temperature and radiative forcings. Building on a 1D-EBM and assuming that the unconditional quantiles of temperature represent temperatures at different latitudes (with the highest quantiles representing northern latitudes), the proposed approach is able to capture climate heterogeneity in the form of non-homogeneous climate sensitivities across the temperature distribution.

The link between a 1D-EBM and a VECM shares similarities with the contributions of [Pretis \(2020\)](#) and [Brock and Miller \(2023\)](#). In [Brock and Miller \(2023\)](#), the authors approximate a theoretical moist 1D-EBM with a two-box model and estimate in its VECM form. Although the two studies are related, the econometric approach to modeling and estimation is completely different. The proposal in the current paper allows for a more detailed characterization of the climate system by including as many unconditional quantiles of temperature as desired; this can be seen as a generalization of the two-box model to a model with more boxes. Moreover, the methodology can be applied in contexts beyond the modeling of EBMs, as long as there is sufficient cross-sectional or high-dimensional variability to estimate the distributional characteristics of temperature. For example, it can be utilized for a specific region, such as Central England, using daily information.

In this case, the quantiles of temperature no longer represent latitudes but rather temperatures at different seasons.

Finally, some other recent contributions address geographical heterogeneity in the climate sensitivity. [Anderson et al. \(2023\)](#) develops a dynamic varying-coefficient panel data model and uses it to measure regional climate sensitivity. The average climate sensitivity is estimated to be around 3.7°C , but strong heterogeneity is found: in northern areas, the estimated sensitivity is above 5°C . [Estrada et al. \(2021\)](#) study regional attribution of climate change by establishing the existence of a common non-linear deterministic trend in regional temperatures and anthropogenic forcing. The analysis is conducted by latitude belts, continents, and countries. Warming is found to be widespread among different regions, with higher sensitivities being observed in high latitudes in the Northern Hemisphere. These two papers conduct very detailed analyses of climate sensitivity, providing estimates at the unit level. My approach focusing on the distributional characteristics of temperature, although more aggregated, offers advantages for other purposes such as forecasting and identification of structural shocks. The closest references to this paper are [Gadea and Gonzalo \(2020\)](#) or [Gadea and Gonzalo \(2023\)](#), who study the dynamics of the distributional characteristics of temperature using individual linear trend models. My contribution consists of adopting a multivariate approach to jointly model the dynamics of the whole temperature distribution in a VAR framework and including the effect of the radiative forcing from GHGs, including CO₂.

3 Energy Balance Models

EBMs are the simplest climate models used to understand and facilitate both analytical and numerical studies of climate sensitivities. These models describe the change in temperatures as a function of incoming and outgoing radiation, with the simplest models approximating climate through global mean surface temperatures and aggregate radiative forcing.¹⁰ In the most elementary, 0D-EBM ([Budyko, 1969](#); [Sellers, 1969](#)), the average global temperature \bar{T}_t satisfies an ordinary differential equation with $d\bar{T}_t/dt$ determined by the balance between the incoming shortwave (solar) radiation and the outgoing longwave (terrestrial) radiation emitted in response to the former. Net heat flux is given by $Z_t = F_t - \lambda\bar{T}_t$, where the incoming heat radiation is represented by the effective radiative forcing F_t , and the outgoing radiation is assumed to depend linearly on \bar{T}_t with slope λ . A 0D-EBM is written as:

¹⁰EBMs are used within IAMs to model the climate response to different forcings from natural and anthropogenic sources

$$C \frac{d\bar{T}_t}{dt} = F_t - \lambda \bar{T}_t, \quad (1)$$

where C is a global thermal inertia or heat capacity coefficient.

The EBM in Equation (1) assumes that the entire Earth can be represented by a homogeneous box and all of the energy balance predictions are based on global averages. Therefore, with this type of models it is not possible to study geographical heterogeneity in the climate relationships. 1D-EBMs extend the framework by introducing spatial dependence in temperature equations. In a simple 1D-EBM, temperature is modeled as a function of latitude, and heat is transported between adjacent latitudes in the direction from the Equator to the poles. This allows for a more accurate representation of climate dynamics and enables the study of processes like PA. Following [Held and Suarez \(1974\)](#), at a given latitude θ , a 1D-EBM can be expressed as:

$$C(\theta) \frac{\partial T_t(\theta)}{\partial t} = [F_t - \lambda(\theta)T_t(\theta)] + \gamma(\theta)[\bar{T}_t - T_t(\theta)], \quad (2)$$

where $T_t(\theta)$ is the surface temperature. The first term in the right-hand-side of Equation (2) is the latitudinal net heat flux. The second term is the energy gained due to latitudinal transport, which is assumed to be proportional to the difference between the temperature at latitude θ and the average temperature. This transport term provides for interaction between latitudes in a very simple way. γ is a measure of the efficiency of the model in transporting energy poleward.

The previous equation can be further generalized by assuming that deviations at a given latitude predict the change of temperature in other latitudes in a diffusion process. The equation of interest becomes:

$$C(\theta_i) \frac{\partial T_t(\theta_i)}{\partial t} = [F_t - \lambda(\theta_i)T_t(\theta_i)] + \gamma(\theta_{ii})[\bar{T}_t - T_t(\theta_i)] + \sum_{j \neq i} \gamma(\theta_{ij})[\bar{T}_t - T_t(\theta_j)], \quad (3)$$

for $i = 1, \dots, I$, where the energy balance at certain latitude θ_i depends on deviations in temperatures at other latitudes— θ_j , $i \neq j$ —with respect to the average.

4 Equivalence Between a 1D-EBM and an Unconditional-Quantile Vector Error Correction Model

[Pretis \(2020\)](#) demonstrates that a 0D-EBM with two layers is equivalent to an econometric coin-

tegrated system and can be estimated in discrete time. More recently, Brock and Miller (2023) shows that a moist 1D-EBM can be approximated by a two-box model, and relates it to a restricted vector error correction model which can be estimated using well-known econometric methods. This section follows a similar line of reasoning. The objective is to establish an equivalence between the 1D-EBM in Equation (3) and a VAR model in its error correction form, where the unconditional distributional characteristics of temperature and the radiative forcing from GHGs are incorporated into the multivariate system.

Lets start by assuming that at global or hemispheric scales, the temperature unconditional distributional characteristics represent temperatures at different locations or latitudes. Colder temperatures—at lower quantiles—are associated to northern locations whereas hotter temperatures—at upper quantiles—correspond to locations closer to the Equator.¹¹ Therefore, for a given local temperature $T_t(\theta_i)$ it is possible to find an equivalent temperature quantile $Q_t(\tau_i)$. If a set of $i = 1, 2, \dots, I$ quantiles are observed, then the quantile version of system (3) is written as follows:

$$C(\tau_i) \frac{\partial Q_t(\tau_i)}{\partial t} = [F_t - \lambda(\tau_i)Q_t(\tau_i)] + \gamma(\tau_{ii})[\bar{T}_t - Q_t(\tau_i)] + \sum_{j \neq i} \gamma(\tau_{ij})[\bar{T}_t - Q_t(\tau_j)], \quad (4)$$

for $i, j = 1, \dots, J$ and $t = 1, \dots, T$. For illustration, when $J = 2$ the system is given by:

$$C(\tau_1) \frac{\partial Q_t(\tau_1)}{\partial t} = [F_t - \lambda(\tau_1)Q_t(\tau_1)] + \gamma(\tau_{11})[\bar{T}_t - Q_t(\tau_1)] + \gamma(\tau_{12})[\bar{T}_t - Q_t(\tau_2)], \quad (5)$$

$$C(\tau_2) \frac{\partial Q_t(\tau_2)}{\partial t} = [F_t - \lambda(\tau_2)Q_t(\tau_2)] + \gamma(\tau_{21})[\bar{T}_t - Q_t(\tau_1)] + \gamma(\tau_{22})[\bar{T}_t - Q_t(\tau_2)]. \quad (6)$$

Assuming stochastic processes and relying on a simple first-order Euler-Maruyama discrete time approximation with $\frac{\partial Q_t(\tau_i)}{\partial t} \approx \Delta Q_t(\tau_i) = Q_t(\tau_i) - Q_{t-1}(\tau_i)$, the system describing the 1D-EBM in discrete time can be expressed as:

$$\Delta Q_t(\tau_i) = \frac{1}{C(\tau_i)}[F_{t-1} - \lambda(\tau_i)Q_{t-1}(\tau_i)] + \frac{\gamma(\tau_{ii})}{C(\tau_i)}[\bar{T}_{t-1} - Q_{t-1}(\tau_i)] + \sum_{j \neq i} \frac{\gamma(\tau_{ij})}{C(\tau_i)}[\bar{T}_{t-1} - Q_{t-1}(\tau_j)] + u_t(\tau_i), \quad (7)$$

for $i, j = 1, \dots, J$ and $t = 1, \dots, T$, where $u_t(\tau_i)$ denote stationary error terms for each τ_i .

Note that each equation has the form of a vector autorregresion model in its error correction form with restrictions, where the changes in the unconditional quantiles of temperature adjusts to two different types of long-run equilibrium relationships: the first, $[F_t - \lambda(\tau_i)Q_t(\tau_i)]$, correspond to the latitudinal net heat flux, while relations of the form $[\bar{T}_t - Q_t(\tau_i)]$ characterize latitudinal heat

¹¹See Appendix A for related evidence.

transport. The next section introduces a methodology to estimate the system using time series methods.

5 Climate Econometrics Methodology

5.1 Temperature Distributional Characteristics

A time series analysis framework similar to that used in [Gadea and Gonzalo \(2020\)](#) and [Gadea and Gonzalo \(2023\)](#) is adopted. Specifically, the temperature is treated as a functional stochastic process denoted by $T = (T_t(\omega), t \in \mathcal{T})$, where \mathcal{T} is an interval in \mathbb{R} , defined on a probability space (Ω, \mathcal{F}, P) . For each $\omega \in \Omega$, the function $t \rightarrow T_t(\omega)$ belongs to some function space \mathbf{G} . The function space \mathbf{G} is equipped with a scalar product, a norm, and a Borel σ -algebra denoted as \mathcal{B}_G . In modeling the temperature process, one can either consider the entire sequence of functions in \mathbf{G} , such as the sequence of state densities $(f_1(\omega), \dots, f_T(\omega))$, or focus on specific characteristics $(C_t(\omega))$ such as the mean, variance, and quantiles of the states. These characteristics can be considered as time series objects and existing econometric tools for modeling, inference, or forecasting can be applied on them. In this research, the latter approach is adopted. To estimate the unconditional quantiles of temperature, it is assumed the availability of a sufficiently high number N of cross-sectional units (temperature stations) or higher frequency observations (daily temperatures) at each time period t . Under certain regularity conditions, it is possible to consistently estimate these unconditional quantiles. From now on, $Q_t(\tau_i)$ denotes the estimated unconditional distributional quantile which is the object at hand in the empirical analysis.

5.2 Estimation and Testing of Co-trending Relationships

Let Z_t denote a m -variate time series vector for $t = 1, 2, \dots, T$. Elements in Z_t are non-stationary and both stochastic and non-linear deterministic trends are allowed. [Guo and Shintani \(2013\)](#) propose a consistent selection procedure of two types of co-trending ranks: r_1 , the number of linearly independent vectors that eliminate both stochastic and deterministic trends at the same time; and r_2 , the number of linearly independent vectors that eliminate the deterministic but not the stochastic trends. $r = r_1 + r_2$ is called the weak co-trending rank, while the number of common non-linear deterministic trends corresponds to $m - r$.

The procedure selects the co-trending rank by minimizing a von Neumann criterion in a multi-variate framework. Concretely, let $\hat{\lambda}_1 \geq \dots \geq \hat{\lambda}_m$ denote the eigenvalues of $S_{11}^{-1}S_{00}$, where

$$S_{11} = T^{-1} \sum_{t=1}^T Z_t Z'_t, \quad S_{00} = T^{-1} \sum_{t=2}^T \Delta Z_t \Delta Z'_t. \quad (8)$$

A “paired” procedure independently selects r and r_1 by minimizing each of the following expressions:

$$VN_1(r_1) = - \sum_{i=1}^{r_1} \hat{\lambda}_i + f(r_1) \frac{C_T}{T}, \quad VN_2(r) = - \sum_{i=1}^r \hat{\lambda}_i + f(r) \frac{C'_T}{T^2}, \quad (9)$$

where $f(s)$, C_T , and C'_T are elements of a penalty function analogous to the ones used in the information criteria literature. A “joint” procedure simultaneously determines r and r_1 by minimising:

$$VN_1(r_1, r) = -T^\alpha \sum_{i=1}^{r_1} \hat{\lambda}_i - \sum_{i=r_1+1}^r \hat{\lambda}_i + f(r_1) \frac{C_T}{T} + f(r) \frac{C'_T}{T^2}, \quad (10)$$

where $0 < \alpha < 1$. Both procedures are consistent in selecting the co-trending rank without specifying a parametric model for trends that belong to a certain class of non-linear function including breaks in the trend function and smooth transitions. For large enough samples the two methods yield similar results.

The knowledge of the co-trending rank offers useful prior information for the full estimation of the multivariate system since it determines the reduced rank structure of the coefficient matrix on non-linear trend functions. Once the co-trending rank is established, and based on insights from the theoretical 1D-EBMs, the next step in the methodology is to estimate the co-trending vectors using a methodology robust to the type of trends in the data. Consider a scenario where the econometrician observes two trending series of the form:

$$y_t = f_t + u_t, \quad (11)$$

$$x_t = g_t + v_t, \quad (12)$$

for $t = 1, 2, \dots, T$, where f_t and g_t are trending components, and u_t and v_t are ergodic stationary disturbances. The trending components are not assumed to be of a particular nature, and therefore, can be linear or a finite polynomial of time, integrated processes of order 1 or larger, piecewise linear, or even combination of these forms. Two different definitions of co-trending are proposed. **Strong co-trending** implies that the difference $y_t - x_t$ is a non-trending process. For stochastic trends,

it implies cointegration with a cointegrating vector $(1, -1)$. For deterministic case, it implies that both series share the same type of trend and that the slopes are equal for all t . This type of co-trending was studied in [Gadea and Gonzalo \(2023\)](#) to test for PA.¹² A weaker form of co-trending assumes that if the trends in y_t and x_t are common, then there exists exactly one β_0 such that there is no trend in the linear combination $y_t - \beta_0 x_t$. If that is the case, then the series satisfy the **Weak co-trending** condition. For stochastic trends, it implies cointegration with a general cointegration vector $(1, -\beta)$. For deterministic trends, it means that the trends in the series are of the same type but differing rates of change are allowed. For example, if y_t and x_t both are linearly trending but their slopes are different, then the weak co-trending condition is satisfied, but the strong co-trending is not. The [Guo and Shintani \(2013\)](#) procedure allows for this second type of co-trending.

[Chen et al. \(2022\)](#) propose a method to estimate and test for weak co-trending in bivariate relationships. Consider the pseudo-structural model:

$$y_t = \alpha_0 + \beta_0 x_t + e_t, \quad (13)$$

$$x_t = g_t + v_t, \quad (14)$$

where g_t is a trend process. This is a pseudo-structural model because e_t and v_t are correlated, and hence the right-hand-side variable in the first equation is endogenous. The authors propose an estimation procedure for β_0 that use powers of (t/T) as legitimate instruments to solve the endogeneity issue in an instrumental variable (IV) framework. The idea is that polynomial functions in time are relevant predictors of the trending variable y_t but are uncorrelated with the non-trending term e_t , regardless of whether the trend g_t is deterministic or stochastic.¹³

Legendre Polynomials of (t/T) are employed as instruments and the estimation of β_0 is obtained using two-stages least squares (2SLS). Let $\phi_j(\tau_t)$ defined on $[0, 1]$ for $\tau_t = t/T$ take the form:

$$\phi_j(\tau_t) = \sqrt{2j+1} \sum_{s=0}^j (-1)^{j+s} \binom{j}{s} \binom{j+s}{s} \tau_t^s, \quad (15)$$

$j = 0, 1, 2, \dots$. In matrix form, $y = (y_1, \dots, y_T)'$, $e = (e_1, \dots, e_T)'$ with $e_t = y_t - \alpha_0 - \beta_0 x_t$, $\gamma_0 = (\alpha_0, \beta_0)'$, and

¹²To test for the co-trending vector $(1, -1)$, [Gadea and Gonzalo \(2023\)](#) implemented a trend test on the series $w_t = y_t - x_t$. If a trend is detected in w_t , then the two series do not satisfy the strong co-trending condition.

¹³The rationale of the procedure is based on [Phillips \(1998\)](#), who shows that any generic trending process can be validly represented using trending regressors that are independent to the process.

$$X = \begin{pmatrix} 1 & x_1 \\ \dots & \dots \\ 1 & x_T \end{pmatrix}, \quad \Phi = \begin{pmatrix} 1 & \phi_1(\tau_1) & \dots & \phi_p(\tau_1) \\ \dots & \dots & & \\ 1 & \phi_1(\tau_T) & \dots & \phi_p(\tau_T) \end{pmatrix}, \quad (16)$$

where p is a integer greater than 2. The 2SLS estimator of γ_0 is written as follows:

$$\hat{\gamma}_{2SLS} = (\hat{\alpha}_{2SLS}, \hat{\beta}_{2SLS})' = (X'\Phi(\Phi'\Phi)^{-1}\Phi'X)^{-1}X'\Phi(\Phi'\Phi)^{-1}\Phi'y. \quad (17)$$

Under certain regularity assumptions, the authors establish the asymptotic properties of the 2SLS estimator. Concretely, as $T \rightarrow \infty$, the estimator satisfies:

$$(U'U)^{1/2}(\hat{\gamma}_{2SLS} - \gamma_0) \xrightarrow{\mathcal{D}} N(0, \lambda_e^2 I_{(2)}), \quad (18)$$

where $U = W^{1/2}\Phi'X$, $W = (\Phi'\Phi)^{-1}$ and λ_e^2 is the long-run variance of e_t . The rate of convergence of the estimator depends on a deterministic matrix D_T ensuring $D_T^{-1}U'UD_T^{-1} \xrightarrow{\mathcal{D}} \xi$, with the assumption that such matrix exists and $\|D_T\|_2^2 \rightarrow \infty$ as $T \rightarrow \infty$, $(D_T^{-1}U'UD_T^{-1}, D_T^{-1}U'\varepsilon) \xrightarrow{\mathcal{D}} (\xi, \eta)$, where ξ is a matrix of positive random variables and η is a 2-dimensional mixture normal radon variable $N(0, \xi\lambda_e^2)$ with $\mathbf{E}\|\xi\|_2 < \infty$.

If the variables share a common trend, the residuals of the co-trending regression should contain no trend and will be uncorrelated with the instruments. A natural test for the null of a common trend among the variables is equivalent to an over-identification test on the residuals of the 2SLS procedure. Alternatively, co-trending can be tested using the trend test of [Gadea and Gonzalo \(2020\)](#) that is useful to detect any type of trend in the residuals of the co-trending regressions.

5.3 Estimation of the Unconditional-Quantile Vector Error Correction Model

The estimation of the restricted unconditional-quantile VECM model is conducted in two steps. In the first step, the co-trending relationships implied by the model are estimated following the procedure by [Chen et al. \(2022\)](#) described in the previous subsection. Specifically, the slope-coefficients for each bivariate co-trending equation involving F_t and a given distributional characteristic of temperature ($Q_t(\tau_i), i = 1, \dots, J$ and \bar{T}_t) are estimated, where F_t represents the radiative forcing. For co-trending relationships involving \bar{T}_t and $Q_t(\tau_i), i = 1, \dots, J$, note that Equation (7) implies a strong co-trending condition. However, the data suggest that the differences between the average temperature and the quantiles are trending processes, which is a consequence of heterogeneous

warming rates along the temperature distribution. Therefore, this condition is relaxed and the co-trending vector is allowed to be different from $(1, -1)$. This ensures that the terms in the right-hand-side of Equation (7) are all non-trending. In other words, co-trending coefficients $\beta(\tau_i)$ in equations of the form $Q_t(\tau_i) = \beta_0(\tau_i) + \beta(\tau_i)\bar{T}_t + u_t(\tau_i)$ are also estimated. After estimating each co-trending equation, the associated vector of residuals are computed.

In the second step, the short-run dynamics of the unconditional-quantile VECM in Equation (7) are estimated.¹⁴ Let $Z_t = [Q_t(\tau_1), \dots, Q_t(\tau_i), \bar{T}_t, F_t]'$. The procedure involves regressing the first difference of Z_t , denoted as ΔZ_t , on the lagged residuals of the co-trending equations and lags of ΔZ_t . However, a normalization is necessary to avoid collinearity among the co-trending vectors. Notice that in a system with $i = 3$ and 5 variables, 7 co-trending relationships are estimated and tested. To maintain consistency with the maximum co-trending rank, only the lagged residuals of the co-trending equations relating $Q_t(\tau_i)$ and \bar{T}_t , along with the lagged co-trending residuals of the relationship between F_t and \bar{T}_t , are included. In simpler terms (omitting the lags of ΔX_t from the specification), equations of the following form are estimated individually through OLS:

$$\begin{aligned} \Delta Q_t(\tau_i) = & \frac{1}{C(\tau_i)}[F_{t-1} - \bar{\lambda}\bar{T}_{t-1}(\tau_i)] - \frac{\gamma(\tau_{ii})}{C(\tau_i)}[Q_{t-1}(\tau_i) - \hat{\beta}(\tau_i)\bar{T}_{t-1}] - \\ & \sum_{j \neq i} \frac{\gamma(\tau_{ij})}{C(\tau_i)}[Q_{t-1}(\tau_j) - \hat{\beta}(\tau_j)\bar{T}_t] + v_t(\tau_i), \end{aligned} \quad (19)$$

for $i = 1, \dots, J$ and $t = 1, \dots, T$. The parameters to be estimated are $\delta_{0i} = \frac{1}{C(\tau_i)}$, $\delta_{ii} = \frac{\gamma(\tau_{ii})}{C(\tau_i)}$, and $\delta_{ij} = \frac{\gamma(\tau_{ij})}{C(\tau_i)}$, which represent the adjustment parameters. The terms $\hat{\lambda}(\tau_i)$ and $\hat{\beta}(\tau_i)$ are the estimated parameters obtained from the first step. Similar equations are estimated for $\Delta\bar{T}_t$ and ΔF_t .

The analysis presented in this document focuses on three specific geographical units: the Globe, the North Hemisphere, and Europe. Importantly, the methodology can be applied to other situations provided that there is a sufficient amount of cross-sectional or higher frequency data available to estimate temperature unconditional quantiles. For example, one could choose a specific region such as Central England and utilize daily temperature data to estimate the annual temperature distribution. By applying Equation (19) to this dataset, it would be possible to analyze the dynamic relationships within the temperature distribution and examine the co-movements and dependencies among different quantiles. However, the interpretation of the results would need to be adapted because there is no geographical dimension to exploit and heat transport across latitudes is not longer a valid mechanism. Instead, the focus would be on capturing seasonal interdependencies or

¹⁴Section 5.4 below shows how an error correction mechanism is obtained in a model with deterministic co-trending.

day-time heterogeneity. Appendix B illustrates this aspect by the application of the methodology to daily mean-temperature observations at Central England.

5.4 Error Correction in a Co-trending Model

This section shows how an error correction mechanism emerges in a model with deterministic co-trending. Consider an initial bivariate model similar to that in [Chen et al. \(2022\)](#). Define:

$$y_t = \beta x_t + u_t, \quad u_t = \rho u_{t-1} + e_t, \quad \Delta y_t = \beta \Delta x_t + \Delta u_t, \quad (20)$$

$$x_t = g_t + \epsilon_t, \quad \epsilon_t = \alpha u_t + v_t, \quad \Delta x_t = [g_t - g_{t-1}] + \Delta \epsilon_t. \quad (21)$$

where the endogeneity in this pseudo-structural model originates from the correlation between ϵ_t and u_t . Since $\Delta u_t = (\rho - 1)u_{t-1} + e_t$, $\Delta \epsilon_t = \alpha \Delta u_t + \Delta v_t = \alpha((\rho - 1)u_{t-1} + e_t) + \Delta v_t$, $u_{t-1} = y_{t-1} - \beta x_{t-1}$, it is possible to write Δy_t and Δx_t as:

$$\Delta y_t = \beta[g_t - g_{t-1}] + (\rho - 1)(1 + \beta\alpha)(y_{t-1} - \beta x_{t-1}) + (\beta\alpha + 1)e_t + \beta\Delta v_t, \quad (22)$$

$$\Delta x_t = [g_t - g_{t-1}] + \alpha(\rho - 1)(y_{t-1} - \beta x_{t-1}) + \alpha e_t + \Delta v_t. \quad (23)$$

Notice that under the assumed structure for ϵ_t , both equations adjust to the past deviations from the long-run relationship between the two variables, $(y_{t-1} - \beta x_{t-1})$ and the stochastic terms are $I(0)$. The first term, $g_t - g_{t-1}$, generally depends on t . If g_t is a linear trend, then it becomes a constant. In fact, for a linear-trend model with $x_t = \gamma_0 + \gamma_1 t + \epsilon_t$, it is possible to write:

$$\Delta y_t = \beta(\gamma_1) + (\rho - 1)(1 + \beta\alpha)(y_{t-1} - \beta x_{t-1}) + (\beta\alpha + 1)e_t + \beta\Delta v_t, \quad (24)$$

$$\Delta y_t = C_0 + C_1(y_{t-1} - \beta x_{t-1}) + [(\beta\alpha + 1)e_t + \beta\Delta v_t], \quad (25)$$

and similarly:

$$\Delta x_t = \gamma_1 + \alpha(\rho - 1)(y_{t-1} - \beta x_{t-1}) + \alpha e_t + \Delta v_t, \quad (26)$$

$$\Delta x_t = C_2 + C_3(y_{t-1} - \beta x_{t-1}) + [\alpha e_t + \Delta v_t]. \quad (27)$$

More generally, consider the parametric co-trending model in [Hatanaka and Yamada \(2003\)](#), with a k -variate time series $y_t = (y_{1t}, \dots, y_{kt})'$ generated by:

$$y_t = g_t + u_t, \quad t = 1, \dots, T, \quad (28)$$

where $g_t = (g_{1t}, \dots, g_{ky})'$ is a non-stochastic trend component and $u_t = (u_{1t}, \dots, u_{kt})'$ is a stochastic component with $\Delta u_t = C(L)\epsilon_t = \sum_{j=0}^{\infty} C_j \epsilon_{t-j}$, $C_0 = I_k$, $\sum_{j=0}^{\infty} j^2 \|C_j\| < \infty$, ϵ_t is iid with zero mean and positive definite covariance matrix $\Sigma_{\epsilon,\epsilon}$. This assumption implies that u_t contains at least one stochastic trend, unless $C(1) = 0$. To rule-out stochastic trends, I assume $C(1) = 0$ so that all elements in u_t are $I(0)$ stationary random variables.

Assumption 2.1 in [Guo and Shintani \(2013\)](#) restricts the class of trends in g_t and the co-trending structure among its elements. A general class of trends in g_t is allowed as long as the trends do not diverge faster than a linear trend in the following sense: $d = \lim_{T \rightarrow \infty} T^{-2} \sum_{i=1}^T g_t$ and $D = \lim_{T \rightarrow \infty} T^{-3} \sum_{i=1}^T g_t g_t'$ exist, all elements in the main diagonal of D are non-zero, and $T^{-3} \sum_{i=1}^T g_t g_t' - D = O(T^{-1/2})$. Linear trends, piecewise linear trends, or smooth transition trends are allowed. Additionally, assume a co-trending structure with r co-trending vectors that eliminate deterministic trends in the absence of stochastic trends. Define B as a $k \times r$ matrix collecting those co-trending vectors and assume $B'D = 0$. Assume there exists a $k \times (k-r)$ matrix B_{\perp} such that $B_{\perp}'GB_{\perp}$ is of full rank.

Under these assumptions, and following [Hatanaka and Yamada \(2003\)](#), the first difference of the trend component can be written as:

$$\Delta g_t = AB'g_{t-1} + Mh_{T,t}, \quad (29)$$

where A and B are $k \times r$ full column rank matrices, r being the co-trending rank, M is an $k \times m$ matrix satisfying $m \geq k-r$, and $h_{T,t} = [1, I(t > [b_1 T]), \dots, I(t > [b_{m-1} T])]'$ with break functions b_j 's satisfying $0 < b_1 < \dots < b_{m-1} < 1$. Notice that an error correction form for the deterministic component g_t is established, with the second part of Equation 29 representing non-linearities in the form of breaks that may appear in the first difference of g_t . The [Guo and Shintani \(2013\)](#) approach allows for pinning-down the dimensions of A and B through the selection of the co-trending rank r , while the climate theory from 1D-EBMs combined with the methodology of [Chen et al. \(2022\)](#) allows for inference regarding the structure of B . Non-linearities in $h_{T,t}$ can be properly accounted for by adding a trend-component in the equation of the VECM or imposing a sufficient number of lags to capture properly the underlying dynamics.

6 Empirical Analysis

6.1 Data

Temperature. Station-level temperature data is obtained from the latest version of the HadCRUT5 dataset (Morice et al., 2021), jointly developed by the Climatic Research Unit (CRU) at the University of East Anglia and the Hadley Centre at the UK Met Office.¹⁵ For land regions across the globe, this dataset compiles monthly-mean temperatures from a network of 10,000 weather stations, spanning the period from 1850 to the present. Data coverage is denser over the more populated regions, particularly, the United States, southern Canada, Europe, and Japan. In contrast, coverage is more limited over the interior of South America and Africa, as well as the Antarctica.

A limitation of this dataset is that the number of observed stations varies from year to year. To address the potential statistical implications arising from this imbalance, the distributional characteristics of interest are estimated using only those stations-month units that have complete observations throughout the entire sample period. Concretely, a station-month unit is included if the station has continuous observations for that month throughout the sample period.¹⁶ The effective number of stations-month units used is 1.263. Utilizing the cross-sectional variation across different locations, the annual unconditional distributional characteristics are estimated following the procedure in Section 5.1. Figure 2 presents the annual unconditional densities of temperature for the Globe, the Northern Hemisphere, and Europe, while Figure 3 shows the corresponding unconditional distributional characteristics. Appendix A provides evidence suggesting that these unconditional quantiles, at the global scale, represent temperatures at different latitudes.

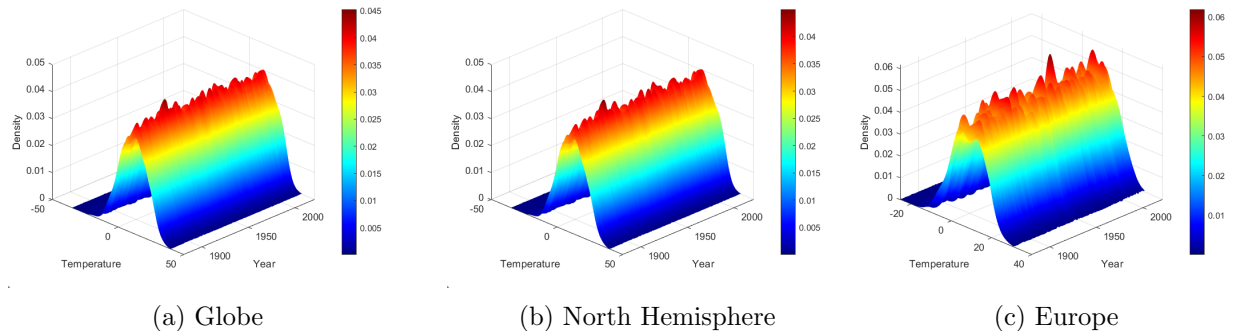


Figure 2: Unconditional densities estimated each year from 1880 to 2021

¹⁵Dataset accessible at the following URL: <https://crudata.uea.ac.uk/cru/data/temperature/>.

¹⁶An alternative approach involves computing the annual temperature for each station by averaging its monthly observations. Empirical results are robust to both methods.

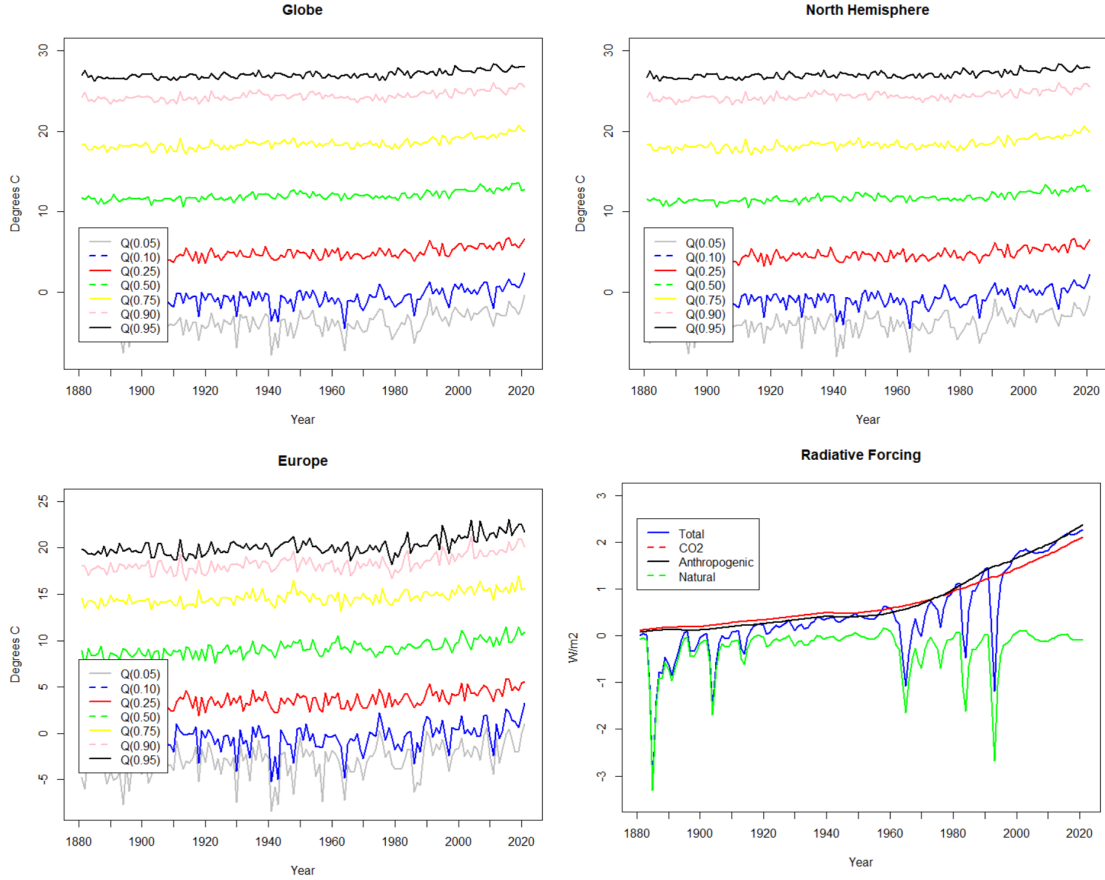


Figure 3: Temperature distributional characteristics (Globe, North Hemisphere, and Europe) and radiative forcing from different sources

Radiative forcing. The latest version of the effective radiative forcing dataset developed by Hansen et al. (2011) is used. This dataset provides information on radiative forcing in units of watts per square meter (W/m^2) originating from various sources, including greenhouse gases (CO_2 , CH_4 , CFCs, N_2O , O_3), changes in land surface, solar irradiance, and volcanic activity. Following the approach of Bennedsen et al. (2023), total radiative forcing (TRF) can be decomposed into natural forcing, which arises from solar and volcanic influences, and anthropogenic forcing attributed to human activities. By examining the corresponding graph in Figure 3, a clear upward trend in the TRF is observed. Notably, this trend is predominantly driven by anthropogenic sources, particularly atmospheric CO_2 emissions.

Table 1: ADF tests for unit roots

Characteristic	Temperature					
	Globe		North Hemisphere		Europe	
	Test-statistic	p-value	Test-statistic	p-value	Test-statistic	p-value
$Q_t(0.05)$	-10.3438	0.0000	-10.3936	0.0000	-9.8402	0.0000
$Q_t(0.10)$	-9.7128	0.0000	-9.6863	0.0000	-9.6418	0.0000
$Q_t(0.25)$	-10.3506	0.0000	-10.2948	0.0000	-10.6979	0.0000
$Q_t(0.50)$	-4.6258	0.0014	-4.3464	0.0036	-10.9592	0.0000
$Q_t(0.75)$	-2.1158	0.5321	-2.2124	0.4786	-6.3808	0.0000
$Q_t(0.90)$	-3.9051	0.0143	-3.9956	0.0109	-3.7950	0.0196
$Q_t(0.95)$	-8.8098	0.0000	-9.3037	0.0000	-3.6483	0.0294

Source	Radiative Forcing					
	Levels		First differences		Second differences	
	Test-statistic	p-value	Test-statistic	p-value	Test-statistic	p-value
Total (TRF)	-4.6950	0.0011	-11.6801	0.0000	-9.2650	0.0000
CO ₂	2.9746	1.0000	-3.5256	0.0406	-13.8463	0.0000
Anthropogenic	-0.0589	0.9951	-2.9437	0.1523	-13.0928	0.0000
Natural	-6.9410	0.0000	-11.6499	0.0000	-9.2705	0.0000

Notes: Test-statistics and p-values of the ADF-tests for unit roots. Intercept and trend included in the test-equation. Lags selected using the BIC criterion.

6.2 Unit Roots

Augmented Dickey-Fuller (ADF) tests are implemented as an attempt to determine the nature of the trends in the temperature and radiative forcing data. The results are presented in Table 1. Based on the test-statistics and p-values, the evidence suggests that the unconditional quantiles of temperature do not contain unit roots but instead follow trend-stationary processes. This evidence aligns with the strand of literature arguing for the existence of deterministic trends, see [Gay-Garcia et al. \(2009\)](#) and [Gadea et al. \(2024\)](#) for a discussion. The only exception is $Q_t(0.75)$ in the Globe and North Hemisphere, where the null hypothesis of the test cannot be rejected perhaps due to the existence of a more prominent structural break that bias the ADF test towards the non-rejection area. Regarding the radiative forcing series, different orders of integration are detected. Results indicate that the natural and total forcing variables in levels do not contain unit roots. In contrast, anthropogenic and CO₂ forcing appear to be integrated of order 2, I(2). [Pretis and Hendry \(2013\)](#) discusses the challenges in establishing the order of integration of CO₂ concentrations due to the pooling of different measurement regimes. Before 1958, CO₂ concentrations were inferred from ice drilling, and it is only from 1959 onwards that this variable started to be measured with instruments. This shift can potentially influence the conclusion of the ADF tests.

Table 2: Testing for trends in distributional characteristics

Characteristic	Globe		North Hemisphere		Europe	
	Test-statistic	p-value	Test-statistic	p-value	Test-statistic	p-value
$Q_t(0.05)$	0.0172	0.0000	0.0173	0.0000	0.0175	0.0000
$Q_t(0.10)$	0.0150	0.0000	0.0151	0.0000	0.0153	0.0000
$Q_t(0.25)$	0.0122	0.0000	0.0121	0.0000	0.0129	0.0000
$Q_t(0.50)$	0.0096	0.0000	0.0097	0.0000	0.0127	0.0000
$Q_t(0.75)$	0.0118	0.0000	0.0114	0.0000	0.0103	0.0000
$Q_t(0.90)$	0.0082	0.0000	0.0083	0.0000	0.0142	0.0000
$Q_t(0.95)$	0.0074	0.0000	0.0074	0.0000	0.0148	0.0000
Mean	0.0112	0.0000	0.0112	0.0000	0.0129	0.0000

Notes: Annual distributional characteristics estimated using the cross-sectional temperature distribution at each year from 1880 to 2021. Test-statistics and p-values correspond to a significance test for the trend-slope in a regression of the distributional characteristic on a constant and a linear trend, using HAC standard-errors.

6.3 Testing for Trends in the Temperature Distribution

[Gadea and Gonzalo \(2020\)](#) propose a simple robust trend-test to detect the existence of an unknown trend component (deterministic or stochastic) in the unconditional distributional characteristics of global temperature. The test involves estimating an OLS regression of the corresponding distributional characteristic on a linear trend, and testing the significance of the slope coefficient using HAC standard errors. Table 2 reports the slope coefficients and corresponding p-values for the null of no-trend. The test identifies an increasing trend in all distributional characteristics of interest. Notably, for the Globe and North Hemisphere, the trend slopes (perceived as linear approximations to the potentially non-linear trend component) are stronger in the lower quantiles compared to the mean, median, and upper quantiles. This is consistent with the evidence in [Serreze et al. \(2009\)](#), [Screen and Simmonds \(2010\)](#) or [Smith et al. \(2019\)](#) regarding trends in the Arctic being about twice the global average as signal of AA. In the case of Europe, the global warming dynamics seem more uniform, although the largest trend slope is estimated for $Q_t(0.05)$.

This section is descriptive and serves as a preliminary analysis of heterogeneity in the trend temperature dynamics. For a more comprehensive “univariate” approach to characterizing, measuring, and testing the existence of climate change heterogeneity, refer to [Gadea and Gonzalo \(2023\)](#).

6.4 A Model for the Unconditional Distributional Characteristics of Temperature

In this section, a multivariate model for the mean and the unconditional quantiles of temperature is analyzed. Define the vector $Z_t = [Q_t(\tau_1), \dots, Q_t(\tau_k), \bar{T}_t]'$. This initial model aims to

capture the interaction between different parts of the temperature distribution without conditioning on the radiative forcing variable. From a 1D-EBM perspective, such type of interactions may arise due to heat transport across latitudes. A parsimonious system comprising four series, $Z_t = [Q_t(0.05), Q_t(0.50), Q_t(0.95), \bar{T}_t]'$, is initially considered. The model can be trivially expanded to include more unconditional quantile series, see Appendix D.

6.4.1 Testing for the co-trending rank

As described in Section 6.3, the elements of Z_t exhibit an upward trend. ADF-tests indicates that these trends are of deterministic nature. To establish co-trending in the sense of by [Guo and Shintani \(2013\)](#), their model-free co-trending rank selection procedure is implemented. For all geographical scales (Globe, North Hemisphere, and Europe), the procedure identifies a co-trending rank of 3. In a vector of 4 variables, it implies the existence of 1 common (possibly non-linear) deterministic trend. This information, together with the equations from the 1D-EBM, provides useful guidance for the estimation of a restricted version of the VECM in Equation (19).

6.4.2 Estimation of co-trending vectors

From the 1D-EBM in Equation (2), the energy gained due to latitudinal transport is assumed to be proportional to the difference between the temperature at a given latitude and the average temperature. Due to the heterogeneity in individual trend-slopes across the temperature distribution (see Table 2), these differences are trending processes and each pair of series do not satisfy the strong co-trending condition.¹⁷ Thus, for relations of the form $[\bar{T}_t - Q_t(\tau_i)]$, instead of enforcing a co-trending vector $(1, -1)$, the co-trending vector is allowed to be of the form $(1, -\beta(\tau_i))$, where $\beta(\tau_i)$ is estimated using the approach of [Chen et al. \(2022\)](#).

The estimated co-trending slopes are reported in Table 3. Across all geographical scales, the estimated $\hat{\beta}(\tau_i)$ -values are statistically significant at the 1% level. For both the Globe and the North Hemisphere, $\hat{\beta}(0.05)$ exceeds 1, whereas $\hat{\beta}(0.95)$ falls below 1. This observation aligns with the expected pattern of accelerated warming at northern latitudes with respect to the average, a phenomenon consistent with the AA effect. In the case of Europe, the variability is comparatively lower with the strongest co-trending coefficients estimated at the tails of the temperature distribution. In all cases, the null hypothesis of a common trend cannot be rejected at a 5% significance level and it is concluded that each pair of series share a common —deterministic and/or stochastic—

¹⁷The trend-test of [Gadea and Gonzalo \(2020\)](#) is applied to the differences of each unconditional quantile with respect to the mean and, in all cases, the null of no-trend is strongly rejected.

Table 3: Co-trending slopes of relationships between unconditional quantiles and the average temperature

Slope	Globe		North Hemisphere		Europe	
	<i>Estimate</i>	<i>Cot-test</i>	<i>Estimate</i>	<i>Cot-test</i>	<i>Estimate</i>	<i>Cot-test</i>
$\beta(0.05)$	1.5310*** (0.1529)	0.9026	1.5283*** (0.1503)	0.8755	1.3975*** (0.2109)	0.9053
$\beta(0.50)$	0.8353*** (0.0482)	0.4198	0.8496*** (0.0463)	0.4536	0.9253*** (0.0745)	0.1556
$\beta(0.95)$	0.6677*** (0.0473)	0.0876	0.6536*** (0.0478)	0.2486	1.2137*** (0.0953)	0.1987

Notes: Column *Estimate* correspond to the estimated co-trending slope—of the quantile with respect to the average temperature—and its standard-error in parenthesis. *, **, *** denote significance at the 10%, 5%, and 1% levels, respectively. Column *Cot-test* reports the p-value of the test for common-trends.

trend.

The estimation of the co-trending vectors presented in this subsection offers an alternative way of quantifying the degree of amplification in the temperature distribution relative to the average. In [Gadea and Gonzalo \(2023\)](#), the same objective is achieved by testing for the presence of trends in the differences between the respective quantile and the mean temperature. Both approaches are equivalent. The procedure presented here is also related to the “statistical downscaling” technique used in climate science to infer local temperatures, considering the average temperature as a sufficient statistic for the global climate [Tebaldi and Arblaster \(2014\)](#). Estimated co-trending vectors and confidence bands can be incorporated into IAM practice for an “empirically-guided” calibration and uncertainty analysis.

6.4.3 Estimation of the error correction model and Trend-Transitory decomposition

A version of the VECM in Equation (19) omitting the radiative forcing variable is estimated. Specifically, the first difference of Z_t , ΔZ_t , is regressed on the lagged residuals derived from the co-trending equations discussed in the previous section, alongside ΔZ_{t-1} .¹⁸ This two-step procedure mirrors the approach of [Engle and Granger \(1987\)](#) for estimating VECM within cointegrated systems. Table 4 reports the coefficients associated to the lagged co-trending residuals, which are informative about the adjustment rate of each dependent variable to deviations from the long-run equilibrium. Notice that for all geographical scales, the first differences of the unconditional quantiles adjust to their own previous deviations from its long-run equilibrium with respect to the average temperature. For the Globe and the North Hemisphere, the rate of adjustment is slower at

¹⁸Lag-length selected using the BIC and a general to particular approach.

the tails of the temperature distribution and all equations adjust to the stationary (non-trending) deviations of $Q_t(0.95)$ from the mean. In contrast, for Europe, the rate of adjustment decreases with the quantile level, and there is less dependence on the stationary deviations of $Q_t(0.95)$ from the average.

Similar to [Gonzalo and Granger \(1995\)](#), it is possible to identify a common trending component in a multivariate system with deterministic co-trending. Identification is achieved by imposing that the component is a linear combination of the original variables, and that the error-correction terms do not cause this component at low frequencies. The proof follows an analogous reasoning to that used when variables are cointegrated. Denote A as the $k \times r$ matrix of adjustment coefficients in the VECM form. The common trending component, f_t , is obtained as $f_t = A'_{\perp} Z_t$, where A'_{\perp} is the orthogonal complement of A satisfying $A'_{\perp} A = 0$. Using the estimates of A presented in Table 4, I compute f_t for the Globe, the Northern Hemisphere, and Europe. Table 5 presents the linear combination coefficients necessary to obtain the common trending components. In all cases, trend dynamics are primarily driven by the mean and the upper quantile, while the lower quantile acts in an opposite direction. Figure 4 plots the resulting components.

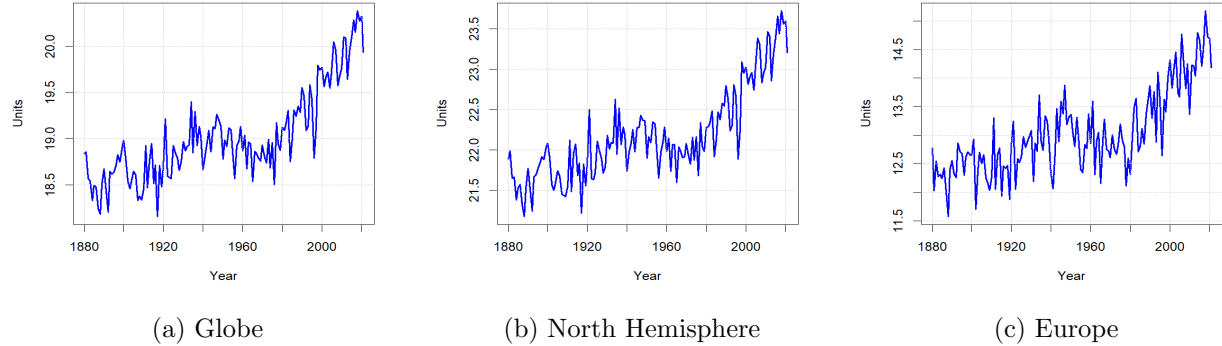


Figure 4: Common Trending Component

6.4.4 Long-term density forecasts

For forecasting purposes, the VAR form of the estimated VECM is conveniently used to generate h -step unconditional density forecasts at origin t with minimal MSE, see chapters 6 and 7 in [Lütkepohl \(2005\)](#). The forecast horizon extends up to 2100, a time-frame commonly used to assess and project climate change dynamics. Prediction graphs, alongside their respective 95% confidence bands, are presented in Figures 5, 6, and 7. The forecasted change in each distributional characteristic reported in Table 6 is computed by comparing the average of the series during the

Table 4: Adjustment coefficients of a vector error correction model of temperatures

Variables	Globe			
	$\Delta Q_t(0.05)$	$\Delta Q_t(0.50)$	$\Delta Q_t(0.95)$	$\Delta \bar{T}_t$
$e_{1,t-1}$	-0.8348*** (0.2034)	-0.0949 (0.0591)	-0.1337*** (0.0490)	-0.0904* (0.0528)
$e_{2,t-1}$	0.4690 (0.4554)	-1.1397*** (0.1251)	0.0512 (0.1449)	-0.0160 (0.1243)
$e_{3,t-1}$	0.8155** (0.3855)	0.3068** (0.1265)	-0.7226*** (0.1111)	0.3774*** (0.1060)
Variables	North Hemisphere			
	$\Delta Q_t(0.05)$	$\Delta Q_t(0.50)$	$\Delta Q_t(0.95)$	$\Delta \bar{T}_t$
$e_{1,t-1}$	-0.8254*** (0.2077)	-0.0681 (0.0620)	-0.1046** (0.0492)	-0.0673 (0.0571)
$e_{2,t-1}$	0.6816 (0.4889)	-1.0295*** (0.1380)	0.0946 (0.1556)	0.0872 (0.1458)
$e_{3,t-1}$	0.7972** (0.4043)	0.3499*** (0.1273)	-0.6856*** (0.1174)	0.4054*** (0.1115)
Variables	Europe			
	$\Delta Q_t(0.05)$	$\Delta Q_t(0.50)$	$\Delta Q_t(0.95)$	$\Delta \bar{T}_t$
$e_{1,t-1}$	-1.3480*** (0.2472)	-0.2173** (0.0907)	-0.0868 (0.1144)	-0.1643** (0.0728)
$e_{2,t-1}$	-1.0438** (0.4793)	-1.0881*** (0.1791)	0.1787 (0.2361)	-0.1139 (0.1607)
$e_{3,t-1}$	-0.4667 (0.3616)	0.1817 (0.1463)	-0.8352*** (0.1750)	0.0636 (0.1288)

Notes: Estimates obtained in a two-steps procedure. HAC Standard-errors in parenthesis. *, **, *** denote significance at the 10%, 5%, and 1% levels, respectively. $e_{1,t-1}$ denotes the lagged residuals of the co-trending equation between $Q_t(0.05)$ and \bar{T}_t . $e_{2,t-1}$ denotes the lagged residuals of the co-trending relation between $Q_t(0.50)$ and \bar{T}_t . $e_{3,t-1}$ denotes the lagged residuals of the co-trending relation between $Q_t(0.95)$ and \bar{T}_t . Short-run dynamics involving lags of ΔZ_t omitted.

Table 5: Linear combination coefficients for the common trending component

Variables	Globe	North Hemisphere	Europe
$Q_t(0.05)$	-0.1438	-0.1273	-0.1388
$Q_t(0.50)$	-0.0587	0.0295	0.0581
$Q_t(0.95)$	0.3037	0.4027	0.1644
\bar{T}_t	0.9400	0.9059	0.9748

Notes: Linear combination coefficients used to obtain the common trending component. Corresponds to the orthogonal complement of the matrix of adjustment coefficients in Table 4. Vectors normalized to have an Euclidean norm equal to 1.

periods 1880-1900 and 1961-1990 to the unconditional point forecast at year 2100 ($h = 79$). The analysis predicts that temperature will continue increasing during the next decades. The magnitude of the change is far from being homogeneous across the temperature distribution. For the Globe and North Hemisphere, $Q_t(0.05)$ is predicted to increase approximately 2.5°C (4.1°C) compared to the 1961-1990 (1880-1900) average, nearly twice the 1.4°C (2.1°C) predicted rise in $Q_t(0.50)$. In Europe, the forecasted change in $Q_t(0.05)$ is about 2.72°C (4.44°C), exceeding the predicted changes in $Q_t(0.50)$ and $Q_t(0.95)$.

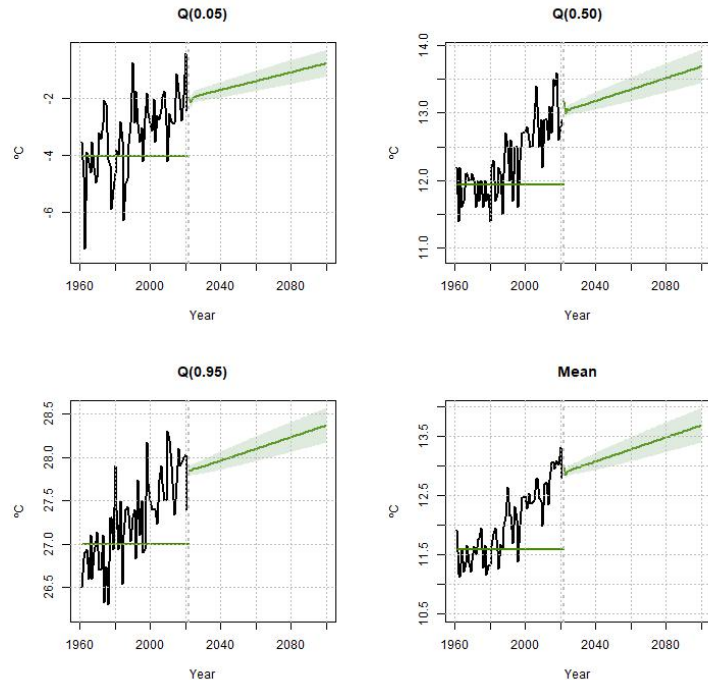


Figure 5: Forecasts (Globe)

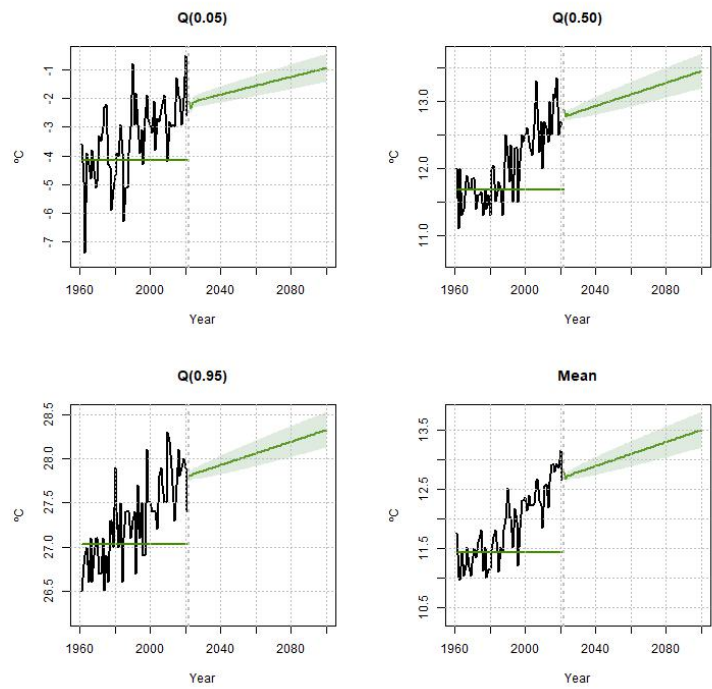


Figure 6: Forecasts (North Hemisphere)

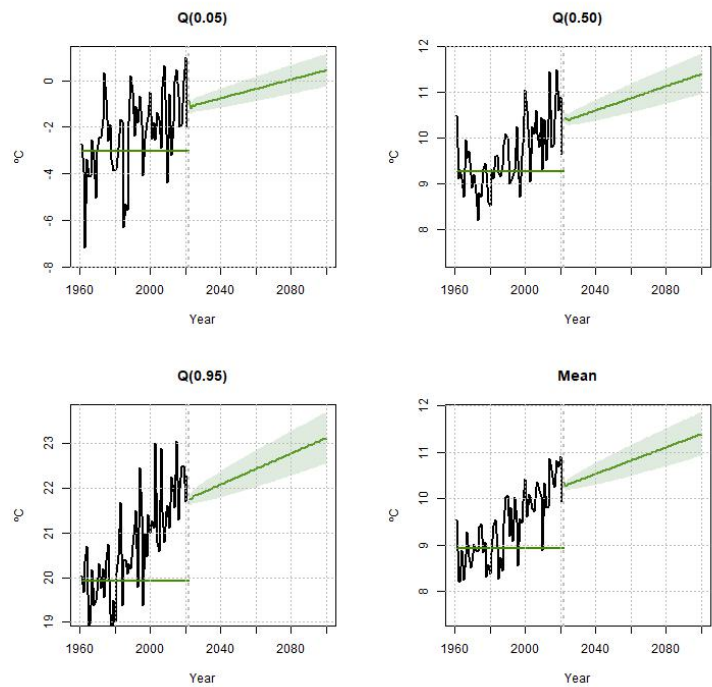


Figure 7: Forecasts (Europe)

Table 6: Changes in temperature characteristics predicted by a model including only temperatures

Characteristic	Globe		North Hemisphere		Europe	
	1961-1990	1880-1900	1961-1990	1880-1900	1961-1990	1880-1900
$\Delta Q_t(0.05)$	2.51	4.12	2.46	4.08	2.72	4.44
$\Delta Q_t(0.50)$	1.36	2.13	1.35	2.12	1.75	2.89
$\Delta Q_t(0.95)$	1.06	1.64	1.01	1.61	2.39	3.45
\bar{T}_t	1.63	2.57	1.60	2.54	1.94	3.04

Notes: Predicted change in the distributional characteristics of temperature obtained in a model including temperature distributional characteristics only. Changes computed as the difference between the observed mean in the periods 1880-1900 and 1961-1990 and the forecast at year 2100.

6.4.5 Identification of distributional structural shocks

To further characterize the interactions in the temperature distribution, this section explores the identification of structural shocks and conducts an impulse response analysis.

The reduced-form residuals are cross-correlated with the correlation matrix given in Table 7. Notice that for all geographical scales, the residuals from the equation for \bar{T}_t are strongly correlated with the residuals associated with $Q_t(0.05)$ and $Q_t(0.50)$, and much less correlated with the residuals from the $Q_t(0.95)$ equation. From climate science theory, there is no clear guidance on how to orthogonalize these residuals and identify meaningful structural shocks. Here, I propose a Cholesky rotation imposing the following ordering of the variables in the system: $[\bar{T}_t, Q_t(0.95), Q_t(0.50), Q_t(0.05)]'$. This ordering assumes that shocks to the quantiles are orthogonal with respect to shocks at the mean. Moreover, shocks occurring at hotter temperatures may generate non-zero impact responses at colder temperatures, while the responses of hotter temperatures to shocks at colder temperatures are zero on impact. The logic behind this ordering comes from the heat transportation pattern from the Equator to the poles as postulated by the theoretical 1D-EBMs. In principle, any other identification assumptions are valid, provided there is a meaningful interpretation of the identified shocks. Further research on this topic is worth doing.

Figures 8, 9, and 10 correspond to the impulse-response functions (IRFs) to the identified structural shocks (Cholesky-rotated residuals) for a horizon of 20 years. These IRFs are estimated using the Local Projections (LPs) approach of Jordà (2005), including one lag of the endogenous variables in the regression equations. Standard errors for inference are robust to auto-correlation. Confidence bands are at the 95% level. The decision to use LPs is based on the recent contribution by Montiel-Olea et al. (2024), who formally proved the claim made by Jordà (2005) regarding the robustness of LPs to misspecification. Specifically, Montiel-Olea et al. (2024) demonstrate that the conventional LP confidence interval has correct coverage even when the misspecification in the VAR model is large. This is a result of a "double robustness" property, which is analogous to the double

Table 7: Correlation between reduced-form residuals

Variables		Globe			
		\bar{T}_t	$Q_t(0.95)$	$Q_t(0.50)$	$Q_t(0.05)$
\bar{T}_t		1.0000			
$Q_t(0.95)$		0.2563	1.0000		
$Q_t(0.50)$		0.6345	0.1892	1.0000	
$Q_t(0.05)$		0.7300	0.0216	0.2040	1.0000
Variables		North Hemisphere			
		\bar{T}_t	$Q_t(0.95)$	$Q_t(0.50)$	$Q_t(0.05)$
\bar{T}_t		1.0000			
$Q_t(0.95)$		0.2512	1.0000		
$Q_t(0.50)$		0.6456	0.1668	1.0000	
$Q_t(0.05)$		0.7236	0.0206	0.2161	1.0000
Variables		Europe			
		\bar{T}_t	$Q_t(0.95)$	$Q_t(0.50)$	$Q_t(0.05)$
\bar{T}_t		1.0000			
$Q_t(0.95)$		0.4695	1.0000		
$Q_t(0.50)$		0.6867	0.1901	1.0000	
$Q_t(0.05)$		0.6964	0.0396	0.2788	1.0000

Notes: This Table contains the correlation coefficients between the reduced form residuals of the estimated unconditional quantile VECM discussed in this section. Sample period 1880-2021.

robustness of modern partially linear regression estimators in the literature on debiased machine learning.

Results for the Globe, the Northern Hemisphere, and Europe are share some similarities. Notice that in all cases, a one-standard-deviation shock to \bar{T}_t increases temperatures at all quantiles on impact; the strongest response is observed at $Q_t(0.05)$, a finding that can be interpreted as consequence of the distribution amplification patterns observed in the data. Regarding the shocks to the unconditional quantiles, their interpretation is quite difficult given the assumptions imposed on the impact responses. Remember that those shocks do not generate impact responses on the mean temperature. Therefore, to maintain the balance in the temperature distribution, an increase in a given quantile must be accompanied by an adjustment in the other quantiles so that the mean does not change. According to the estimated IRFs, this adjustment occurs at $Q_t(0.05)$, where a temperature reduction is observed after a shock in $Q_t(0.95)$ and $Q_t(0.50)$. Adjustments to shocks at $Q_t(0.05)$ must occur in the tails of the distribution at quantiles that are not included in the system.

The identified distributional structural shocks can be used to complement and extend the recent literature that quantifies the macroeconomic impact of climate change by exploiting time-series variability in global temperature (see [Neal \(2023\)](#) and [Bilal and Käenzig \(2024\)](#)). The unconditional-quantile VECM produces shocks based on the physical climate theory underlying the relationships among the variables. Furthermore, it leverages information from the entire temperature distribution, rather than just the average temperature, providing a wider amount of information. I develop this idea in more detail in subsection [6.5.7](#).

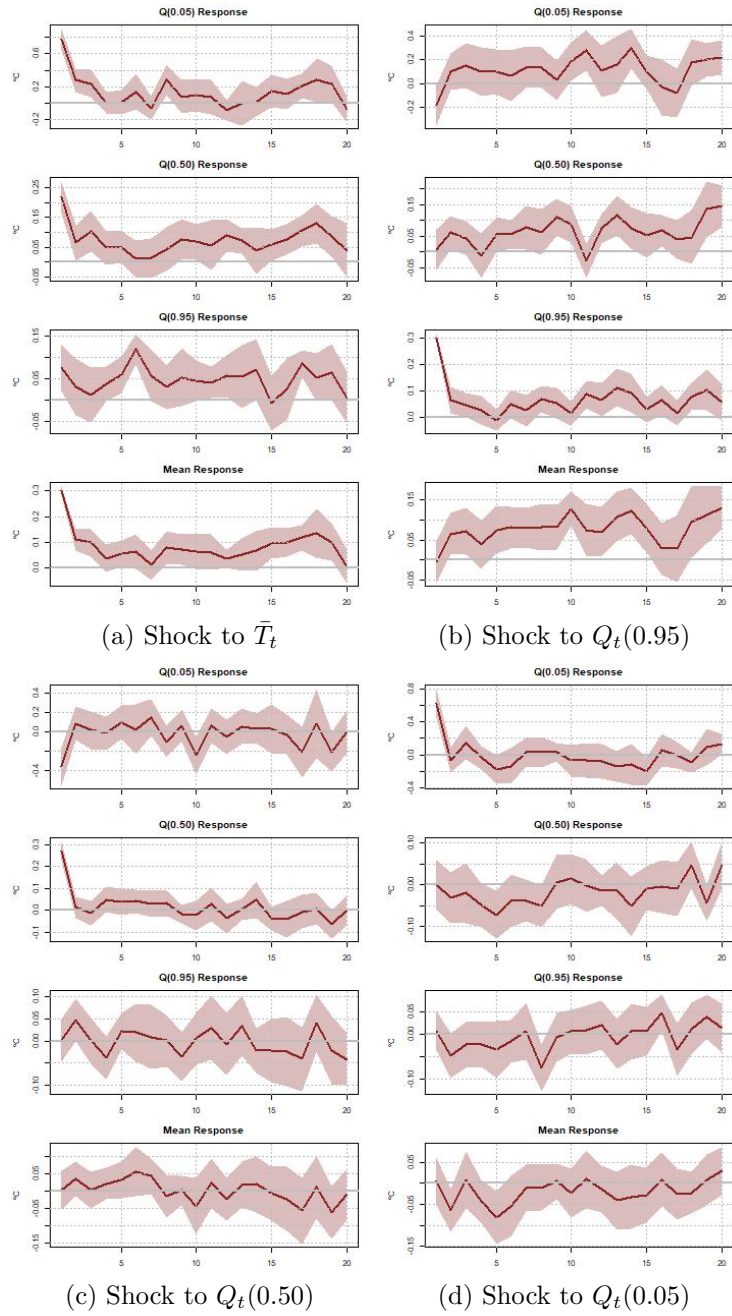


Figure 8: IRFs to identified structural shocks (Globe)

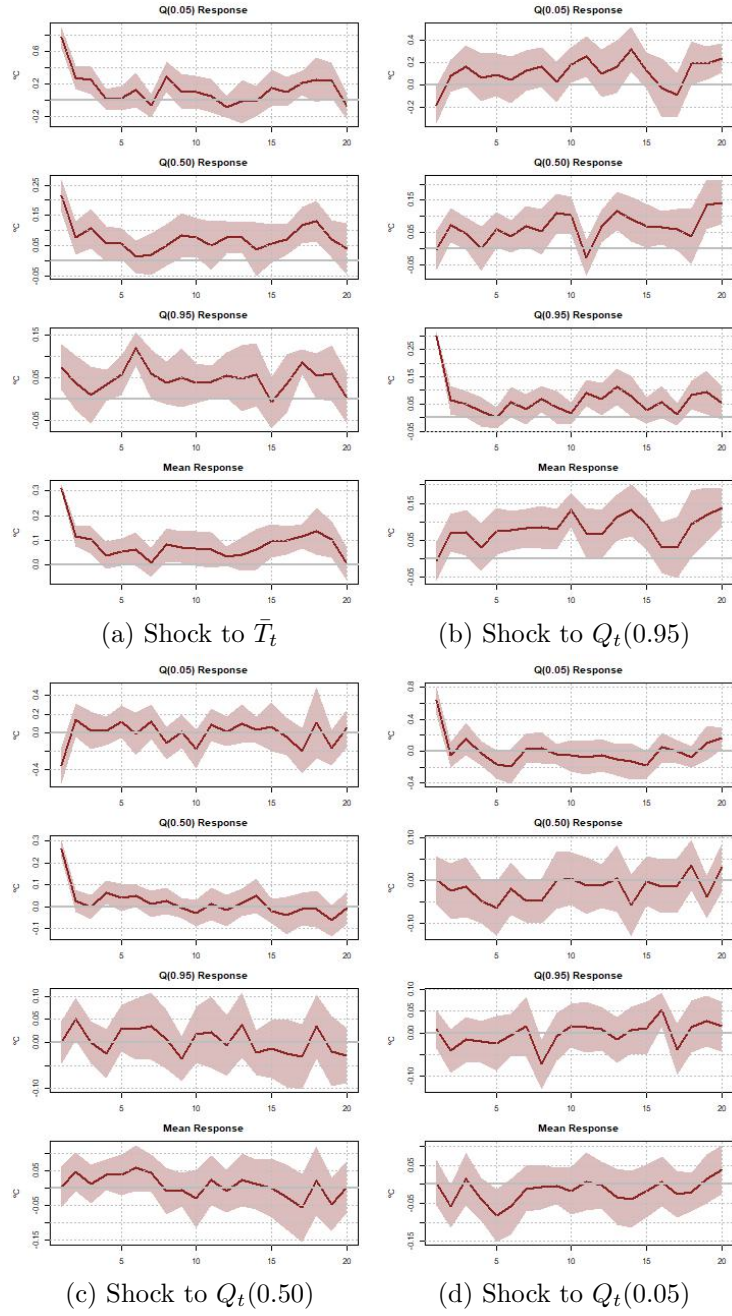


Figure 9: IRFs to identified structural shocks (North Hemisphere)

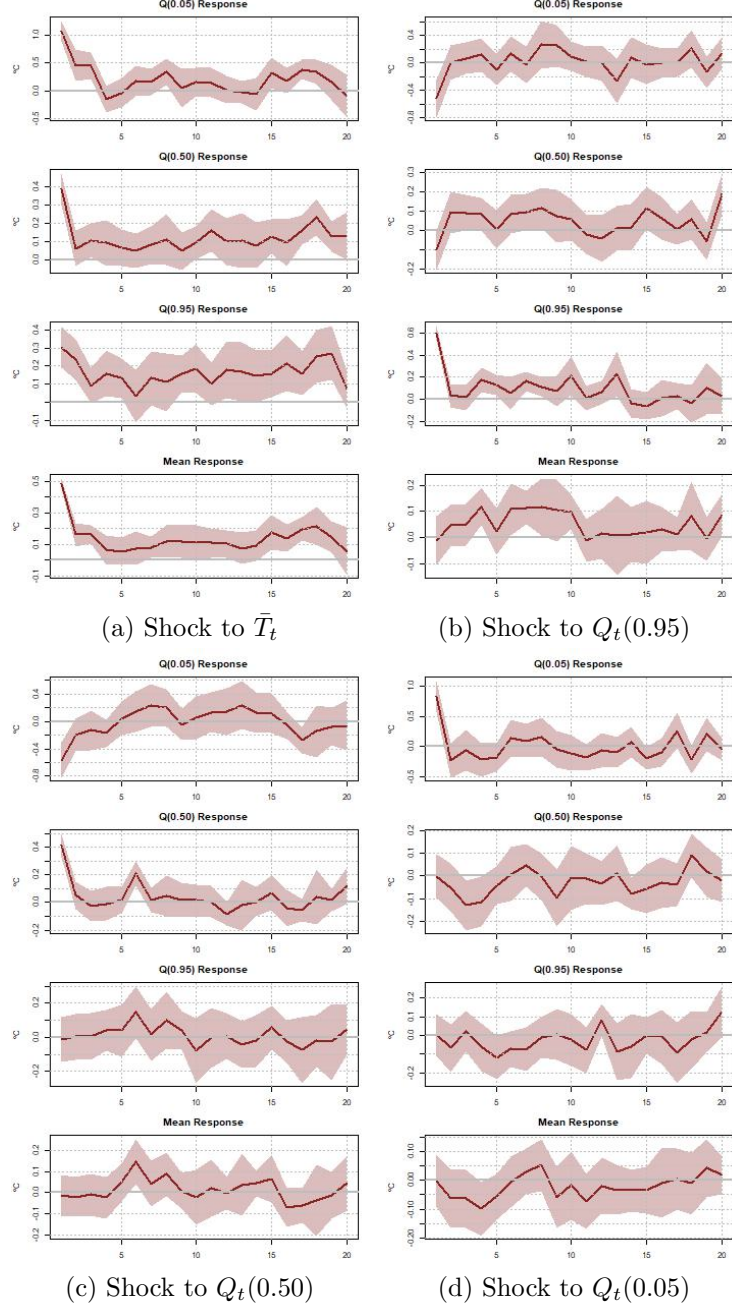


Figure 10: IRFs to identified structural shocks (Europe)

6.5 A Model for the Unconditional Distributional Characteristics of Temperature and Radiative Forcing

The initial vector of unconditional distributional characteristics of temperature is now augmented by the inclusion of the radiative forcing series, F_t . Let $Z_t = [Q_t(0.05), Q_t(0.50), Q_t(0.95), \bar{T}_t, F_t]'$. In the baseline analysis F_t is the total radiative forcing and includes both anthropogenic and natural

sources, see blue line in Figure 3. Appendix C reproduces the analysis considering two alternative versions of F_t that are commonly studied in the empirical literature: the radiative forcing from CO₂ ($F_t^{CO_2}$) and the anthropogenic forcing (F_t^{ant}). Results are qualitatively similar. This application is a generalization of the bi-variate VAR model for the average temperature and CO₂ in Goulet-Coulombe and Göbel (2021), to a expanded model including more unconditional distributional characteristics of temperature into the system.

6.5.1 Testing for the co-trending rank

The Guo and Shintani (2013) test is applied to establish the presence of deterministic co-trending among the variables in Z_t . For the Globe, the North-Hemisphere, and Europe, the procedure identifies a co-trending rank of 4, implying the existence of one common (possibly non-linear) deterministic trend. Compared to the model in Section 6.4, this result suggests an additional co-trending vector involving a relationship between one (or more) of the unconditional distributional characteristics of temperature and F_t . Estrada et al. (2021) obtain a similar result: applying the same test to a system including average regional temperature (latitude belts, continents, and countries), radiative forcing of GHGs, and total radiative forcing, the authors obtain a single common trend driven by the anthropogenic forcing. This information, together with the equations from the 1D-EBM, provides useful guidance for estimating the VECM in Equation (19).

6.5.2 Estimation of co-trending vectors

This section discusses the estimation of co-trending slopes in relationships between the unconditional distributional characteristics of temperature and F_t . Compared to Chen et al. (2022), who computed the co-trending vector for F_t and \bar{T}_t , $\bar{\lambda}$, this analysis is more general and extends to other characteristics of the temperature distribution. Table 8 reports the estimated coefficients and their corresponding standard-errors. Some noteworthy patterns emerge from the results. Firstly, across all geographical scales, the estimated coefficients are positive and statistically significant at the 1% level. Furthermore, the null hypothesis of a common trend cannot be rejected at a 5% significance level, indicating that each unconditional distributional characteristic share a common trend with F_t . Secondly, for the Globe and the North Hemisphere, the estimated slopes decrease with the quantile level. For example, at $\tau_i = 0.05$, the estimated slope for the North Hemisphere is 0.9887, while at $\tau_i = 0.95$, the slope decreases to 0.4186. In contrast, in Europe, the variability is less pronounced, with the extreme quantile levels yielding the higher estimates. These observed regularities have significant implications for climate sensitivity analysis, as discussed next.

Table 8: Co-trending slopes of relationships between the distributional characteristics of temperature and F_t

Slope	Globe		North Hemisphere		Europe	
	<i>Estimate</i>	<i>Cot-test</i>	<i>Estimate</i>	<i>Cot-test</i>	<i>Estimate</i>	<i>Cot-test</i>
$\lambda(0.05)$	0.9897*** (0.1167)	0.8649	0.9887*** (0.1160)	0.9148	1.0323*** (0.1725)	0.7042
$\lambda(0.50)$	0.5395*** (0.0504)	0.5753	0.5479*** (0.0494)	0.5145	0.6936*** (0.0699)	0.6303
$\lambda(0.95)$	0.4255*** (0.0374)	0.2643	0.4186*** (0.0327)	0.0559	0.8860*** (0.1043)	0.1150
$\bar{\lambda}$	0.6443*** (0.0428)	0.3721	0.6442*** (0.0431)	0.3964	0.7404*** (0.0507)	0.3380

Notes: Column *Estimate* correspond to the estimated co-trending slope—of the distributional characteristic with respect to the radiative forcing F_t —and its standard-error in parenthesis. *, **, *** denote significance at the 10%, 5%, and 1% levels, respectively. Column *Cot-test* reports the p-value of the test for common-trends.

6.5.3 Distributional climate sensitivities

Following [Pretis \(2020\)](#), [Chen et al. \(2022\)](#), [Bennedsen et al. \(2023\)](#), and [Brock and Miller \(2023\)](#), this section utilizes the co-trending slopes reported in Table 8 to derive the quantile-dependent climate sensitivities with respect to the total radiative forcing series. Concretely, at each τ_i , the climate sensitivity is obtained as $CS(\tau_i) = \lambda(\tau_i) \times 5.35 \times \ln(2)$, with standard errors derived via the delta method based on the standard errors of $\lambda(\tau_i)$. This approach explodes the fact that long-term relationships can be linearly and independently estimated across different regions or units ([Leduc et al., 2016](#); [Brock and Miller, 2023](#)).¹⁹

Focus first on the climate sensitivities for the Globe and the North Hemisphere, plotted in the left and central panels of Figure 11. The estimates indicate that the average temperature in the North Hemisphere would increase by approximately 2.39°C following doubling in total radiative forcing. This value is slightly below the 2.5°C to 3.5°C range estimated using instrumental records in the IPCC AR6 report ([AR6-IPCC, 2021](#)), and align with empirical estimates from related literature, such as [Bennedsen et al. \(2023\)](#) and [Anderson et al. \(2023\)](#). The analysis reveals substantial heterogeneity in the climate sensitivity across the temperature distribution. For $Q_t(0.05)$ (representing the coldest temperatures), the confidence interval for the climate sensitivity ranges from 2.82°C to 4.51°C, while for $Q_t(0.95)$ (representing the warmest temperatures) the range of variation is from 1.31°C to 1.79°C. The distinct, non-overlapping confidence intervals across quantile levels

¹⁹An alternative method involves adjusting the climate sensitivity for the average temperature based on $\bar{\lambda}$ by the co-trending slopes $\beta(\tau_i)$ of the unconditional quantiles relative to the mean. Even though both approaches lead to the same results, the direct use of $\lambda(\tau_i)$ is preferred for its simplicity, requiring the estimation of only a single equation.

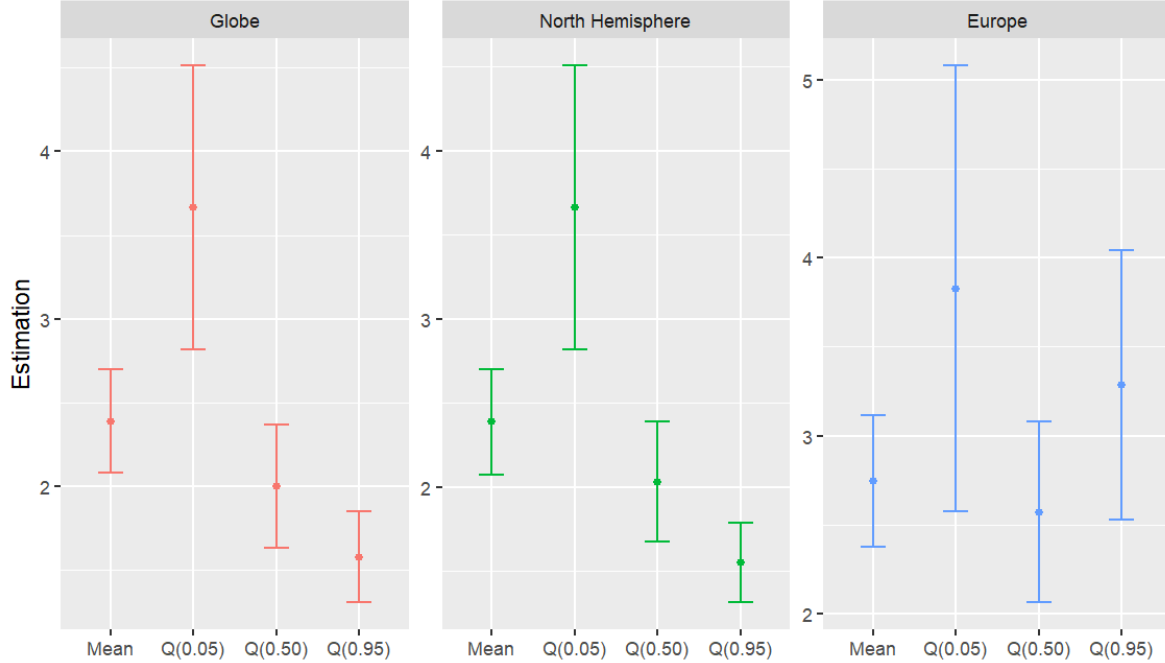


Figure 11: Climate sensitivities

suggest significant differences and provide evidence of AA. Even though a climate sensitivity of 4.5°C may seem high, similar estimates have been estimated for northern locations by [Anderson et al. \(2023\)](#) and [Brock and Miller \(2023\)](#). Regarding Europe, a distinct qualitative pattern of results emerges. The climate sensitivity for the average temperature is estimated at 2.74°C . Stronger climate sensitivities are obtained for extreme temperatures compared to the median, with the point estimates being higher at $Q_t(0.05)$. However, the overlap between the confidence intervals indicates a less marked heterogeneity.

In climate science, climate sensitivities are typically obtained using simulations from large-scale GCMs, for example, by simulating a known radiative forcing perturbation (such as a doubling of CO₂ concentrations) and computing the resultant temperature change with respect to an initial equilibrium ([Knutti et al., 2017](#); [Zhu et al., 2021](#)). However, GCMs are highly non-linear, require large amounts of input data, are computationally expensive to solve, and are heavily dependent on the system's initial conditions. As an alternative, the unconditional quantile VECM provides an estimation of the same physical quantity using a simpler, less time-consuming, reduced-form approach, leveraging the information contained in historical data. Moreover, while most climate models produce climate sensitivity estimates for the average temperature, the unconditional quantile VECM yields a set of quantile-dependent climate sensitivities, which exhibit strong patterns of heterogeneity. IAM practitioners can directly use the estimated climate sensitivities to guide

the calibration of the climate module and utilize the confidence bands, which reflect estimation uncertainty, to assess the effect of uncertainty on quantities of interest, such as optimal taxes or welfare (Hassler et al., 2018).

6.5.4 Estimation of the error correction model and Trend-Transitory decomposition

The VECM defined in Equation (19) is estimated using a two-step approach similar to the Engle and Granger (1987) method. The first differences of the elements in Z_t , ΔZ_t , are regressed against the lagged residuals of the corresponding co-trending equations. Remember that to maintain consistency with the co-trending rank determined in the Guo and Shintani (2013) test, the lagged residual series $F_{t-1} - \bar{\lambda}\bar{T}_{t-1}$ is included, while residuals of the form $F_{t-1} - \hat{\lambda}(\tau_i)Q_t(\tau_i)$ are omitted to avoid collinearity. The adjustment coefficients for the Globe, the North Hemisphere, and Europe are detailed in Table 9. Across all geographical scales, temperature unconditional quantiles adjust to their own past deviations from the co-trending relationship with the average temperature, as well as to past deviations from the equilibrium between the mean temperature and the radiative forcing. Interactions across quantiles is observed, specially for the case of Europe. Regarding the equation for ΔF_t , it adjusts only to its lagged long-run equilibrium deviations in relation to average temperature.

Residual diagnosis.— Figures 12, 13, and 14 display the residuals, auto-correlation functions (ACF), and partial auto-correlation functions (PACF) for each estimated model. The corresponding p-values for the individual Ljung and Box (1978) (LB) modified portmanteau tests and the Epps (1987) tests for normality are detailed in Table 10. These diagnostic tests reveal good properties in the residuals. The null hypothesis of no auto-correlation is not rejected in all cases according to the LB tests applied to each individual residual series. For the multivariate tests, the p-values are 0.5536, 0.5473, and 0.7329 for the Globe, the North Hemisphere, and Europe, respectively.²⁰ The assumption of normality in the residuals holds in all cases except for the forcing series. This particular deviation is consistent with findings in Bruns et al. (2020) and Pretis (2020), and can be explained by the presence of sudden volcanic forcings that likely introduces outliers and changes in the series dynamics.

²⁰Results from the Box and Pierce (1970) (BP) test are similar. Different values for the number of lags ranging from 1 to 15 lead to the same conclusion of no-auto-correlation.

Table 9: Adjustment coefficients of a vector error correction model of temperatures and total radiative forcing

Variables	Globe				
	$\Delta Q_t(0.05)$	$\Delta Q_t(0.50)$	$\Delta Q_t(0.95)$	$\Delta \bar{T}_t$	ΔF_t
$e_{1,t-1}$	-0.7729*** (0.2108)	-0.0559 (0.0646)	-0.1043** (0.0492)	-0.0510 (0.0567)	-0.1175 (0.0905)
$e_{2,t-1}$	0.4228 (0.4157)	-1.1234*** (0.1242)	0.0508 (0.1354)	-0.0189 (0.1168)	-0.1370 (0.1938)
$e_{3,t-1}$	0.5865 (0.4173)	0.1786 (0.1256)	-0.8241*** (0.1101)	0.2407** (0.1185)	0.0588 (0.1566)
$e_{4,t-1}$	-0.6043* (0.3182)	-0.3124*** (0.0854)	-0.2553* (0.1332)	-0.3455*** (0.0971)	0.5703*** (0.1585)
Variables	North Hemisphere				
	$\Delta Q_t(0.05)$	$\Delta Q_t(0.50)$	$\Delta Q_t(0.95)$	$\Delta \bar{T}_t$	ΔF_t
$e_{1,t-1}$	-0.7675*** (0.2123)	-0.0306 (0.0655)	-0.0766 (0.0480)	-0.02968 (0.0586)	-0.0845 (0.0844)
$e_{2,t-1}$	0.5742 (0.4415)	-1.0451*** (0.1300)	0.0691 (0.1494)	0.0510 (0.1309)	-0.0327 (0.2030)
$e_{3,t-1}$	0.5277 (0.4314)	0.1986 (0.1280)	-0.8050*** (0.1156)	0.2444 (0.1254)	0.1421 (0.1413)
$e_{4,t-1}$	-0.6350** (0.3181)	-0.3230*** (0.0909)	-0.2647** (0.1299)	-0.3583*** (0.1014)	0.5715*** (0.1584)
Variables	Europe				
	$\Delta Q_t(0.05)$	$\Delta Q_t(0.50)$	$\Delta Q_t(0.95)$	$\Delta \bar{T}_t$	ΔF_t
$e_{1,t-1}$	-1.2654*** (0.2568)	-0.1524* (0.0913)	-0.0301 (0.1115)	-0.0920 (0.0717)	-0.0539 (0.0429)
$e_{2,t-1}$	-1.0947*** (0.4675)	-1.1492*** (0.1636)	0.0994 (0.2355)	-0.1831 (0.1440)	-0.0522 (0.0936)
$e_{3,t-1}$	-0.5177 (0.3617)	0.1373 (0.1356)	-0.8793*** (0.1567)	0.0139 (0.1165)	0.0899 (0.0863)
$e_{4,t-1}$	-0.5356 (0.3316)	-0.4503*** (0.1472)	-0.4290** (0.1654)	-0.5032*** (0.1112)	0.3876*** (0.1130)

Notes: Estimates obtained in a two-steps procedure. HAC Standard-errors in parenthesis. * ** *** denote significance at the 10%, 5%, and 1% levels, respectively. $e_{1,t-1}$, $e_{2,t-1}$, and $e_{3,t-1}$ as before. $e_{4,t-1}$ denotes the lagged residuals of the co-trending relation between F_t and \bar{T}_t . Short-run dynamics involving ΔX_t omitted.

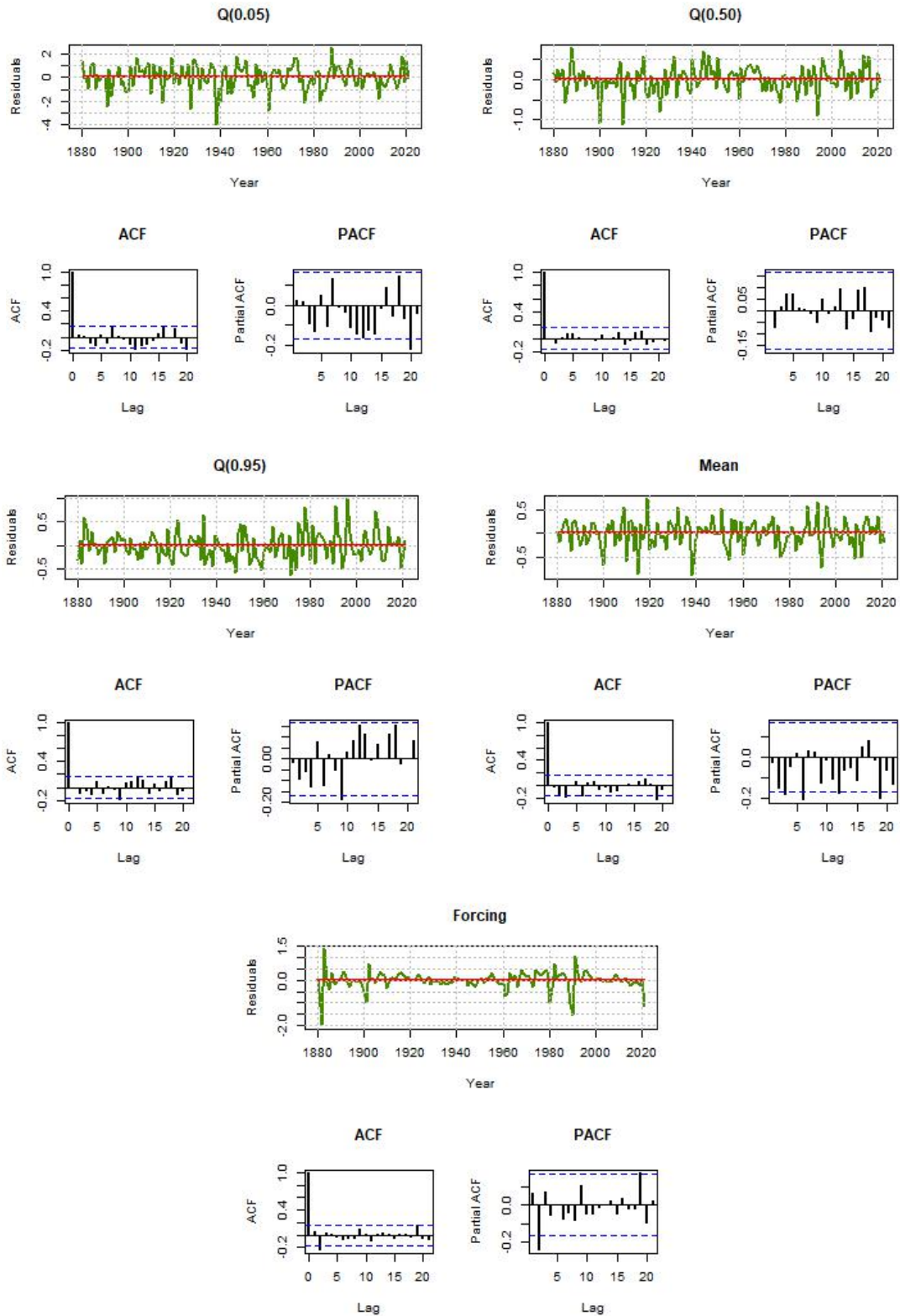


Figure 12: Residuals, ACF, and PACF (Globe)

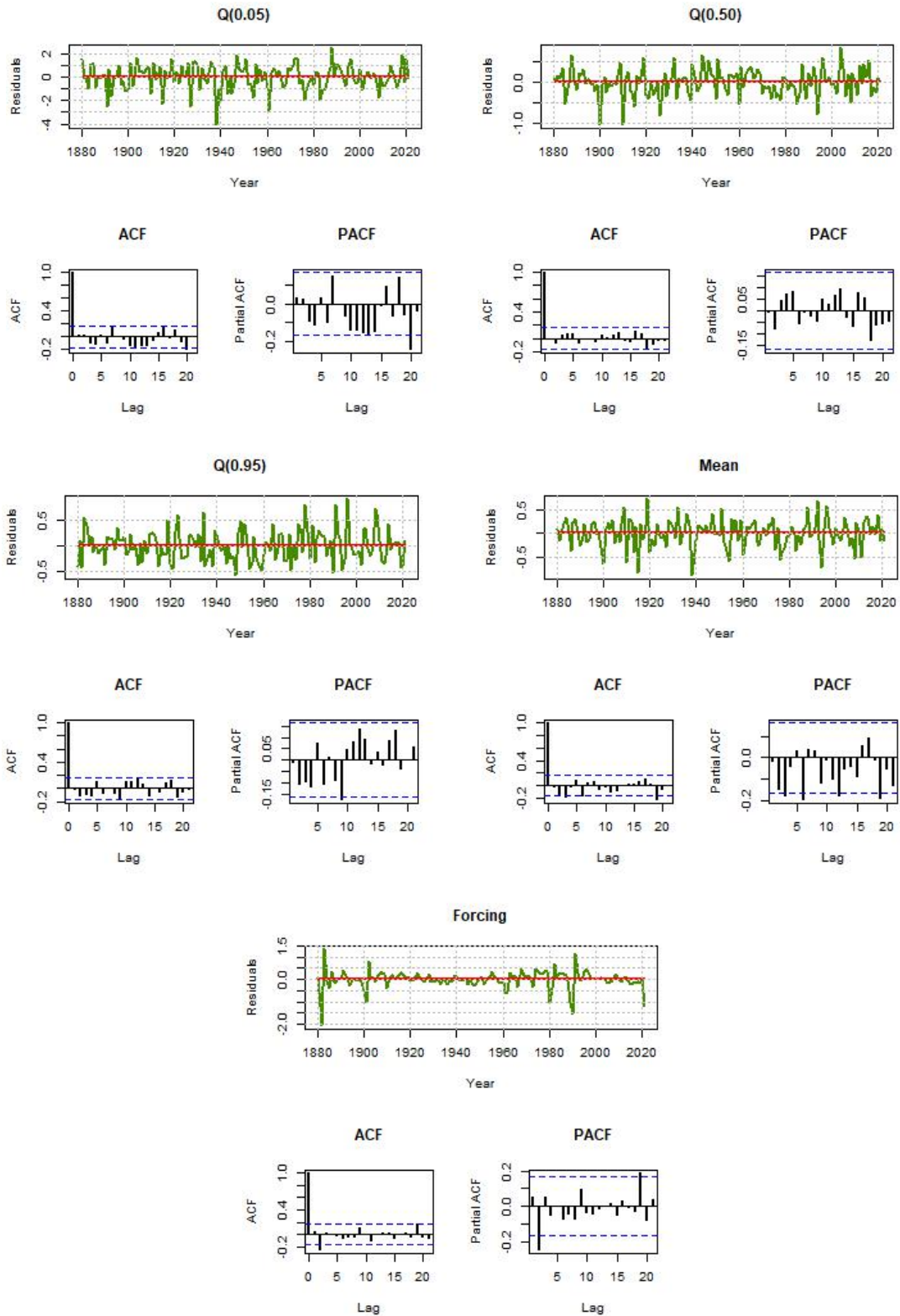


Figure 13: Residuals, ACF, and PACF (North Hemisphere)

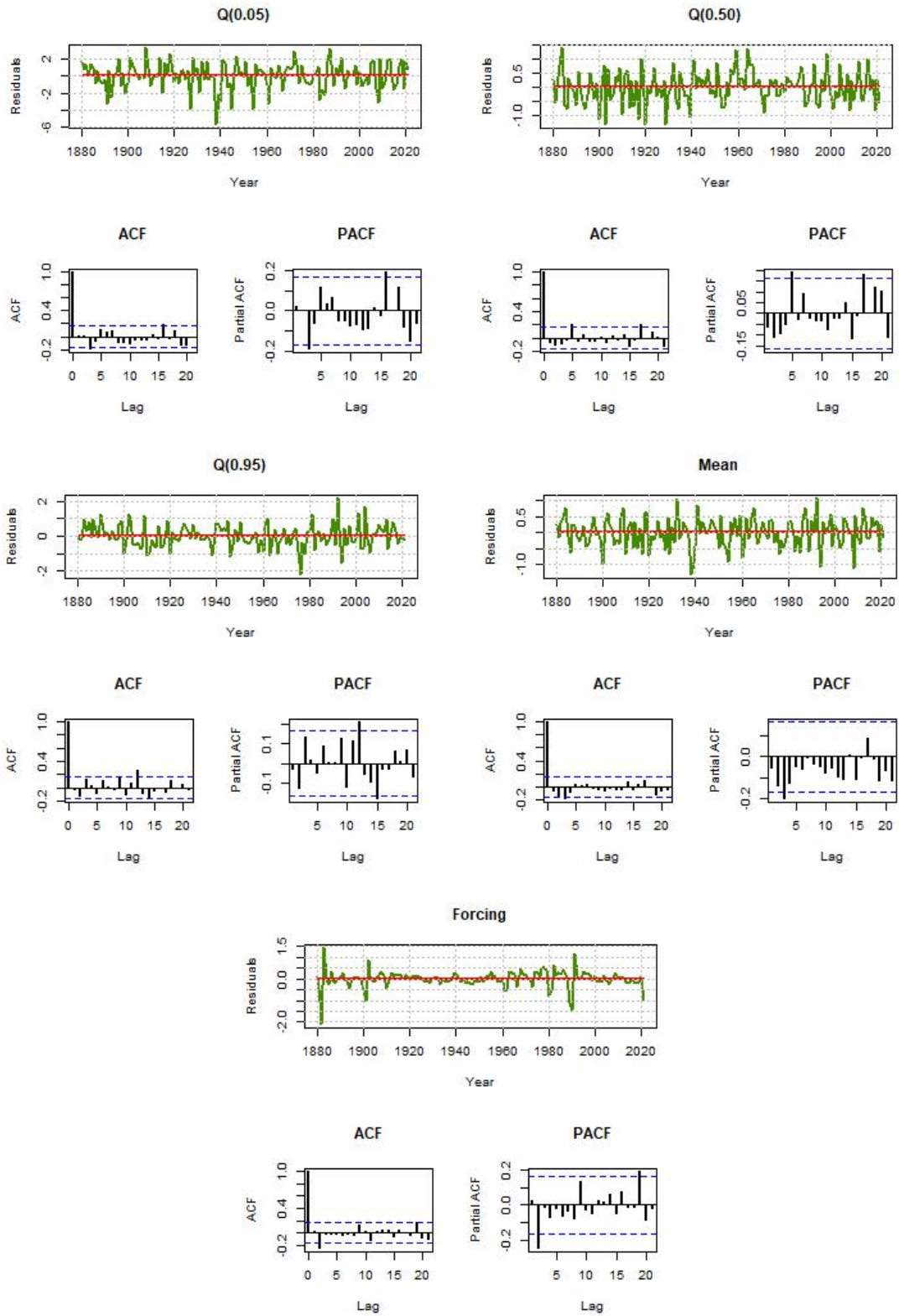


Figure 14: Residuals, ACF, and PACF (Europe)

Table 10: Autocorrelation and normality tests for residual diagnosis

Characteristic	Globe		North Hemisphere		Europe	
	Auto-correlation	Normality	Auto-correlation	Normality	Auto-correlation	Normality
$\Delta Q_t(0.05)$	0.3958	0.3018	0.3275	0.3778	0.2430	0.1887
$\Delta Q_t(0.50)$	0.9803	0.2462	0.9523	0.3914	0.3182	0.9680
$\Delta Q_t(0.95)$	0.2565	0.8850	0.2028	0.6836	0.2668	0.5340
\bar{T}_t	0.1889	0.0797	0.2155	0.0621	0.4584	0.4744
F_t	0.3128	0.0088	0.2970	0.0100	0.2628	0.0095

Notes: Auto-correlation column reports the p-values of the [Ljung and Box \(1978\)](#) modified portmanteau tests applied to each individual residual series. Lag set at 10. Normality column reports the p-values of the [Epps \(1987\)](#) test applied to each individual residual series.

Table 11: Linear combination coefficients for the common trending component

Variables	Globe	North Hemisphere	Europe
$Q_t(0.05)$	-0.1348	-0.1115	-0.0744
$Q_t(0.50)$	-0.1076	-0.0198	-0.0515
$Q_t(0.95)$	0.1672	0.2589	0.1246
\bar{T}_t	0.8812	0.8195	0.6149
F_t	0.4071	0.4986	0.7734

Notes: Linear combination coefficients used to obtain the common trending component. Corresponds to the orthogonal complement of the matrix of adjustment coefficients in Table 9. Vectors normalized to have an Euclidean norm equal to 1.

Trend-Transitory decomposition.— The orthogonal complements of the matrices of adjustment coefficients are detailed in Table 11. These vectors are informative about the linear combinations required to obtain the common trending component. In this model, the trend dynamics of the system are driven by the mean and the upper quantile of temperature, as well as by radiative forcing. In the case of Europe, the coefficient associated with radiative forcing is higher. Figure 15 plots the derived common trending components. That both temperatures and radiative forcing load positively on the common trend component suggests the presence of feedback mechanisms within the long-run equilibrium of the climate system. Further research is required to interpret these components and their influence on the dynamics of climate change. Moreover, understanding the properties of this common trend component and exploring its potential as a sufficient statistic for forecasting and projection is an interesting possibility that is part of the ongoing research.

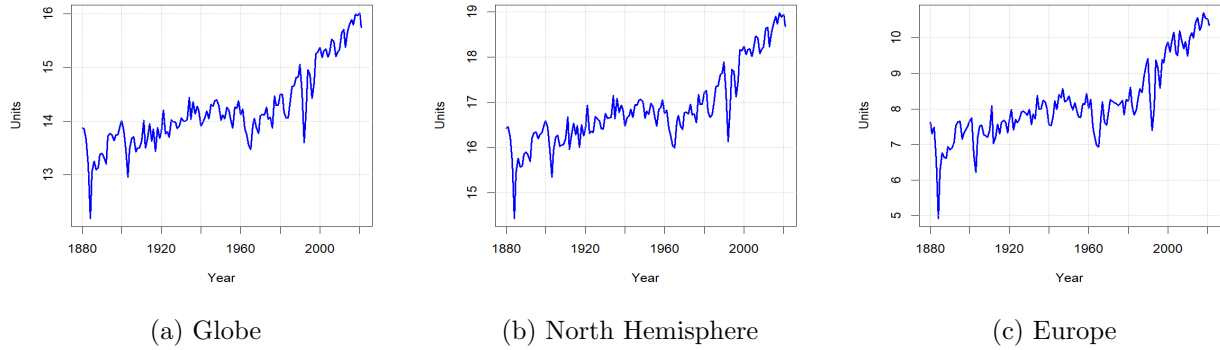


Figure 15: Common Trending Component

6.5.5 Long-term density forecasts

Similar to Section 6.4.4, the VAR form of the estimated VECM is employed to generate h -step unconditional density forecasts at origin t with minimal MSE, now incorporating the dynamics of the radiative forcing series into the system. Predicted trajectories of the temperature distribution for the Globe, North Hemisphere, and Europe, along with their respective 95% confidence bands, are presented in Figures 16, 17, and 18, for a forecasting horizon up to 2100. Complementary, Table 12 reports the forecasted change in each distributional characteristic computed as the difference between the observed mean of the series during the periods 1880-1900 or 1961-1990, and the point forecast at year 2100. Results are similar to those obtained in the model of the previous section. For both the Globe and North Hemisphere, the model predicts a substantial increase in $Q_t(0.05)$ of approximately 2.6°C (4.2°C) compared to the 1961-1990 (1880-1900) average, the strongest change compared to any other distributional characteristic. The magnitude of the temperature increases are slightly higher in this model including the total radiative forcing than in the model of the previous section. For Europe, the forecasted change in $Q_t(0.05)$ is around 2.67°C (4.38°C), higher than the predicted changes in $Q_t(0.50)$ and $Q_t(0.95)$. Compared to the scenario analysis conditional on the SSP trajectories discussed in the next subsection, the unconditional predictions of the model produce an intermediate outcome between the SSP 1-2.6 and the SSP 2-4.5. The current analysis can be interpreted as the long-term density forecasts in a “business-as-usual” scenario.

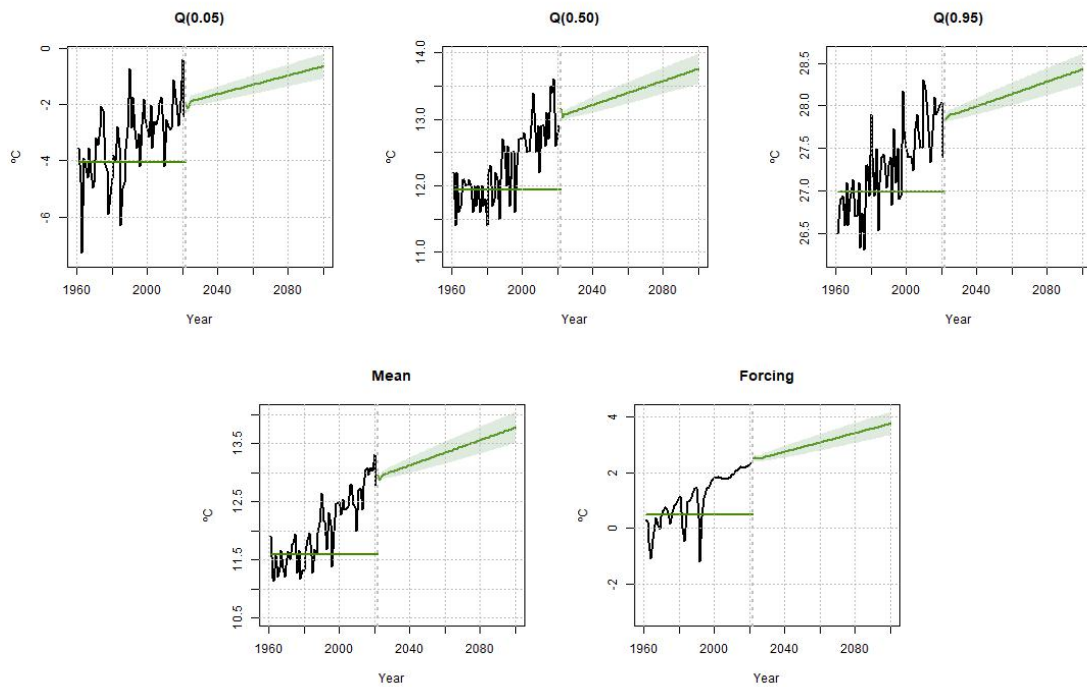


Figure 16: Long-term density forecasts including forcing dynamics (Globe)

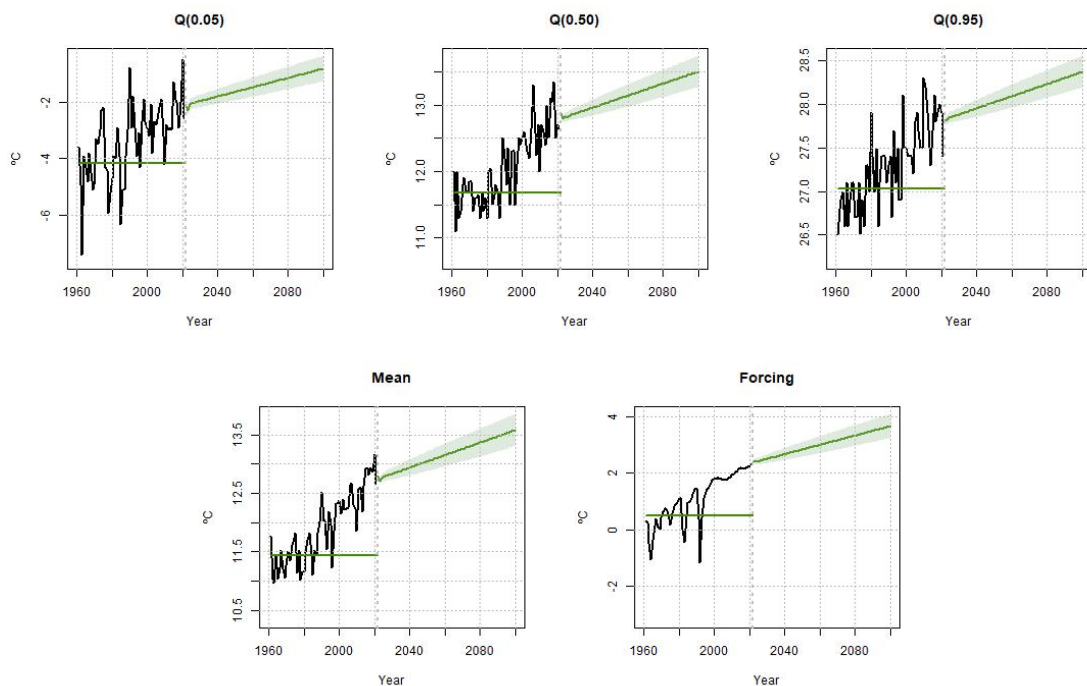


Figure 17: Long-term density forecasts including forcing dynamics (North Hemisphere)

Table 12: Changes in temperature characteristics predicted by a model including temperatures and radiative forcing

Characteristic	Globe		North Hemisphere		Europe	
	1961-1990	1880-1900	1961-1990	1880-1900	1961-1990	1880-1900
$\Delta Q_t(0.05)$	2.64	4.25	2.56	4.18	2.67	4.38
$\Delta Q_t(0.50)$	1.43	2.20	1.41	2.18	1.72	2.85
$\Delta Q_t(0.95)$	1.12	1.69	1.06	1.65	2.34	3.40
\bar{T}_t	1.72	2.65	1.67	2.61	1.90	3.00

Notes: Predicted change in the distributional characteristics of temperature obtained in a model including temperature distributional characteristics and radiative forcing. Changes computed as the difference between the observed mean in the periods 1880-1900 and 1961-1990 and the forecast at year 2100.

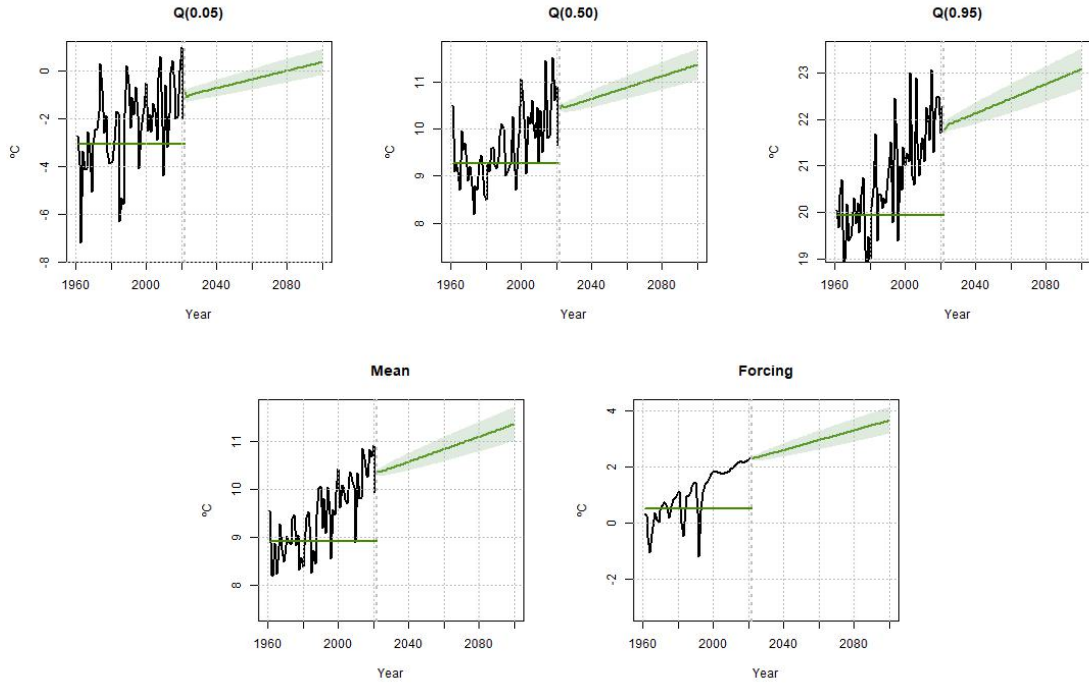


Figure 18: Long-term density forecasts including forcing dynamics (Europe)

6.5.6 Scenario analysis

In this section, the estimated model is used to generate conditional point forecasts for the distributional characteristics of temperature, conditional on a range of Shared Socioeconomic Pathways (SSP) scenarios.²¹ A SSP scenario describes a potential future development path, grounded on a coherent and internally consistent set of assumptions regarding driving forces like demography, eco-

²¹In macroeconomics, a similar conditional forecasting exercise might involve projecting variables such as GDP growth or inflation based on assumed trajectories of monetary or fiscal policy variables. Relevant examples of this practice include [Baumeister and Kilian \(2014\)](#) and [Giannone et al. \(2014\)](#).

nomic processes, technological innovation, and their wide-ranging implications for energy use, land utilization, and emissions (Riahi et al., 2017; AR6-IPCC, 2021).²² Originally, the SSP framework outlined five broad narratives for future socioeconomic development (O'Neill et al., 2014): Sustainability (SSP1), Middle of the Road (SSP2), Regional Rivalry (SSP3), Inequality (SSP4), and Fossil-fueled Development (SSP5). The AR6 report by the IPCC (AR6-IPCC, 2021) utilized the SSP framework to construct a suite of future scenarios implying different trajectories of emissions and warming. A single SSP “family” might encompass several emissions trajectories, leading to varied levels of radiative forcing. This variation originates from different mitigation ambition levels, which can cause divergent emissions outcomes even within the same socioeconomic narrative. For instance, SSP1-1.9 and SSP1-2.6 both originate from the Sustainability narrative, yet they project different emissions and radiative forcing levels targets in 2100 (1.9 W/m^2 vs 2.6 W/m^2) attributable to distinct mitigation efforts implemented in each scenario. For further details on how SSP scenarios are developed and used by the scientific community, refer to Chapters 1, 3, and 4 of the AR6 report (AR6-IPCC, 2021) and the references cited therein.

The conditional projection exercise considers five illustrative SSP scenarios, which are also considered in the AR6-IPCC (2021) report: SSP1-1.9, SSP1-2.6, SSP2-4.5, SSP3-7.0, and SSP5-8.5. These scenarios cover a broad spectrum of plausible societal and climatic futures for the upcoming decades. Figure 19 shows the SSP radiative forcing projections for the period 2022-2100. Conditional long-term projections for the three geographical scales of analysis (Globe, North Hemisphere, and Europe) are plotted in Figures 20, 21, and 22, respectively. These projections are obtained by evaluating the estimated model, in its VAR form, on the external SSP data. For each SSP scenario and each distributional characteristic, the projected change, reported in Table 13, is calculated as the difference between the observed mean in the periods 1880-1900 or 1961-1990 with respect to the the conditional prediction at year 2100. The projected change is informative about the expected impact of each SSP trajectory on the temperature distribution.

Observe that under all SSP scenarios, the distributional characteristics of temperature are projected to increase, with the magnitude of the change depending on the level of radiative forcing targeted at each scenario. When focusing on a specific scenario, the projected increase in temperature is not uniform across the temperature distribution. Specifically, for the Globe and the North Hemisphere, across all scenarios, the change in $Q_t(0.05)$ is approximately twice the change in $Q_t(0.50)$, and this proportion is even more pronounced when comparisons are made with respect to $Q_t(0.95)$. In the extreme scenario of SSP5-8.5, the average temperature is projected to be about

²²SSP scenarios refine the previously used Representative Concentration Pathways (RCPs) scenarios and allow for a standardized comparison of society’s choices and their resulting levels of climate change.

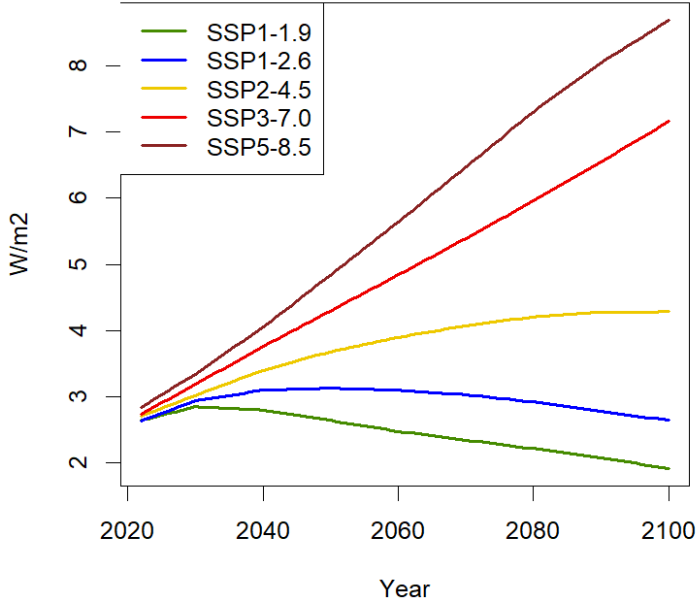


Figure 19: Annual radiative forcing under five different SSP-based scenarios

4.79°C above the observed average in the period 1961-1990, while that increase in $Q_t(0.05)$ is expected to exceed 7.3°C. For Europe, the variability in temperature changes across the distribution is less heterogeneous, yet the most significant changes are still projected for $Q_t(0.05)$. Compared to the Globe or the North Hemisphere, the projected changes for Europe are uniformly stronger.

Bennedsen et al. (2023) and Chen et al. (2022) conduct a similar analysis but using the previous RCP scenarios to produce conditional projections of global average temperature. This analysis extends and complements the above mentioned references by considering a more actual version of the scenarios and projecting not only the mean but also other distributional characteristics of temperature. The projected heterogeneous trajectories of the temperature distribution can have significant environmental and societal implications. Further research in this direction within the domains of climate modeling and climate economics is required for a better understanding of this phenomenon and its implications. It is important to note that the projections are conditional on SSPs scenarios and also conditional on all else remaining constant (i.e. remaining as they were during the estimation sample). This means that they are conditional on the feedback from temperature to GHGs concentrations remaining insignificant and assuming no additional mechanisms starting to operate as temperatures rise. This ceteris paribus assumption may not be a good approximation if there are climate tipping points or new mechanisms that amplify the temperature appear.

Projection outcomes are alternatively produced in climate science using simulations from large-scale GCMs. In this case, temperature paths are obtained by simulating the whole climate system, conditional on the specific emissions or concentration scenarios. Uncertainty measures are obtained by running the model multiple times from slightly different initial conditions ([Lupo et al., 2013](#)). As mentioned several times in this paper, GCMs are highly complex and computationally expensive to solve. The unconditional-quantile VECM offers a simpler, reduced-form alternative to obtain comparable outcomes, not only for the average, as is often the case in GCMs, but also for other characteristics of the temperature distribution. It also provides a different measure of uncertainty through forecast confidence bands.

These outcomes serve as useful inputs for analyzing the economic damages of climate change. Typically, researchers rely on long-term average temperature projections to quantify the expected local or global impacts of climate change on economic variables such as GDP growth, agricultural and labor productivity, mortality, and more. Instead of using projections from climate models, researchers can rely on projections from the unconditional-quantile VECM to provide a more comprehensive characterization of the consequences of climate change, accounting for heterogeneity in temperature dynamics. This type of analysis opens the door to a new class of research that explicitly incorporates heterogeneity into economic studies. Such analyses can be applied at any geographical scale and offer valuable insights to better inform both local and global adaptation and mitigation policies. A similar argument is valid for the long-term density forecasts of the previous section, but in that case the future implies a “business-as-usual” scenario.

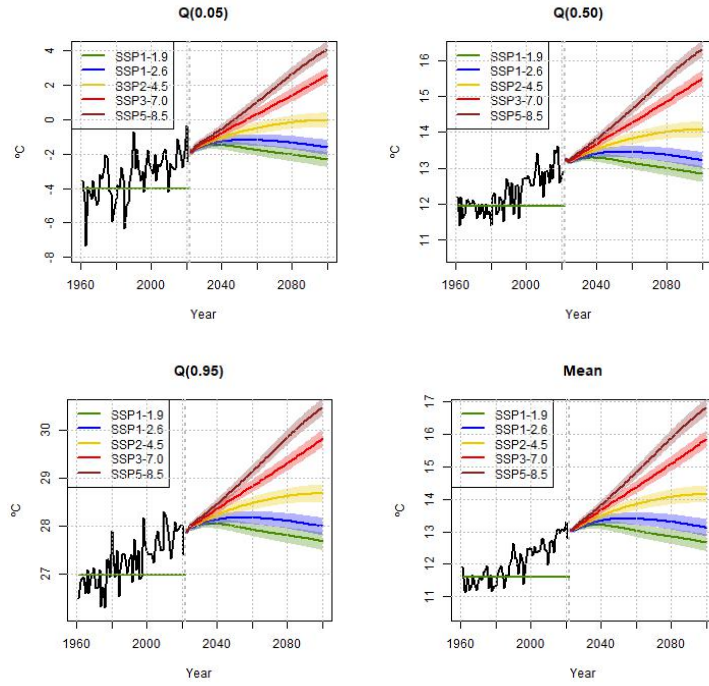


Figure 20: Long-term projections under RCP scenarios (Globe)

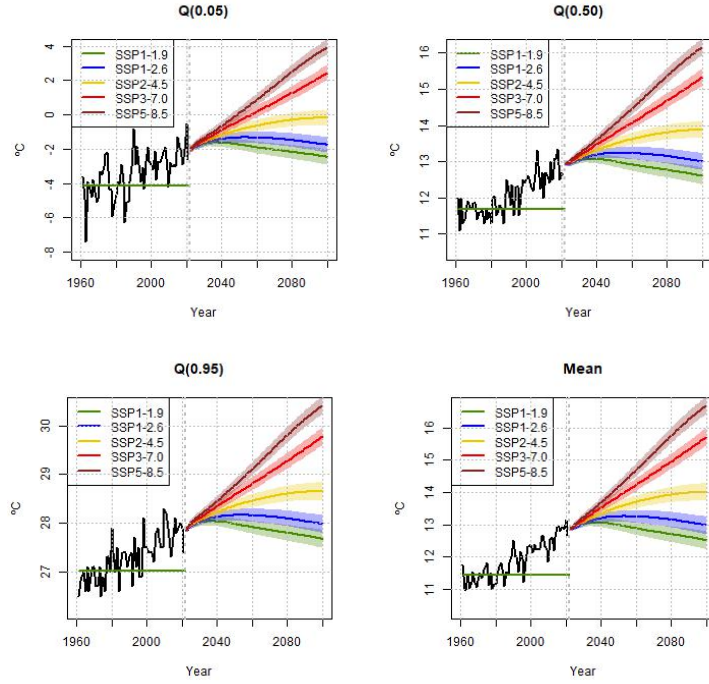


Figure 21: Long-term projections under RCP scenarios (North Hemisphere)

Table 13: Changes in temperature characteristics predicted conditional on RCP scenarios

Characteristic	Globe									
	SSP1-1.9		SSP1-2.6		SSP2-4.5		SSP3-7.0		SSP5-8.5	
	1961-1990	1880-1900	1961-1990	1880-1900	1961-1990	1880-1900	1961-1990	1880-1900	1961-1990	1880-1900
$\Delta Q_t(0.05)$	1.78	3.40	2.08	3.70	3.22	4.84	5.85	7.45	7.35	8.97
$\Delta Q_t(0.50)$	0.96	1.73	1.12	1.90	1.75	2.52	3.18	3.95	3.99	4.77
$\Delta Q_t(0.95)$	0.74	1.31	0.87	1.45	1.37	1.94	2.52	3.09	3.17	3.74
\bar{T}_t	1.16	2.09	1.35	2.29	2.10	3.04	3.81	4.75	4.79	5.72

Characteristic	North Hemisphere									
	SSP1-1.9		SSP1-2.6		SSP2-4.5		SSP3-7.0		SSP5-8.5	
	1961-1990	1880-1900	1961-1990	1880-1900	1961-1990	1880-1900	1961-1990	1880-1900	1961-1990	1880-1900
$\Delta Q_t(0.05)$	1.78	3.41	2.08	3.70	3.22	4.84	5.85	7.45	7.35	8.97
$\Delta Q_t(0.50)$	0.98	1.75	1.14	1.91	1.78	2.55	3.24	4.01	4.07	4.84
$\Delta Q_t(0.95)$	0.72	1.32	0.58	1.45	1.34	1.94	2.47	3.06	3.11	3.70
\bar{T}_t	1.16	2.10	1.35	2.29	2.10	3.04	3.82	4.76	4.80	5.73

Characteristic	Europe									
	SSP1-1.9		SSP1-2.6		SSP2-4.5		SSP3-7.0		SSP5-8.5	
	1961-1990	1880-1900	1961-1990	1880-1900	1961-1990	1880-1900	1961-1990	1880-1900	1961-1990	1880-1900
$\Delta Q_t(0.05)$	1.87	3.59	2.17	3.89	3.37	5.09	6.16	7.88	7.73	9.45
$\Delta Q_t(0.50)$	1.18	2.32	1.39	2.52	2.18	3.31	4.04	5.17	5.08	6.22
$\Delta Q_t(0.95)$	1.64	2.70	1.91	2.96	2.95	4.01	5.38	6.44	6.75	7.80
\bar{T}_t	1.32	2.42	1.54	2.64	2.40	3.50	4.41	5.51	5.54	6.64

Notes: Projected change in the distributional characteristics of temperature under different SSPs scenarios. Changes computed as the difference between the observed mean in the periods 1880-1900 and 1961-1990 and the forecast at year 2100.

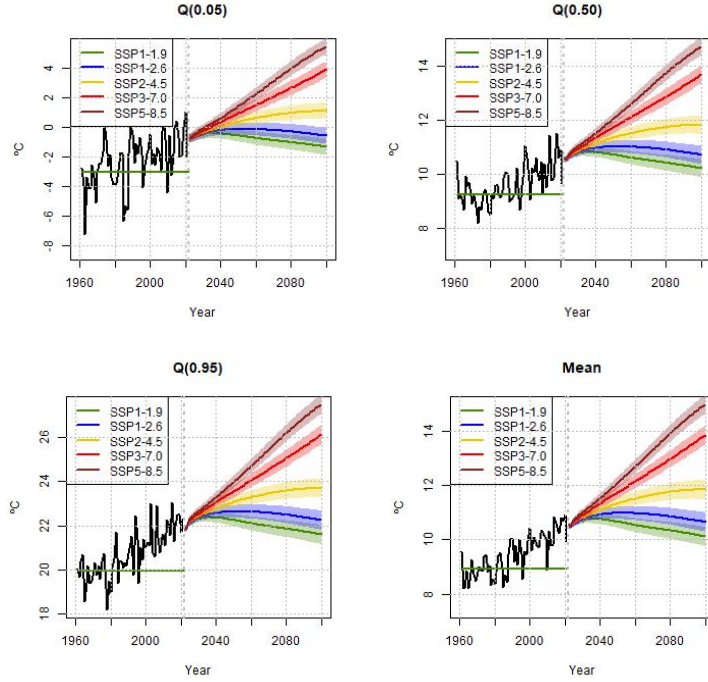


Figure 22: Long-term projections under RCP scenarios (Europe)

6.5.7 Identification of distributional structural shocks

Similar to Section 6.4.5, this section explores the identification of distributional structural shocks and conducts an impulse-response analysis within a system of variables that now includes the total

radiative forcing, F_t . For the Globe and the Northern Hemisphere, the correlation patterns in the reduced-form residuals of the temperature equations are similar to those described in Section 6.4.5. Concerning F_t , the strongest correlation is observed with the $Q_t(0.95)$ residuals. It is important to note that the inclusion of the forcing variable significantly modifies the correlation structure within the model for Europe.

The reduced-form residuals are rotated using a Cholesky decomposition with the following ordering: $[F_t, \bar{T}_t, Q_t(0.95), Q_t(0.50), Q_t(0.05)]'$. This specific ordering, with F_t as the first variable and \bar{T}_t as the second, is also supported by Bruns et al. (2020), and implies that the reduced-form residuals of \bar{T}_t are decomposed into a component associated with shocks to F_t and an orthogonal component that does not instantaneously affect F_t . The latter component is what I interpret as the structural shock at the mean. The ordering of the distributional characteristics of temperature remains the same as before. This analysis extends the framework presented in Goulet-Coulombe and Göbel (2021) by incorporating the entire distribution of temperature into the vector of variables, rather than focusing solely on the average, thereby providing a richer set of information.

The impulse-response functions to the identified shocks, computed using LPs (Jordà, 2005), and their respective 95% confidence bands, are presented in Figures 23, 24, and 25, for the Globe, the Northern Hemisphere, and Europe, respectively. For the Globe and the Northern Hemisphere, an increase in radiative forcing of around 0.4 W/m^2 induces a rise in all distributional characteristics in the medium run. The peak response for the average temperature is about 0.1°C and occurs between five to six years after the shock. As expected, the strongest peak response is observed for the lower quantile $Q_t(0.05)$, with a magnitude of about 0.2°C . Even 20 years after the shock, some responses remain significant, suggesting long-lasting effects of a forcing shock. The responses to the shocks for each distributional characteristic are similar to those described in Section 6.4.5. For Europe, the temperature distribution responds in a similar manner; however, the figures corresponding to the responses to other shocks are completely different compared to those obtained in a model without radiative forcing.

The identification of structural shocks to the temperature distribution complements the most recent literature on the macroeconomic impacts of climate change, which exploits variations in global rather than local temperatures to estimate economic damages. In a panel data context, Neal (2023) extends the standard linear and non-linear regression models of economic growth on local weather conditions considered in Dell et al. (2012) and Burke et al. (2015) to incorporate external weather effects through a cross-sectional weighted average of global temperature (and rainfall). The main identifying assumption is the conditional exogeneity of local and global temperatures with

respect to economic variables. [Bilal and Käenzig \(2024\)](#) propose a similar idea within a time series framework. Global “temperature shocks” are identified as potentially persistent deviations from the long-run trend in global mean temperature, following the method proposed by [Hamilton \(2018\)](#). In both cases, the estimated impacts of climate change on economic activity are significantly stronger than those from previous literature using only local weather/climate variation.

My contribution to this framework is to propose an alternative identification strategy that *i*) integrates elements from climate theory within a multivariate statistical model and identifies shocks based on the unexplained variability in the dynamic system, and *ii*) produces information for the entire temperature distribution, rather than just for the average, thus offering a wider amount of data for damage and subsequent policy analysis. Appendix F presents an analysis of this nature and estimates the World GDP per-capita responses when the identified shocks are used in a time-series framework similar to [Bilal and Käenzig \(2024\)](#). The results for the period 1960-2022 suggest that the main negative GDP effects are produced by shocks at the mean and $Q_t(0.95)$, while shocks at $Q_t(0.50)$ and, to some extent, $Q_t(0.05)$, generate positive responses. This finding aligns well with the literature on the geographical and seasonal heterogeneity in the impacts of climate change.

Table 14: Correlation between reduced-form residuals

Variables	Globe				
	F_t	\bar{T}_t	$Q_t(0.95)$	$Q_t(0.50)$	$Q_t(0.05)$
\bar{F}_t	1.0000				
\bar{T}_t	0.1203	1.0000			
$Q_t(0.95)$	0.2746	0.1920	1.0000		
$Q_t(0.50)$	0.0225	0.6000	0.1275	1.0000	
$Q_t(0.05)$	-0.0098	0.7326	-0.0136	0.1812	1.0000
Variables	North Hemisphere				
	F_t	\bar{T}_t	$Q_t(0.95)$	$Q_t(0.50)$	$Q_t(0.05)$
\bar{F}_t	1.0000				
\bar{T}_t	0.1168	1.0000			
$Q_t(0.95)$	0.2936	0.1846	1.0000		
$Q_t(0.50)$	0.0515	0.6109	0.1000	1.0000	
$Q_t(0.05)$	-0.0329	0.7246	-0.0173	0.1927	1.0000
Variables	Europe				
	F_t	\bar{T}_t	$Q_t(0.95)$	$Q_t(0.50)$	$Q_t(0.05)$
\bar{F}_t	1.0000				
\bar{T}_t	0.3516	1.0000			
$Q_t(0.95)$	0.1640	0.4343	1.0000		
$Q_t(0.50)$	-0.0340	0.1992	0.6878	1.0000	
$Q_t(0.05)$	0.0106	0.2128	0.6312	0.8935	1.0000

Notes: This Table contains the correlation coefficients between the reduced form residuals of the estimated unconditional quantile VECM discussed in this section. Sample period 1880-2021.

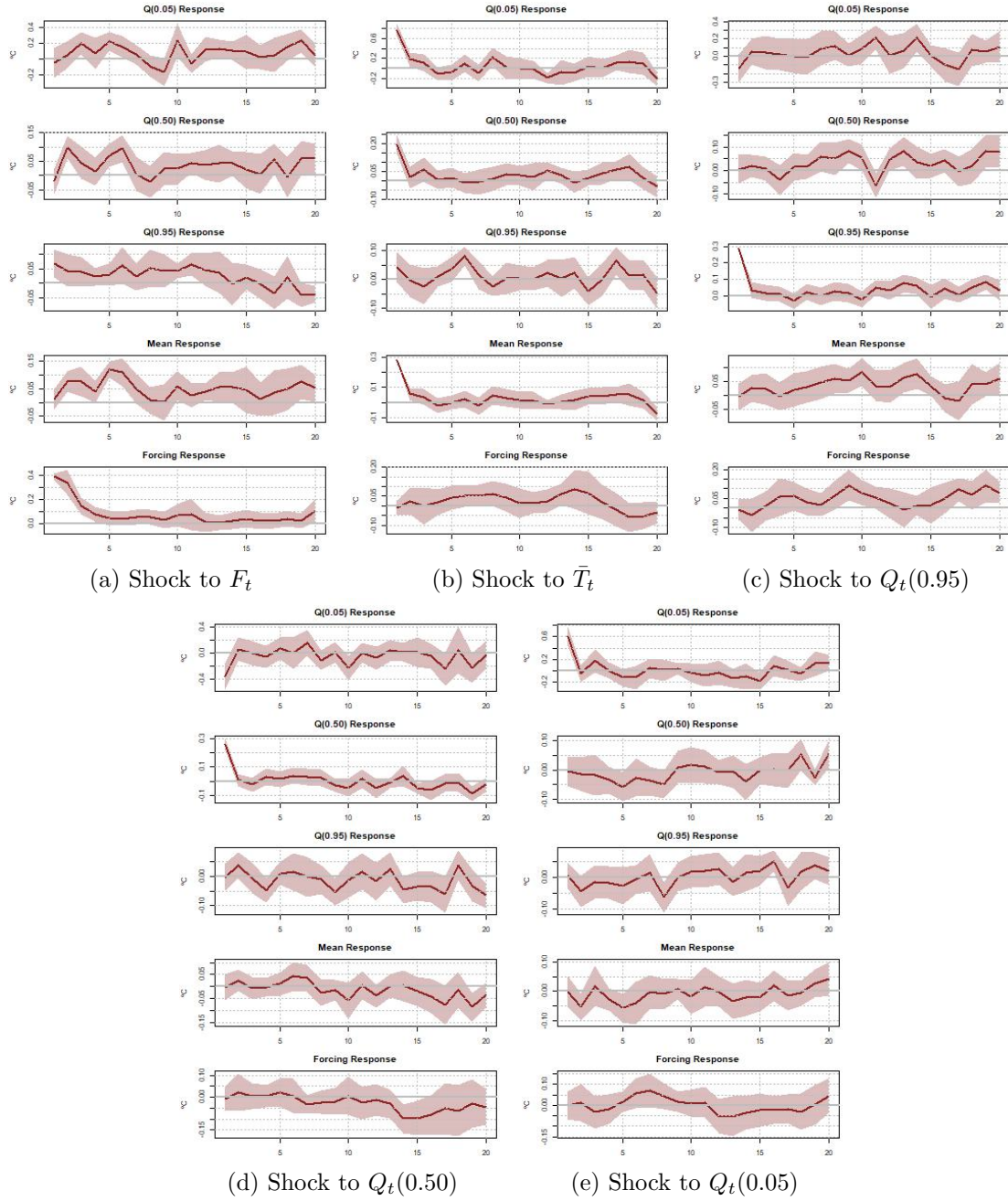


Figure 23: IRFs to identified structural shocks (Globe)

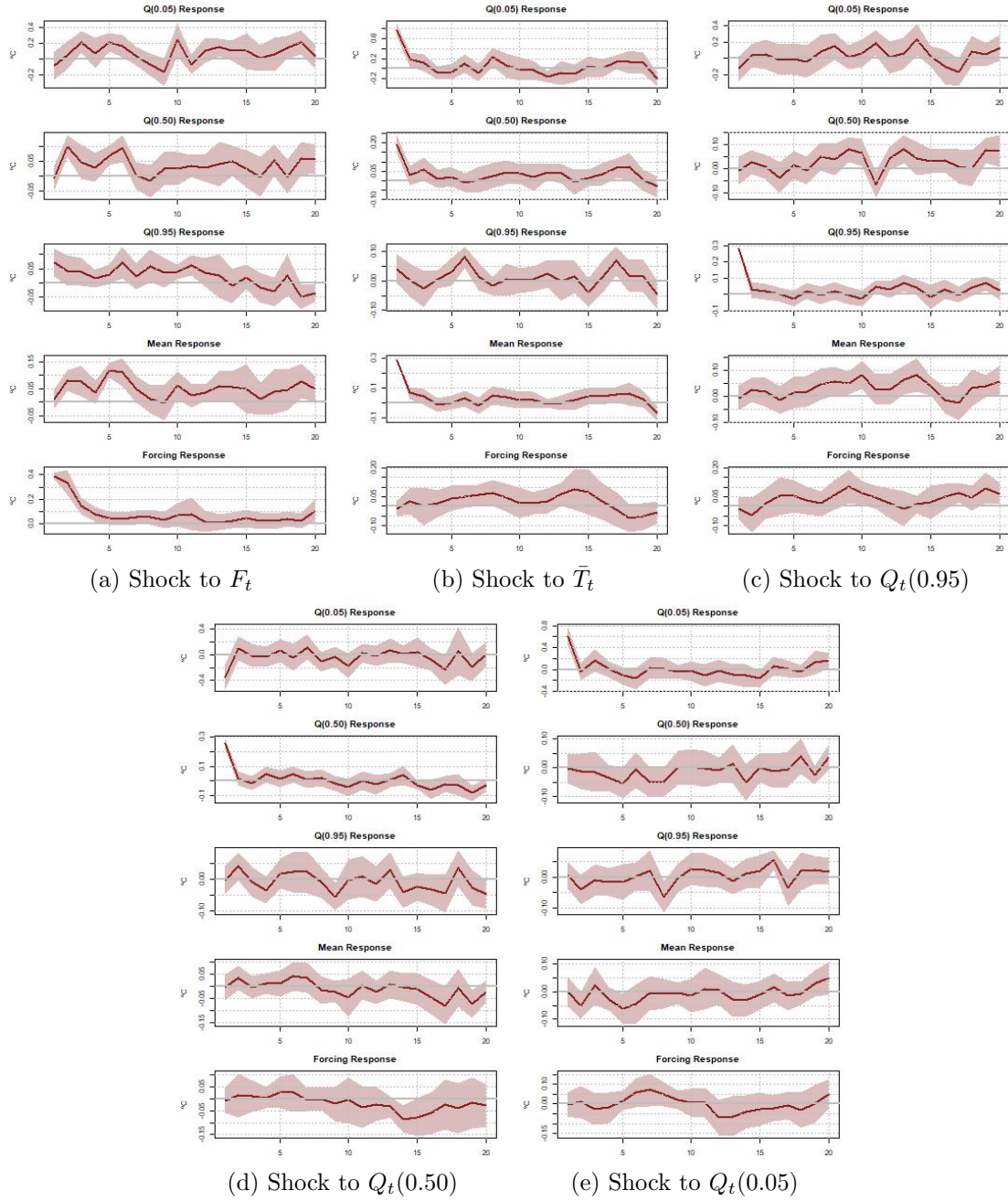


Figure 24: IRFs to identified structural shocks (North Hemisphere)

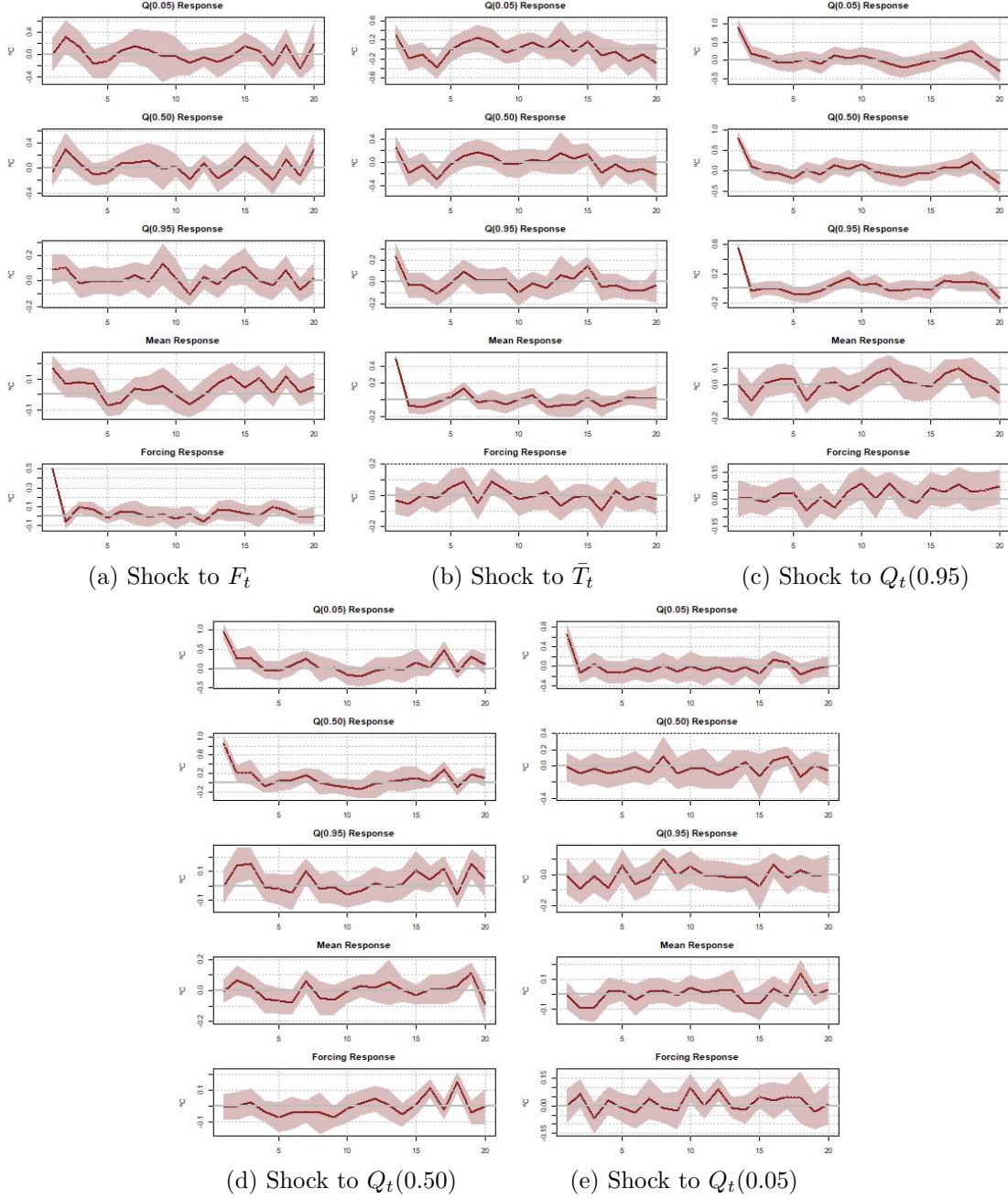


Figure 25: IRFs to identified structural shocks (Europe)

6.5.8 Additional analyses

A set of complementary analysis are conducted within this research. Appendix B presents the application of the methodology to the case of Central England, where the availability of high-frequency (daily) temperature data enables the estimation of temperature distributional characteristics at lower frequencies. In this application, the unconditional quantiles represent seasonal temperatures

and the interpretations of the results need to be adapted in that direction. In Appendix D, the information set is enlarged by the inclusion of more quantile series into the vector Z_t . The main conclusions of the baseline analysis remain robust. Appendix E zooms the analysis to the reduced sample from 1958 to 2021 in order to avoid the criticism raised by Pretis and Hendry (2013) about the combination of proxy-based and observed historical forcing series constructed with changing methodologies. Even though the qualitative patterns of heterogeneity are preserved, the magnitudes of the estimated distributional climate sensitivities and the long-term density forecasted and projected changes are stronger. Finally, Appendix G expands the information set by including ice extent and sea surface temperature. In the context of Arctic sea ice, this exercise extends the existing literature on ice coverage forecasting (see Coulombe and Göbel (2021), Diebold and Rudebusch (2022), Diebold et al. (2023), Diebold and Rudebusch (2023), or Blazsek et al. (2024)) by introducing more complex dynamics between temperature distribution, GHG concentrations, and the ongoing reduction of Arctic ice.

Next section discusses possible extensions and complementary applications that are motivated by the outcomes in this research.

7 Limitations and Future Research

The proposed methodology is subject to certain limitations that warrant further investigation.

First, as exposed by Folini et al. (2024), in 150 years of historical data, the anthropogenic signal due to CO₂ and other GHGs emissions comes in combination with a range of other relevant effects. Reliably disentangling the different contributions is a challenging task. This is a limitation common to all studies using observed climate data. Consequently, it is important to complement and compare the results obtained from observational data with those derived from climate model simulations. Exploring the use of paleoclimate data over past centuries to millennia offers a promising avenue for future research, extending the study of climate heterogeneity across a broader historical canvas.

Second, unconditional quantiles imperfectly represent temperatures at different latitudes (or seasons) and the obtained results must be interpreted with caution. An alternative approach involves estimating average temperatures for different latitude belts, like in Brock and Miller (2023) and Estrada et al. (2021), and subsequently estimating a VAR model with these average temperature series instead of the unconditional quantiles. This approach also faces challenges, particularly in capturing the heterogeneous dynamics in locations situated at similar latitudes. For instance,

New York and Madrid share approximate latitudes yet exhibit distinct climate characteristics, especially in their responses to increasing GHG concentrations. The use of unconditional quantiles relies on the strength of the concept of order-statistics and provides a robust statistical framework that aligns with that of the functional analysis. Furthermore, when the methodology is applied to characterize seasonal heterogeneity, as in the Central England case, the correspondence between unconditional quantiles and seasons is more justifiable, thereby enhancing the method's applicability and interpretative value.

Third, the empirical analysis conducted within this study assumes uniformity in radiative forcing across all geographical units and seasons. This assumption overlooks potential variations in radiative forcing that can arise from diverse factors, including changes in land use, cloud cover variability, and the localized concentrations of aerosols with either cooling or warming effects. Incorporating heterogeneity in radiative forcing into the analysis significantly increases the complexity of the problem and is left as a subject for future research. The main difficulty in conducting this type of analysis lies in the availability of long-term, high-resolution data necessary for reliable inference and forecasting. An alternative approach might involve a more agnostic view regarding local forcing, opting instead to infer forcing signals directly from the temperature series. This could be achieved through the use of flexible analytical frameworks, such as State-Space modeling, see [Durbin and Koopman \(2012\)](#).

Several ideas for future research are derived from this paper. First, the methodology can be employed to conduct more granular regional analyses of climate heterogeneity at various levels, such as continental, latitude-belts, country, or sub-regional. Research outcomes from this type of applications can be integrated in to economic studies to forecast and project local damages from climate change. This would provide policymakers with more precise, localized information on climate heterogeneity, aiding in the formulation of targeted mitigation/adaptation policy interventions that account not only for variations in the average temperature, but also in the whole temperature distribution.

Second, the model's flexibility allows for the inclusion of socioeconomic factors such as GDP, poverty, and inequality to explore the interplay between climate dynamics and economic variables. A recent example of this type of analysis is provided by [Nguyen \(2024\)](#), who investigates the impact of seasonal temperature variations within U.S. counties on economic outcomes. This paper finds that higher winter temperatures potentially boost private sector employment growth, whereas the rise in summer temperatures may have the opposite effect, and highlights the importance of accounting for seasonal variability in accounting for economic damages. Seasonal heterogeneity and its influence

on economic indicators can be further explored using the proposed unconditional-quantile VECM not only for the US counties but also for other regions, for instance, Europe at the NUTS-2 level.

Finally, the identification of structural shocks to the temperature distribution showed a promising complementarity to the most recent literature on the macroeconomic impacts of climate change, which exploits variations in global rather than local temperatures ([Neal, 2023](#); [Bilal and Känzig, 2024](#)). Concretely, this type of studies can be enhanced by considering not only shocks to the average temperature, but also shocks to the whole temperature distribution with potential heterogeneous effects on economic variables, as obtained in the preliminary analysis in Appendix F. A related idea involves using the unconditional-quantile VECM to obtain country-specific distributional temperature shocks. For example, [Nath et al. \(2024\)](#) identify temperature shocks as the innovations from an AR(p) model of temperature, where the parameters depend on the country's mean temperature. Implementing the unconditional-quantile VECM at local or regional levels would allow the estimation of distributional temperature shocks for each unit, which could then be used in damage analysis. This type of study enables the examination of how shocks in different parts of the distribution (representing, in this case, seasons) heterogeneously affect economic variables. More research in this direction is required.

8 Conclusion

Climate heterogeneity holds important implications not only for the climate system equilibrium but also for the economic analysis of climate change. This paper introduced a time series methodology capable of accounting for different forms of heterogeneity in the dynamics of the temperature distribution and its association with various climate drivers, including CO₂. The proposed unconditional-quantile VECM combines elements of physics theory from 1D-EBMs with recent advances in time series econometrics regarding the estimation of models with deterministic (and possibly stochastic) co-trending. The methodology produces estimation, forecasting, and projection outcomes that can be integrated as inputs in other types of economic studies. For example, the estimates of global or hemispheric climate sensitivities at different parts of the temperature distribution can be used for calibration and uncertainty analysis in IAMs featuring geographical heterogeneity (for example [Krusell and Smith \(2022\)](#) or [Cruz and Rossi-Hansberg \(2024\)](#)), as an alternative to statistical downscaling. Additionally, unconditional long-term density forecasts and projections under different scenarios provide valuable inputs for estimating the global and local expected damages from climate change accounting for heterogeneity. An alternative to produce this type of inputs is to use simulations from complex large-scale General Circulation Models. How-

ever, these models are highly non-linear, require large amounts of input data, are computationally expensive to solve and heavily dependent on the initial conditions of the system. In contrast, the unconditional quantile VECM achieves a desirable balance between a purely statistical multivariate approach and the theoretical/structural model of the climate system, allowing the production of estimation and forecasting/projection results and for the assessment of estimation uncertainty in a simpler statistical reduced-form procedure. The potential application of this methodology at different geographical levels opens the door to a new type of research focused on the evolution of the entire temperature distribution and its economic implications. This approach enables the production of research outcomes that can better inform adaptation and mitigation policies.

References

- Acevedo, S., M. Mrkaic, N. Novta, E. Pugacheva, and P. Topalova (2020). The Effects of Weather Shocks on Economic Activity: What are the Channels of Impact? *Journal of Macroeconomics* 65, 103207.
- Anderson, H., J. Gao, F. Vahid, W. Wei, and Y. Yang (2023). Does Climate Sensitivity Differ Across Regions? A Varying-Coefficient Approach. Available at SSRN: <https://ssrn.com/abstract=4437576>.
- Andrews, T., C. J. Smith, G. Myhre, P. M. Forster, R. Chadwick, and D. Ackerley (2021). Effective Radiative Forcing in a GCM With Fixed Surface Temperatures. *Journal of Geophysical Research: Atmospheres* 126(4), e2020JD033880.
- AR6-IPCC (2021). *Climate Change 2021: The Physical Science Basis*. [Masson-Delmotte V, Zhai P, Pirani A et al. (eds)]. Cambridge and New York: Cambridge University Press.
- Balling, R. C., P. J. Michaels, and P. C. Knappenberger (1998). Analysis of Winter and Summer Warming Rates in Gridded Temperature Time Series. *Climate Research* 9(3), 175–181.
- Barnett, T., F. Zwiers, G. Hegerl, M. Allen, T. Crowley, N. Gillett, K. Hasselmann, P. Jones, B. Santer, R. Schnur, P. Scott, K. Taylor, and S. Tett (2005). Detecting and Attributing External Influences on the Climate System: A Review of Recent Advances. *Journal of Climate* 18(9), 1291–1314.
- Baumeister, C. and L. Kilian (2014). Real-Time Analysis of Oil Price Risks Using Forecast Scenarios. *IMF Economic Review* 62(1), 119–145.
- Bekryaev, R. V., I. V. Polyakov, and V. A. Alexeev (2010). Role of polar amplification in long-term surface air temperature variations and modern arctic warming. *Journal of Climate* 23(14), 3888–3906.
- Benati, L. (2023). Forecasting Global Temperatures by Exploiting Cointegration with Radiative Forcing. *Discussion Papers, No. 23-08, University of Bern, Department of Economics, Bern*.
- Bennedsen, M., E. Hillebrand, and J. Z. Lykke (2023). Global Temperature Projections from a Statistical Energy Balance Model Using Multiple Sources of Historical Data. *Journal of Climate* 36(19), 6817–6838.
- Bierens, H. J. (2000). Nonparametric Nonlinear Cotrending Analysis, With an Application to Interest and Inflation in the United States. *Journal of Business & Economic Statistics* 18(3), 323–337.
- Bilal, A. and D. R. Käenzig (2024, May). The Macroeconomic Impact of Climate Change: Global vs. Local Temperature. NBER Working Papers 32450, National Bureau of Economic Research, Inc.
- Blazsek, S., A. Escribano, and E. Kristof (2024). Global, arctic, and antarctic sea ice volume predictions using score-driven threshold climate models. *Energy Economics* 134, 107591.
- Borgerson, S. G. (2008). Arctic Meltdown - The Economic and Security Implications of Global Warming Essay. *Foreign Affairs* 87(2), 63–77.
- Box, G. E. P. and D. A. Pierce (1970). Distribution of Residual Autocorrelations in Autoregressive-Integrated Moving Average Time Series Models. *Journal of the American Statistical Association* 65(332), 1509–1526.
- Brock, W. and A. Xepapadeas (2017). Climate Change Policy Under Polar Amplification. *European Economic Review* 94, 263–282.

- Brock, W. A. and J. I. Miller (2023). Polar Amplification in a Moist Energy Balance Model: A Structural Econometric Approach to Estimation and Testing. Available at SSRN: <https://ssrn.com/abstract=4450492>.
- Bruns, S. B., Z. Csereklyei, and D. I. Stern (2020). A Multicointegration Model of Global Climate Change. *Journal of Econometrics* 214(1), 175–197.
- Budyko, M. (1969). The Effect of Solar Radiation Variations on the Climate of the Earth. *Tellus* 21, 611–619.
- Burke, M., S. M. Hsiang, and E. Miguel (2015). Global Non-Linear Effect of Temperature on Economic Production. *Nature* 527, 235–239.
- Chapman, S., D. Stainforth, and N. Watkins (2013). On Estimating Local Long-term Climate Trends. *Phil Trans R Soc A* 371:20120287.
- Chen, L., J. J. Dolado, J. Gonzalo, and A. Ramos (2023). Heterogeneous Predictive Association of CO₂ with Global Warming. *Economica* 90(360), 1397–1421.
- Chen, L., J. Gao, and F. Vahid (2022). Global Temperatures and Greenhouse Gases: A Common Features Approach. *Journal of Econometrics* 230, 240–254.
- Chen, X., X. Zhang, J. A. Church, C. S. Watson, M. A. King, D. Monselesan, B. Legresy, and C. Harig (2017). The Increasing Rate of Global Mean Sea-Level Rise During 1993–2014. *Nature Climate Change* 7, 492–495.
- Cohen, J. L., J. C. Furtado, M. Barlow, V. A. Alexeev, and J. E. Cherry (2012). Asymmetric Seasonal Temperature Trends. *Geophysical Research Letters* 39(4).
- Coulombe, P. G. and M. Göbel (2021). Arctic Amplification of Anthropogenic Forcing: A Vector Autoregressive Analysis. *Journal of Climate* 34(13), 5523 – 5541.
- Cruz, J.-L. and E. Rossi-Hansberg (2024). The Economic Geography of Global Warming. *Review of Economic Studies*, forthcoming.
- d'Autume, A., K. Schubert, and C. Withagen (2016). Should the Carbon Price Be the Same in All Countries? *Journal of Public Economic Theory* 18(5), 709–725.
- Davy, R., I. Esau, A. Chernokulsky, S. Outten, and S. Zilitinkevich (2017). Diurnal Asymmetry to the Observed Global Warming. *International Journal of Climatology* 37(1), 79–93.
- Dell, M., B. F. Jones, and B. A. Olken (2012, July). Temperature Shocks and Economic Growth: Evidence from the Last Half Century. *American Economic Journal: Macroeconomics* 4(3), 66–95.
- Dell, M., B. F. Jones, and B. A. Olken (2014, September). What Do We Learn from the Weather? The New Climate-Economy Literature. *Journal of Economic Literature* 52(3), 740–98.
- Desmet, K. and E. Rossi-Hansberg (2024, March). Climate Change Economics over Time and Space. Working Paper 32197, National Bureau of Economic Research.
- Diebold, F. X. and G. D. Rudebusch (2022). Probability Assessments of an Ice-free Arctic: Comparing Statistical and Climate Model Projections. *Journal of Econometrics* 231(2), 520–534. Special Issue: The Econometrics of Macroeconomic and Financial Data.
- Diebold, F. X. and G. D. Rudebusch (2023). Climate models underestimate the sensitivity of Arctic sea ice to carbon emissions. *Energy Economics* 126, 107012.
- Diebold, F. X., G. D. Rudebusch, M. Göbel, P. Goulet Coulombe, and B. Zhang (2023). When Will Arctic Sea Ice Disappear? Projections of Area, Extent, Thickness, and Volume. *Journal of Econometrics* 236(2), 105479.

- Donat, M. G. and L. V. Alexander (2012). The Shifting Probability Distribution of Global Daytime and Night-time Temperatures. *Geophysical Research Letters* 39.
- Dong, Y., K. C. Armour, C. Proistosescu, T. Andrews, D. S. Battisti, P. M. Forster, D. Paynter, C. J. Smith, and H. Shiogama (2021). Biased Estimates of Equilibrium Climate Sensitivity and Transient Climate Response Derived From Historical CMIP6 Simulations. *Geophysical Research Letters* 48(24), e2021GL095778.
- Durbin, J. and S. J. Koopman (2012). *Time Series Analysis by State Space Methods*. Oxford University Press.
- Engle, R. F. and C. W. J. Granger (1987). Co-Integration and Error Correction: Representation, Estimation, and Testing. *Econometrica* 55(2), 251–276.
- Epps, T. W. (1987). Testing That a Stationary Time Series is Gaussian. *The Annals of Statistics* 15(4), 1683–1698.
- Estrada, F., D. Kim, and P. Perron (2021). Anthropogenic Influence in Observed Regional Warming Trends and the Implied Social Time of Emergence. *Communications Earth and Environment* 2(31), 1–9.
- Estrada, F. and P. Perron (2017). Extracting and Analyzing the Warming Trend in Global and Hemispheric Temperatures. *Journal of Time Series Analysis* 38(5), 711–732.
- Estrada, F., P. Perron, and B. Martínez-López (2013). Statistically Derived Contributions of Diverse Human Influences to Twentieth-Century Temperature Changes. *Nature Geoscience* 6, 1050–1055.
- Fernández-Villaverde, J., K. Gillingham, and S. Scheidegger (2024). Climate Change through the Lens of Macroeconomic Modeling. Working Paper 32963, National Bureau of Economic Research.
- Folini, D., A. Friedl, F. Kübler, and S. Scheidegger (2024). The Climate in Climate Economics. *The Review of Economic Studies*, rdae011.
- Francis, J. A. and S. J. Vavrus (2015). Evidence for a Wavier Jet Stream in Response to Rapid Arctic Warming. *Environmental Research Letters* 10(1), 014005.
- Gadea, M. and J. Gonzalo (2020). Trends in Distributional Characteristics: Existence of Global Warming. *Journal of Econometrics* 214, 153–174.
- Gadea, M. and J. Gonzalo (2023). Climate Change Heterogeneity: A New Quantitative Approach. *arXiv:2301.02648*.
- Gadea, M., J. Gonzalo, and A. Ramos (2024). Trends in temperature data: Micro-foundations of their nature. *Economics Letters* 244, 111992.
- Gao, J. and K. Hawthorne (2006). Semiparametric Estimation and Testing of the Trend of Temperature Series. *The Econometrics Journal* 9(2), 332–355.
- Gay-Garcia, C., F. Estrada, and A. Sánchez (2009). Global and Hemispheric Temperatures Revisited. *Climatic Change* 94(3), 333–349.
- Giannone, D., M. Lenza, D. Momferatou, and L. Onorante (2014). Short-term Inflation Projections: A Bayesian Vector Autoregressive Approach. *International Journal of Forecasting* 30(3), 635–644.
- Gonzalo, J. and C. Granger (1995). Estimation of Common Long-Memory Components in Cointegrated Systems. *Journal of Business Economic Statistics* 13(1), 27–35.
- Goulet-Coulombe, P. and M. Göbel (2021). On Spurious Causality, CO₂, and Global Temperature. *Econometrics* 99(3), 33.

- Guo, Z.-F. and M. Shintani (2013). Consistent Co-trending Rank Selection when Both Stochastic and Non-linear Deterministic Trends are Present. *The Econometrics Journal* 16(3), 473–484.
- Hamilton, J. D. (2018, 12). Why You Should Never Use the Hodrick-Prescott Filter. *The Review of Economics and Statistics* 100(5), 831–843.
- Hansen, J., M. Sato, P. Kharecha, and K. von Schuckmann (2011). Earth's Energy Imbalance and Implications. *Atmospheric Chemistry and Physics* 11, 13421–13449.
- Hassler, J., P. Krusell, and C. Olovsson (2018). The Consequences of Uncertainty: Climate Sensitivity and Economic Sensitivity to the Climate. *Annual Review of Economics* 10, 189–205.
- Hassler, J., P. Krusell, and C. Olovsson (2024). The Macroeconomics of Climate Change: Starting Points, Tentative Results, and a Way Forward. Working Paper 24-8, Peterson Institute for International Economics.
- Hatanaka, M. (2000). How to Determine the Number of Relations Among Deterministic Trends. *The Japanese Economic Review* 51(3), 349–374.
- Hatanaka, M. and H. Yamada (2003). *Co-trending: A Statistical System Analysis of Economic Trends*. Springer Tokyo.
- Held, I. M. and M. J. Suarez (1974). Simple Albedo Feedback Models of the Icecaps. *Tellus* 26(6), 613–629.
- Hillebrand, E. and T. Proietti (2017). Phase Changes and Seasonal Warming in Early Instrumental Temperature Records. *Journal of Climate* 30(17), 6795 – 6821.
- Hsiang, S., R. Kopp, A. Jina, J. Rising, M. Delgado, S. Mohan, D. J. Rasmussen, R. Muir-Wood, P. Wilson, M. Oppenheimer, K. Larsen, and T. Houser (2017). Estimating Economic Damage from Climate Change in the United States. *Science* 356(6345), 1362–1369.
- Ji, F., Z. Wu, J. Huang, and E. Chassignet (2014). Evolution of Land Surface Air Temperature Trend. *Nature Climate Change* 4, 462–466.
- Jordà, (2005, March). Estimation and Inference of Impulse Responses by Local Projections. *American Economic Review* 95(1), 161–182.
- Kaufmann, R. K., K. Kauppi, and J. Stock (2006). Emissions, Concentrations, and Temperature: A Time Series Analysis. *Climatic Change* 77, 249–278.
- Kaufmann, R. K. and D. I. Stern (2002). Cointegration Analysis of Hemispheric Temperature Relations. *Journal of Geophysical Research: Atmospheres* 107(D2), ACL 8–1–ACL 8–10.
- Kerr, R. A. (2010). 'Arctic Armageddon' Needs More Science, Less Hype. *Science* 329(5992), 620–621.
- Knutti, R., M. A. Rugenstein, and G. C. Hegerl (2017). Beyond Equilibrium Climate Sensitivity. *Nature Geoscience* 10(10), 727–736.
- Krusell, P. and A. Smith (2022). Climate Change Around the World. Working Paper 30338, National Bureau of Economic Research.
- Kwok, R. (2018, oct). Arctic Sea Ice Thickness, Volume, and Multiyear Ice Coverage: Losses and Coupled Variability (1958–2018). *Environmental Research Letters* 13(10), 105005.
- Leduc, M., H. D. Matthews, and R. de Elía (2016). Regional Estimates of the Transient Climate Response to Cumulative CO₂ Emissions. *Nature Climate Change* 6, 474—478.
- Lee, S., T. Gong, S. B. Feldstein, J. A. Screen, and I. Simmonds (2017). Revisiting the Cause of the 1989–2009 Arctic Surface Warming Using the Surface Energy Budget: Downward Infrared Radiation Dominates the Surface Fluxes. *Geophysical Research Letters* 44(20), 10.654–10.661.

- Ljung, G. M. and G. E. P. Box (1978). On a Measure of Lack of Fit in Time Series Models. *Biometrika* 65(2), 297–303.
- Luo, B., D. Luo, L. Wu, L. Zhong, and I. Simmonds (2017, may). Atmospheric Circulation Patterns Which Promote Winter Arctic Sea Ice Decline. *Environmental Research Letters* 12(5), 054017.
- Lupo, A., W. Kininmonth, J. Armstrong, and K. Green (2013). Global Climate Models and Their Limitations. *Climate change reconsidered II: Physical science* 9, 148.
- Lütkepohl, H. (2005). *New Introduction to Multiple Time Series Analysis*. Number 978-3-540-27752-1 in Springer Books. Springer.
- McKittrick, R., T. Vogelsang, and J. Christy (2023). Temperature Trends, Climate Attribution and the Nonstationarity Question. *Earth System Dynamics Discussions* 2023, 1–32.
- Montiel-Olea, J. L., M. Plagborg-Møller, E. Qian, and C. K. Wolf (2024). Double Robustness of Local Projections and Some Unpleasant VARithmetic. Working Paper 32495, National Bureau of Economic Research.
- Morice, C. P., J. J. Kennedy, N. A. Rayner, J. P. Winn, E. Hogan, R. E. Killick, R. J. H. Dunn, T. J. Osborn, P. D. Jones, and I. R. Simpson (2021). An Updated Assessment of Near-Surface Temperature Change From 1850: The HadCRUT5 Data Set. *Journal of Geophysical Research: Atmospheres* 126(3), e2019JD032361.
- Nath, I. B., V. A. Ramey, and P. J. Klenow (2024, July). How much will global warming cool global growth? Working Paper 32761, National Bureau of Economic Research.
- Neal, T. (2023). The Importance of External Weather Effects in Projecting the Macroeconomic Impacts of Climate Change. UNSW Economics Working Paper 2023-09, Available at SSRN: <https://ssrn.com/abstract=4471379>.
- Nelson, C. R. and C. R. Plosser (1982). Trends and random walks in macroeconomic time series: Some evidence and implications. *Journal of Monetary Economics* 10(2), 139–162.
- Nguyen, H. M. (2024). Beyond the Annual Averages: Impact of Seasonal Temperature on Employment Growth in US Counties. *Journal of Environmental Economics and Management* 125, 102946.
- Nordhaus, W. D. (1993). Rolling the ‘DICE’: An Optimal Transition Path for Controlling Greenhouse Gases. *Resource and Energy Economics* 15(1), 27–50.
- O’Neill, B. C., E. Kriegler, K. Riahi, K. L. Ebi, S. Hallegatte, T. R. Carter, R. Mathur, and D. P. van Vuuren (2014). A New Scenario Framework for Climate Change Research: The Concept of Shared Socioeconomic Pathways. *Climatic Change* 122(3), 387–400.
- Parker, D. E., T. P. Legg, and C. K. Folland (1992). A New Daily Central England Temperature Series, 1772–1991. *International Journal of Climatology* 12(4), 317–342.
- Phillips, P. (1998). New Tools for Understanding Spurious Regressions. *Econometrica* 66(6), 1299–1325.
- Phillips, P. C., T. Leirvik, and T. Storelvmo (2020). Econometric Estimates of Earth’s Transient Climate Sensitivity. *Journal of Econometrics* 214(1), 6–32. Annals Issue: Econometric Models of Climate Change.
- Pindyck, R. S. (2021). What We Know and Don’t Know about Climate Change, and Implications for Policy. *Environmental and Energy Policy and the Economy* 2, 4–43.
- Pretis, F. (2020). Econometric Modelling of Climate Systems: The Equivalence of Energy Balance Models and Cointegrated Vector Autoregressions. *Journal of Econometrics* 214(1), 256–273.

Pretis, F. and D. F. Hendry (2013). Comment on "polynomial cointegration tests of anthropogenic impact on global warming" by beenstock et al. (2012) - some hazards in econometric modelling of climate change. *Earth System Dynamics* 4(2), 375–384.

Riahi, K., D. P. van Vuuren, E. Kriegler, J. Edmonds, B. C. O'Neill, S. Fujimori, N. Bauer, K. Calvin, R. Dellink, O. Fricko, W. Lutz, A. Popp, J. C. Cuaresma, S. KéC, M. Leimbach, L. Jiang, T. Kram, S. Rao, J. Emmerling, K. Ebi, T. Hasegawa, P. Havlik, F. Humpenöder, L. A. Da Silva, S. Smith, E. Stehfest, V. Bosetti, J. Eom, D. Gernaat, T. Masui, J. Rogelj, J. Strefler, L. Drouet, V. Krey, G. Luderer, M. Harmsen, K. Takahashi, L. Baumstark, J. C. Doelman, M. Kainuma, Z. Klimont, G. Marangoni, H. Lotze-Campen, M. Obersteiner, A. Tabeau, and M. Tavoni (2017). The Shared Socioeconomic Pathways and their energy, land use, and greenhouse gas emissions implications: An overview. *Global Environmental Change* 42, 153–168.

Schaefer, K., H. Lantuit, V. E. Romanovsky, E. A. G. Schuur, and R. Witt (2014). The Impact of the Permafrost Carbon Feedback on Global Climate. *Environmental Research Letters* 9(8), 085003.

Schuur, E. A. G., A. D. McGuire, C. Schädel, G. Grosse, J. W. Harden, D. J. Hayes, G. Hugelius, C. D. Koven, P. Kuhry, D. M. Lawrence, S. M. Natali, D. Olefeldt, V. E. Romanovsky, K. Schaefer, M. R. Turetsky, C. C. Treat, and J. E. Vonk (2015). Climate Change and the Permafrost Carbon Feedback. *Nature* 520(7546), 171–179.

Screen, J. A. and I. Simmonds (2010). The Central Role of Diminishing Sea Ice in Recent Arctic Temperature Amplification. *Nature* 464, 1334—1337.

Sellers, W. D. (1969). A Global Climatic Model Based on the Energy Balance of the Earth-Atmosphere System. *Journal of Applied Meteorology and Climatology* 8(3), 392–400.

Serreze, M. C., A. P. Barrett, J. C. Stroeve, D. N. Kindig, and M. M. Holland (2009). The Emergence of Surface-based Arctic Amplification. *The Cryosphere* 3(1), 11–19.

Shepherd, T. G. (2016). Effects of a Warming Arctic. *Science* 353(6303), 989–990.

Simmonds, I. (2015). Comparing and Contrasting the Behaviour of Arctic and Antarctic Sea Ice Over the 35 Year Period 1979-2013. *Annals of Glaciology* 56(69), 18–28.

Smith, C. J., R. J. Kramer, G. Myhre, K. Alterskjær, W. Collins, A. Sima, O. Boucher, J.-L. Dufresne, P. Nabat, M. Michou, S. Yukimoto, J. Cole, D. Paynter, H. Shiogama, F. M. O'Connor, E. Robertson, A. Wiltshire, T. Andrews, C. Hannay, R. Miller, L. Nazarenko, A. Kirkevåg, D. Olivié, S. Fiedler, A. Lewinschal, C. Mackallah, M. Dix, R. Pincus, and P. M. Forster (2020). Effective Radiative Forcing and Adjustments in CMIP6 Models. *Atmospheric Chemistry and Physics* 20(16), 9591–9618.

Smith, D. M., J. A. Screen, C. Deser, J. Cohen, J. C. Fyfe, J. Garcia-Serrano, T. Jung, V. Kattsov, D. Matei, R. Msadek, Y. Peings, M. Sigmond, J. Ukita, J.-H. Yoon, and X. Zhang (2019). The polar amplification model intercomparison project (pamip) contribution to cmip6: investigating the causes and consequences of polar amplification. *Geoscientific Model Development* 12(3), 1139–1164.

Stock, J., C. Sims, and M. Watson (1990). Inference in Linear Time Series Models with Some Unit Roots. *Econometrica* 58(1), 113–144.

Tang, Q., X. Zhang, and J. A. Francis (2014). Extreme Summer Weather in Northern Mid-Latitudes Linked to a Vanishing Cryosphere. *Nature Climate Change* 4(1), 45–50.

Taylor, K. E., R. J. Stouffer, and G. A. Meehl (2012). An Overview of CMIP5 and the Experiment Design. *Bulletin of the American Meteorological Society* 93(4), 485 – 498.

Tebaldi, C. and J. M. Arblaster (2014). Pattern scaling: Its strengths and limitations, and an update on the latest model simulations. *Climatic Change* 122, 459–471.

- Vihma, T. (2014). Effects of Arctic Sea Ice Decline on Weather and Climate: A Review. *Surveys in Geophysics* 35(5), 1175–1214.
- Vogelsang, T. J. and P. H. Franses (2005). Are winters getting warmer? *Environmental Modelling Software* 20(11), 1449–1455.
- Wu, Z., X. Li, Y. Li, and Y. Li (2016). Potential Influence of Arctic Sea Ice to the Interannual Variations of East Asian Spring Precipitation. *Journal of Climate* 29(8), 2797 – 2813.
- You, Q., Z. Cai, N. Pepin, D. Chen, B. Ahrens, Z. Jiang, F. Wu, S. Kang, R. Zhang, T. Wu, P. Wang, M. Li, Z. Zuo, Y. Gao, P. Zhai, and Y. Zhang (2021). Warming Amplification over the Arctic Pole and Third Pole: Trends, Mechanisms and Consequences. *Earth-Science Reviews* 217, 103625.
- Zhang, R., C. Sun, J. Zhu, R. Zhang, and W. Li (2020). Increased European Heat Waves in Recent Decades in Response to Shrinking Arctic Sea Ice and Eurasian Snow Cover. *Climate and Atmospheric Science* 3(1), 620–621.
- Zhu, J., B. L. Otto-Bliesner, E. C. Brady, C. J. Poulsen, J. E. Tierney, M. Lofverstrom, and P. DiNezio (2021). Assessment of Equilibrium Climate Sensitivity of the Community Earth System Model Version 2 Through Simulation of the Last Glacial Maximum. *Geophysical Research Letters* 48(3), e2020GL091220.

A Quantiles and Latitudes

At global and hemispheric scales, the proposed methodology is motivated by the physics of a simple 1D-EBM ([Held and Suarez, 1974](#)), assuming that temperature unconditional quantiles represent temperatures at different latitudes. Figure A1 shows the geographical locations of temperature stations around the 5%, 50%, and 95% quantiles. It is clear from this figure that colder stations are situated in northern latitudes above 45 °N, whereas stations recording the higher temperatures are located closer to the Equator, with a notable concentration in India. Supporting this observation, Table A1 reports the average latitude associated with each quantile level, revealing that an increase in the quantile level corresponds to a decrease in the average latitude.

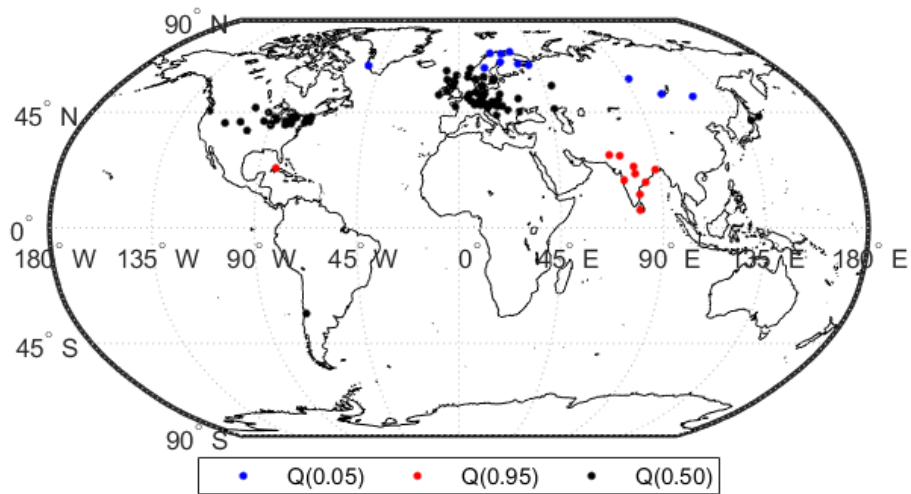


Figure A1: Stations by quantile levels

Table A1: Average latitude by quantile level

Characteristic	Avg. Latitude
$Q_t(0.05)$	60.39
$Q_t(0.10)$	57.94
$Q_t(0.25)$	54.21
$Q_t(0.50)$	47.65
$Q_t(0.75)$	26.96
$Q_t(0.90)$	21.41
$Q_t(0.95)$	20.30

B Application to Central England

The Hadley Centre Central England Temperature (HadCET) dataset is the longest instrumental record of temperature in the world.²³ These data are measured monthly and annually since 1659 for a roughly triangular area of UK enclosed by Lancashire, London and Bristol. There are also daily mean-temperature observations starting from 1772 (Parker et al., 1992) and updated continuously until the present. The availability of high-frequency (daily) temperature data enables the estimation of temperature distributional characteristics at lower frequencies and the application of the unconditional-quantile VAR methodology under no-geographical variation. Using the daily observations from 1772 to 2021, the distributional characteristics of interest are estimated and converted into the series objects depicted in Figure B1. The analysis is limited to the period post-1880, due to the availability of radiative forcing data. Trend-tests reported in Table B1 indicate an increasing trend in the mean and the unconditional quantiles of temperature, with steeper trends observed at the lower and central quantiles. Moreover, ADF tests strongly reject the hypothesis of unit roots in all instances.

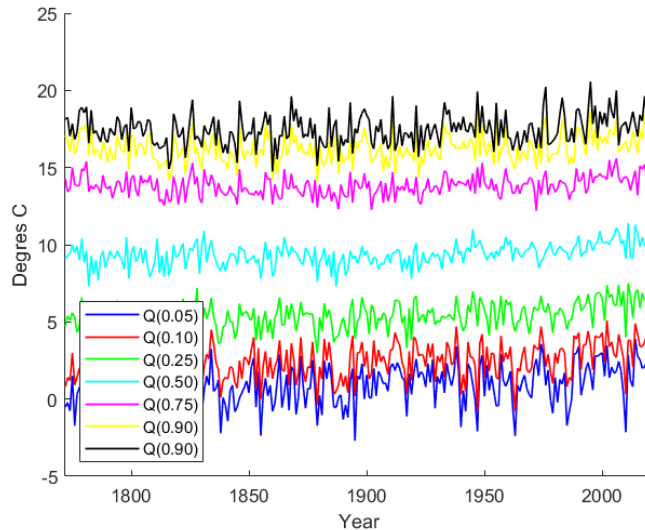


Figure B1: Temperature distributional characteristics (Central England)

The methodology is applied to a multivariate system where X_t contains more than three quantile series. Specifically, $X_t = [Q_t(0.05), Q_t(0.10), Q_t(0.25), Q_t(0.50), Q_t(0.75), Q_t(0.90), Q_t(0.95), \bar{T}_t, F_t]',$ where F_t denotes the radiative forcing. The Guo and Shintani (2013) test reveals 7 co-trending vectors. Table B2 reports the estimates of the co-trending slopes used to compute the climate

²³The dataset is accessible at the following URL: <https://www.metoffice.gov.uk/hadobs/hadcet/>.

Table B1: Testing for trends in distributional characteristics (Central England)

Characteristic	Trend-test		ADF-test	
	Test-statistic	p-value	Test-statistic	p-value
$Q_t(0.05)$	0.0086	0.0015	-14.3868	0.0000
$Q_t(0.10)$	0.0092	0.0001	-14.3614	0.0000
$Q_t(0.25)$	0.0097	0.0000	-14.4393	0.0000
$Q_t(0.50)$	0.0100	0.0000	-14.3042	0.0000
$Q_t(0.75)$	0.0077	0.0000	-14.1496	0.0000
$Q_t(0.90)$	0.0077	0.0000	-14.4480	0.0000
$Q_t(0.95)$	0.0074	0.0003	-15.0577	0.0000
Mean	0.0091	0.0000	-14.3491	0.0000

Notes: Annual distributional characteristics estimated using daily observations from 1880 to 2021. Test-statistics and p-values in column *Trend – test* correspond to a significance test for the trend-slope in a regression of the distributional characteristic on a constant and a linear trend, using HAC standard-errors. Column *ADF – test* report the test-statistics and p-values of the ADF-tests for unit roots. Intercept and trend included in the test-equation. Lags selected using the BIC criterion.

sensitivities plotted in Figure B2. When comparing these findings with CRU data, the local data from Central England displays less heterogeneity. Although the climate sensitivity estimates for the lower and central part of the temperature distribution are higher, the confidence intervals largely overlap. Notably, these climate sensitivities are lower than those derived for the Globe, the Northern Hemisphere, and Europe. The estimated model is used to produce the forecasts and projections under hypothetical SSP scenarios plotted in Figure B3 and Figure B4 respectively.

The application to Central England data illustrates the adaptability of the proposed methodology for its use in contexts with no geographical variation, but having sufficient high-frequency observations for the estimation of temperature distributional characteristics. Here, unconditional quantiles reflect temperatures at various seasons or times of the year —rather than across different latitudes—, allowing an investigation of seasonal sensitivities in the sense of Balling et al. (1998), Vogelsang and Franses (2005), Cohen et al. (2012), and Hillebrand and Proietti (2017). This approach yields interesting insights into climate heterogeneity for specific locations and allows the extension of the methodology to include economic variables as GDP or inequality to study the impact of seasonal temperatures on the economy as in Nguyen (2024).

Table B2: Co-trending slopes of relationships between the distributional characteristics of temperature and F_t (Central England)

Slope	Central England	
	<i>Estimate</i>	<i>Cot-test</i>
$\lambda(0.05)$	0.5449*** (0.1402)	0.4505
$\lambda(0.10)$	0.5596*** (0.1122)	0.5913
$\lambda(0.25)$	0.5417*** (0.0559)	0.9495
$\lambda(0.50)$	0.5016*** (0.0708)	0.0616
$\lambda(0.75)$	0.4301*** (0.0549)	0.8743
$\lambda(0.90)$	0.4247*** (0.0816)	0.9391
$\lambda(0.95)$	0.4141*** (0.0980)	0.9925
$\bar{\lambda}$	0.5090*** (0.0463)	0.8890

Notes: Column *Estimate* correspond to the estimated co-trending slope—of the distributional characteristic with respect to the radiative forcing F_t —and its standard-error in parenthesis. *, **, *** denote significance at the 10%, 5%, and 1% levels, respectively. Column *Cot-test* reports the p-value of the test for common-trends.

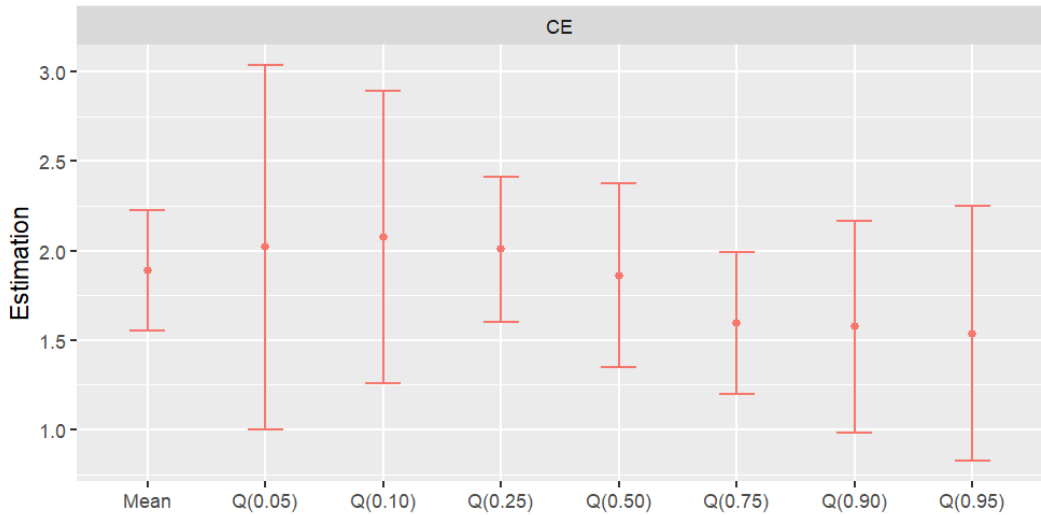


Figure B2: Climate sensitivities (Central England)

Table B3: Autocorrelation and normality tests for residual diagnosis (Central England)

Characteristic	Central England	
	Auto-correlation	Normality
$\Delta Q_t(0.05)$	0.9459	0.0827
$\Delta Q_t(0.10)$	0.8373	0.0847
$\Delta Q_t(0.25)$	0.6080	0.8232
$\Delta Q_t(0.50)$	0.7867	0.5099
$\Delta Q_t(0.75)$	0.9640	0.1284
$\Delta Q_t(0.90)$	0.3346	0.0547
$\Delta Q_t(0.95)$	0.0546	0.0171
$\Delta \bar{T}_t$	0.2538	0.7733
ΔF_t	0.3458	0.0170

Notes: Auto-correlation column reports the p-values of the Ljung and Box (1978) modified portmanteau tests applied to each individual residual series. Lag set at 10. Normality column reports the p-values of the Epps (1987) test applied to each individual residual series.

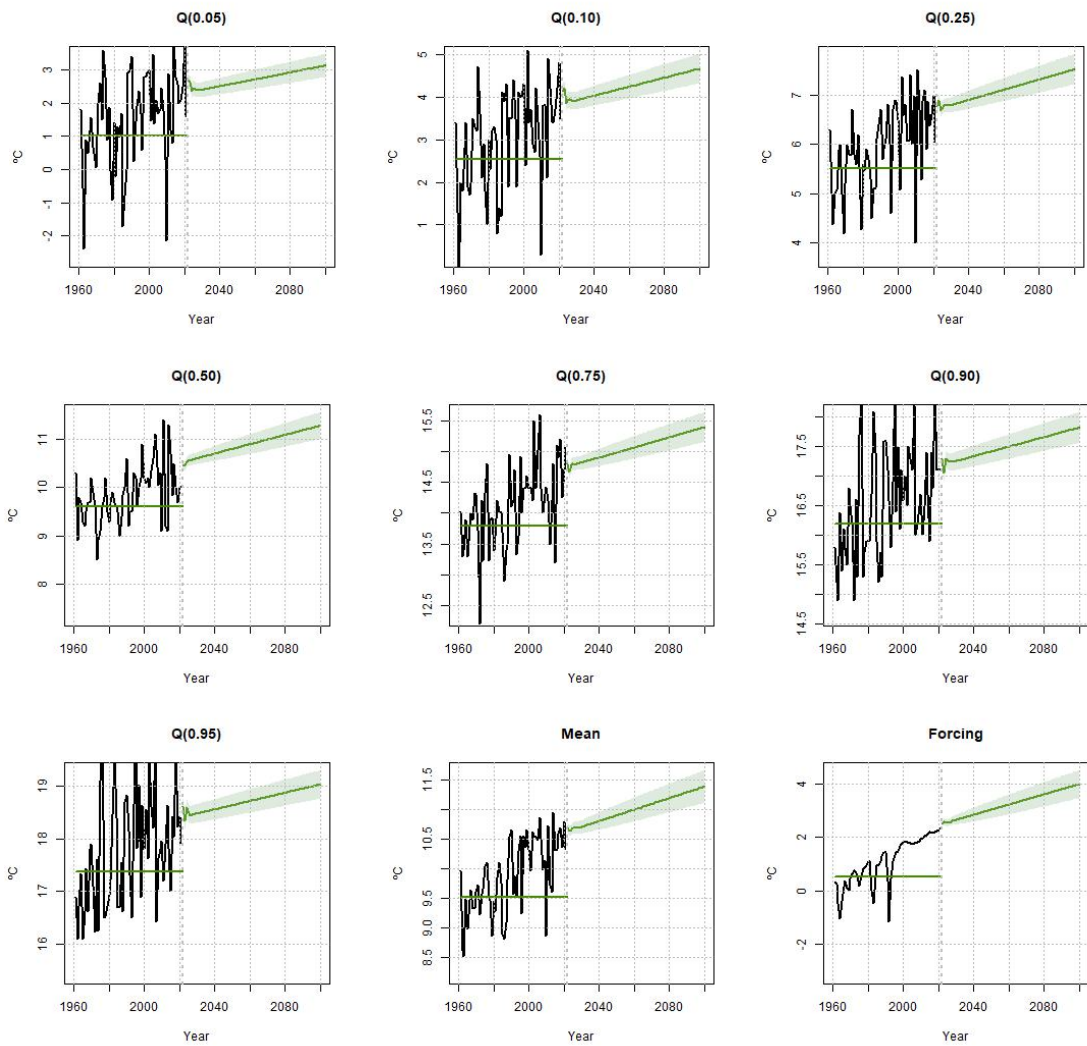


Figure B3: Forecasts including forcing dynamics (Central England)

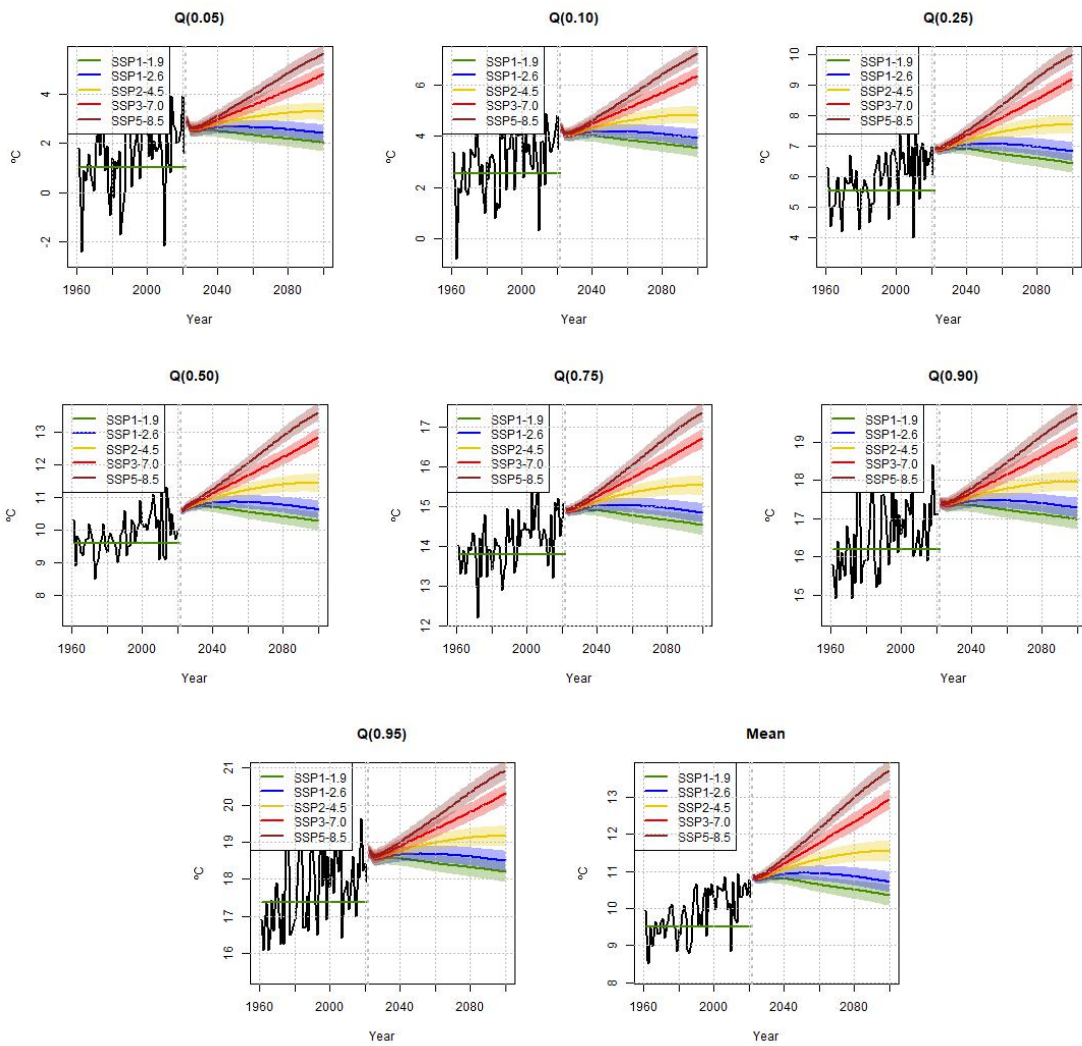


Figure B4: Long-term projections under RCP scenarios (Central England)

C Alternative Radiative Forcing Series

As an attempt to replicate the analysis in [Estrada et al. \(2021\)](#), this section explores specific radiative forcing sources and computes the corresponding temperature sensitivity. Specifically, two alternative versions of F_t are considered: F_t^{co2} , representing the radiative forcing associated with CO₂, and F_t^{ant} , which encompasses anthropogenic forcing from additional GHGs. Observe in Table [C1](#) that the point estimates of the co-trending slopes for the long-run relationships between temperature distributional characteristics and F_t^{co2} are uniformly larger compared to the other versions of radiative forcing. Similar to the baseline analysis, for the Globe and the North Hemisphere, the estimated slopes decrease with the quantile level. For example, at $\tau_i = 0.05$ and focusing on F_t^{co2} , the estimated slope is 1.3505 (0.1769), while at $\tau_i = 0.95$, the slope decreases to 0.6056 (0.0484). In contrast, in Europe, the variability in estimates is less pronounced, with extreme quantile levels yielding the higher estimates.

Co-trending slopes in Table [C1](#) are used to compute the climate sensitivities in Figure [C1](#). Climate sensitivities for F_t^{co2} are consistently higher than those for F_t^{ant} and F_t^{tot} . This finding is not surprising considering that the anthropogenic and total forcing series include forcings from additional sources, some of which have global cooling effects. A similar result is obtained by [Estrada et al. \(2021\)](#). Finally, the VECM is estimated. The main difference with respect to the baseline model is obtained in the equation for ΔF_t . Note that when anthropogenic forcing or the radiative forcing of CO₂ are analyzed, all adjustment coefficients are statically zero. The non-response of ΔF_t to the equilibrium errors is a necessary condition for its exogeneity and indicate no significant feedback from the temperature distribution to the radiative forcing of greenhouse gases. This observation aligns with the evidence in [Chen et al. \(2022\)](#) and the model restrictions in [Pretis \(2020\)](#). When total forcing is examined in the baseline, ΔF_t does adjust to its lagged long-run equilibrium deviations in relation to average temperature. This suggests that any feedback between temperature and radiative forcing primarily occurs through natural forcing dynamics.

Table C1: Co-trending slopes of relationships between the distributional characteristics of temperature and F_t (additional forcing sources)

F_t	Slope	Globe		North Hemisphere		Europe	
		<i>Estimate</i>	<i>Cot-test</i>	<i>Estimate</i>	<i>Cot-test</i>	<i>Estimate</i>	<i>Cot-test</i>
F_t^{co2}	$\lambda(0.05)$	1.3505*** (0.1769)	0.2637 (0.1777)	1.3472*** (0.1777)	0.2601 (0.2408)	1.4120*** (0.2408)	0.3774
	$\lambda(0.50)$	0.7497*** (0.0801)	0.5493 (0.0803)	0.7617*** (0.0803)	0.5287 (0.0971)	0.9568*** (0.0971)	0.2496
	$\lambda(0.95)$	0.6056*** (0.0484)	0.4118 (0.0453)	0.5909*** (0.0453)	0.5304 (0.1490)	1.2395*** (0.1490)	0.1776
	$\bar{\lambda}$	0.8874*** (0.0725)	0.0971 (0.0747)	0.8858*** (0.0747)	0.0923 (0.0821)	1.0207*** (0.0821)	0.0946
	$\lambda(0.05)$	1.1026*** (0.1503)	0.1644 (0.1513)	1.0993*** (0.1513)	0.1607 (0.2003)	1.1547*** (0.2003)	0.2894
	$\lambda(0.50)$	0.6143*** (0.0721)	0.3718 (0.0721)	0.6242*** (0.0721)	0.3631 (0.0890)	0.7815*** (0.0890)	0.1541
F_t^{ant}	$\lambda(0.95)$	0.4994*** (0.0406)	0.4263 (0.0389)	0.4863*** (0.0389)	0.3916 (0.1251)	1.0200*** (0.1251)	0.1615
	$\bar{\lambda}$	0.7262*** (0.0661)	0.0579 (0.0679)	0.7246*** (0.0679)	0.0556 (0.0743)	0.8356*** (0.0743)	0.0547

Notes: Column *Estimate* correspond to the estimated co-trending slope—of the distributional characteristic with respect to the radiative forcing F_t —and its standard-error in parenthesis. *, **, *** denote significance at the 10%, 5%, and 1% levels, respectively. Column *Cot-test* reports the p-value of the test for common-trends.

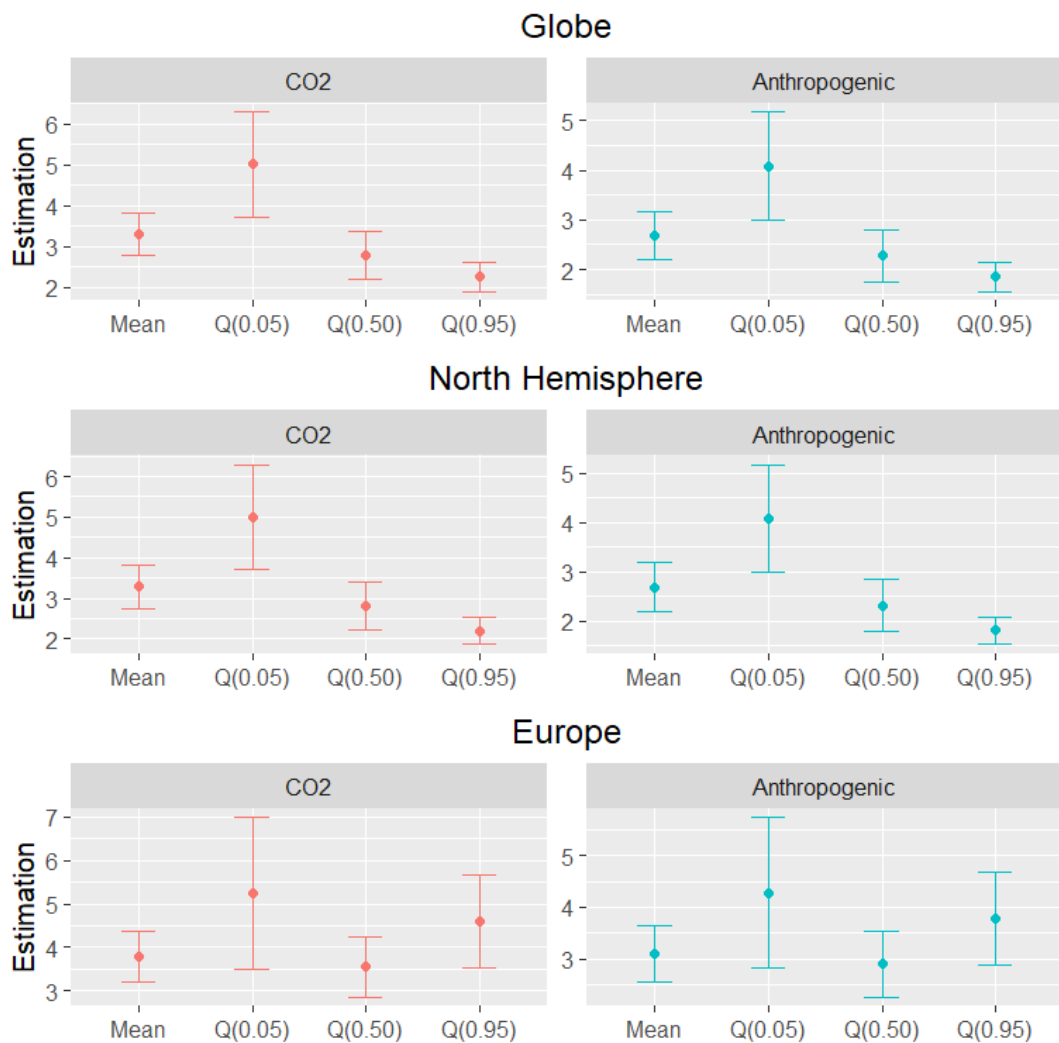


Figure C1: Climate sensitivities

Table C2: Adjustment coefficients of a vector error correction model of temperatures and radiative forcing (Globe, additional forcing sources)

Variables	CO2				
	$\Delta Q_t(0.05)$	$\Delta Q_t(0.50)$	$\Delta Q_t(0.95)$	$\Delta \bar{T}_t$	ΔF_t
$e_{1,t-1}$	-0.7957*** (0.1964)	-0.0649 (0.0679)	-0.0829 (0.0536)	-0.0500 (0.0571)	0.0000 (0.0010)
$e_{2,t-1}$	0.5146 (0.5509)	-1.1107*** (0.1280)	0.0995 (0.1400)	0.0228 (0.1202)	0.0011 (0.0024)
$e_{3,t-1}$	0.5926 (0.4531)	0.1716 (0.1317)	-0.9463*** (0.1095)	0.1968 (0.1218)	-0.0050* (0.0027)
$e_{4,t-1}$	-0.5185 (0.4336)	-0.3479** (0.1476)	-0.5821*** (0.1302)	-0.4670*** (0.1212)	-0.0043 (0.0026)
Anthropogenic					
$e_{1,t-1}$	-0.7975*** (0.2100)	-0.0691 (0.0665)	-0.0885* (0.0529)	-0.0554 (0.0564)	-0.0003 (0.0011)
$e_{2,t-1}$	0.5272 (0.4507)	-1.1095*** (0.1303)	0.1095 (0.1387)	0.0285 (0.1200)	-0.0003 (0.0030)
$e_{3,t-1}$	0.5842 (0.4420)	0.1838 (0.1302)	-0.9578*** (0.1100)	0.1977 (0.1209)	-0.0042 (0.0031)
$e_{4,t-1}$	-0.5137 (0.4665)	-0.3098** (0.1447)	-0.5670*** (0.1260)	-0.4361*** (0.1182)	-0.0048 (0.0032)

Notes: Estimates obtained in a two-steps procedure. HAC Standard-errors in parenthesis. *, **, *** denote significance at the 10%, 5%, and 1% levels, respectively. $e_{1,t-1}$, $e_{2,t-1}$, and $e_{3,t-1}$ as before. $e_{4,t-1}$ denotes the lagged residuals of the co-trending relation between F_t and \bar{T}_t . Short-run dynamics involving ΔX_t omitted.

Table C3: Adjustment coefficients of a vector error correction model of temperatures and radiative forcing (North Hemisphere, additional forcing sources)

Variables	CO2				
	$\Delta Q_t(0.05)$	$\Delta Q_t(0.50)$	$\Delta Q_t(0.95)$	$\Delta \bar{T}_t$	ΔF_t
$e_{1,t-1}$	-0.7972*** (0.2119)	-0.0435 (0.0670)	-0.0636 (0.0500)	-0.0351 (0.0579)	0.0002 (0.0010)
$e_{2,t-1}$	0.6824 (0.4759)	-1.0320*** (0.1352)	0.0893 (0.1462)	0.0834 (0.1284)	0.0013 (0.0026)
$e_{3,t-1}$	0.5550 (0.4662)	0.1828 (0.1386)	-0.9450*** (0.1133)	0.1959 (0.1327)	-0.0047* (0.0027)
$e_{4,t-1}$	-0.4917 (0.4780)	-0.3699*** (0.1403)	-0.5910*** (0.1259)	-0.4716*** (0.1249)	-0.0042 (0.0026)
Anthropogenic					
$e_{1,t-1}$	-0.7981*** (0.2122)	-0.0459 (0.0663)	-0.0693 (0.0494)	-0.0393 (0.0573)	0.0001 (0.0011)
$e_{2,t-1}$	0.6947 (0.4689)	-1.0309*** (0.1345)	0.0982 (0.1437)	0.0889* (0.1266)	0.0008 (0.0031)
$e_{3,t-1}$	0.5482 (0.4622)	0.2013 (0.1391)	-0.9478*** (0.1145)	0.2028 (0.1325)	-0.0035 (0.0030)
$e_{4,t-1}$	-0.4901 (0.4533)	-0.3361** (0.1374)	-0.5648*** (0.1227)	-0.4416*** (0.1211)	-0.0046 (0.0032)

Notes: Estimates obtained in a two-steps procedure. HAC Standard-errors in parenthesis. *, **, *** denote significance at the 10%, 5%, and 1% levels, respectively. $e_{1,t-1}$, $e_{2,t-1}$, and $e_{3,t-1}$ as before. $e_{4,t-1}$ denotes the lagged residuals of the co-trending relation between F_t and \bar{T}_t . Short-run dynamics involving ΔX_t omitted.

Table C4: Adjustment coefficients of a vector error correction model of temperatures and radiative forcing (Europe, additional forcing sources)

Variables	CO2				
	$\Delta Q_t(0.05)$	$\Delta Q_t(0.50)$	$\Delta Q_t(0.95)$	$\Delta \bar{T}_t$	ΔF_t
$e_{1,t-1}$	-1.3238*** (0.2537)	-0.1882* (0.0964)	-0.0480 (0.0944)	-0.1358* (0.0766)	0.0002 (0.0008)
$e_{2,t-1}$	-1.2384*** (0.4637)	-1.2546*** (0.1770)	-0.0018 (0.2195)	-0.2769* (0.1482)	0.0014 (0.0021)
$e_{3,t-1}$	-0.6721* (0.3699)	-0.0099 (0.1548)	-1.0561*** (0.1724)	-0.1237 (0.1380)	-0.0002 (0.0011)
$e_{4,t-1}$	-0.8239* (0.4533)	-0.7336*** (0.1485)	-0.8186*** (0.1779)	-0.7175*** (0.1279)	0.0006 (0.0014)
Anthropogenic					
$e_{1,t-1}$	-1.3251*** (0.2530)	-0.1947** (0.0975)	-0.0515 (0.0928)	-0.1401* (0.0779)	-0.0002 (0.0009)
$e_{2,t-1}$	-1.2307*** (0.4626)	-1.2336*** (0.1812)	0.0134 (0.2192)	-0.2612* (0.1475)	0.0016 (0.0023)
$e_{3,t-1}$	-0.6734* (0.3823)	-0.0055 (0.1562)	-1.0994*** (0.1786)	-0.1326 (0.1436)	-0.0016 (0.0013)
$e_{4,t-1}$	-0.8122* (0.4465)	-0.6750*** (0.1423)	-0.8507*** (0.1723)	-0.6943*** (0.1224)	-0.0008 (0.0016)

Notes: Estimates obtained in a two-steps procedure. HAC Standard-errors in parenthesis. *, **, *** denote significance at the 10%, 5%, and 1% levels, respectively. $e_{1,t-1}$, $e_{2,t-1}$, and $e_{3,t-1}$ as before. $e_{4,t-1}$ denotes the lagged residuals of the co-trending relation between F_t and \bar{T}_t . Short-run dynamics involving ΔX_t omitted.

D Including More Quantiles

The baseline models in the paper include three unconditional quantile series. The methodology, however, allows for straightforward extension to include additional quantile series based on research requirements. In this section, I extend the analysis to include an enhanced vector $X_t = [Q_t(0.05), Q_t(0.10), Q_t(0.25), Q_t(0.50), Q_t(0.75), Q_t(0.90), Q_t(0.95), \bar{T}_t, F_t]'$. The main findings obtained in the baseline analysis are upheld in this expanded framework. For instance, as demonstrated in Figure D1, the observed pattern of heterogeneity in the climate sensitivity remains, with a stronger climate sensitivity at lower quantiles for the Globe and the North Hemisphere, and at the tails of the distribution in Europe. Once the residual properties are checked as in D3, the model is also used to produce both unconditional and conditional long-term forecasts/projections for each variable within the system, with similar insights as in the baseline analysis.

Table D1: Co-trending slopes of relationships between unconditional quantiles and the average temperature (expanded model)

Slope	Globe		North Hemisphere		Europe	
	<i>Estimate</i>	<i>Cot-test</i>	<i>Estimate</i>	<i>Cot-test</i>	<i>Estimate</i>	<i>Cot-test</i>
$\beta(0.05)$	1.5310*** (0.1529)	0.9026	1.5283*** (0.1503)	0.8755	1.3975*** (0.2109)	0.9053
$\beta(0.10)$	1.3861*** (0.1339)	0.6336	1.3990*** (0.1356)	0.6990	1.2647*** (0.1774)	0.5743
$\beta(0.25)$	1.0613*** (0.0463)	0.2325	1.0616*** (0.0476)	0.3646	0.9980*** (0.0527)	0.7210
$\beta(0.50)$	0.8353*** (0.0482)	0.4198	0.8496*** (0.0463)	0.4536	0.9253*** (0.0745)	0.1556
$\beta(0.75)$	1.0866*** (0.0575)	0.1763	1.0613*** (0.0604)	0.0689	0.7793*** (0.0625)	0.7223
$\beta(0.90)$	0.7549*** (0.0561)	0.5523	0.7634 (0.0551)	0.7174	1.1548*** (0.0812)	0.1624
$\beta(0.95)$	0.6677*** (0.0473)	0.0876	0.6536*** (0.0478)	0.2486	1.2137*** (0.0953)	0.1987

Notes: Column *Estimate* correspond to the estimated co-trending slope—of the quantile with respect to the average temperature—and its standard-error in parenthesis. *, **, *** denote significance at the 10%, 5%, and 1% levels, respectively. Column *Cot-test* reports the p-value of the test for common-trends.

Table D2: Co-trending slopes of relationships between the distributional characteristics of temperature and F_t (expanded model)

Slope	Globe		North Hemisphere		Europe	
	<i>Estimate</i>	<i>Cot-test</i>	<i>Estimate</i>	<i>Cot-test</i>	<i>Estimate</i>	<i>Cot-test</i>
$\lambda(0.05)$	0.9897*** (0.1167)	0.8649	0.9887*** (0.1160)	0.9148	1.0323*** (0.1725)	0.7042
$\lambda(0.10)$	0.8907*** (0.0950)	0.3671	0.8985*** (0.0968)	0.4013	0.9312*** (0.1433)	0.3977
$\lambda(0.25)$	0.6885*** (0.0419)	0.9537	0.6878*** (0.0432)	0.8956	0.7414*** (0.0526)	0.5895
$\lambda(0.50)$	0.5395*** (0.0504)	0.5753	0.5479*** (0.0494)	0.5145	0.6936*** (0.0699)	0.6303
$\lambda(0.75)$	0.6937*** (0.0689)	0.1501	0.6755*** (0.0702)	0.0964	0.5780*** (0.0597)	0.6005
$\lambda(0.90)$	0.4831*** (0.0542)	0.3138	0.4893*** (0.0537)	0.4054	0.8435*** (0.0954)	0.1094
$\lambda(0.95)$	0.4255*** (0.0374)	0.2643	0.4186*** (0.0327)	0.0559	0.8860*** (0.1043)	0.1150
$\bar{\lambda}$	0.6443*** (0.0428)	0.3721	0.6442*** (0.0431)	0.3964	0.7404*** (0.0507)	0.3380

Notes: Column *Estimate* correspond to the estimated co-trending slope—of the distributional characteristic with respect to the radiative forcing F_t —and its standard-error in parenthesis. *, **, *** denote significance at the 10%, 5%, and 1% levels, respectively. Column *Cot-test* reports the p-value of the test for common-trends.

Table D3: Autocorrelation and normality tests for residual diagnosis (expanded model)

Characteristic	Globe		North Hemisphere		Europe	
	<i>Auto-correlation</i>	<i>Normality</i>	<i>Auto-correlation</i>	<i>Normality</i>	<i>Auto-correlation</i>	<i>Normality</i>
$\Delta Q_t(0.05)$	0.6420	0.4172	0.6316	0.7814	0.3892	0.2186
$\Delta Q_t(0.10)$	0.7301	0.2910	0.7254	0.2705	0.4103	0.1980
$\Delta Q_t(0.25)$	0.0417	0.8006	0.0212	0.7622	0.2741	0.9422
$\Delta Q_t(0.50)$	0.9892	0.3068	0.9790	0.4382	0.5736	0.9282
$\Delta Q_t(0.75)$	0.3637	0.0734	0.4566	0.0607	0.9038	0.2237
$\Delta Q_t(0.90)$	0.6314	0.2574	0.5691	0.3322	0.4366	0.5856
$\Delta Q_t(0.95)$	0.6183	0.6504	0.3083	0.2365	0.3816	0.6887
$\Delta \bar{T}_t$	0.1108	0.5376	0.1046	0.3316	0.4749	0.6443
ΔF_t	0.2841	0.0146	0.2444	0.0184	0.5785	0.0138

Notes: *Auto-correlation* column reports the p-values of the [Ljung and Box \(1978\)](#) modified portmanteau tests applied to each individual residual series. Lag set at 10. *Normality* column reports the p-values of the [Epps \(1987\)](#) test applied to each individual residual series.

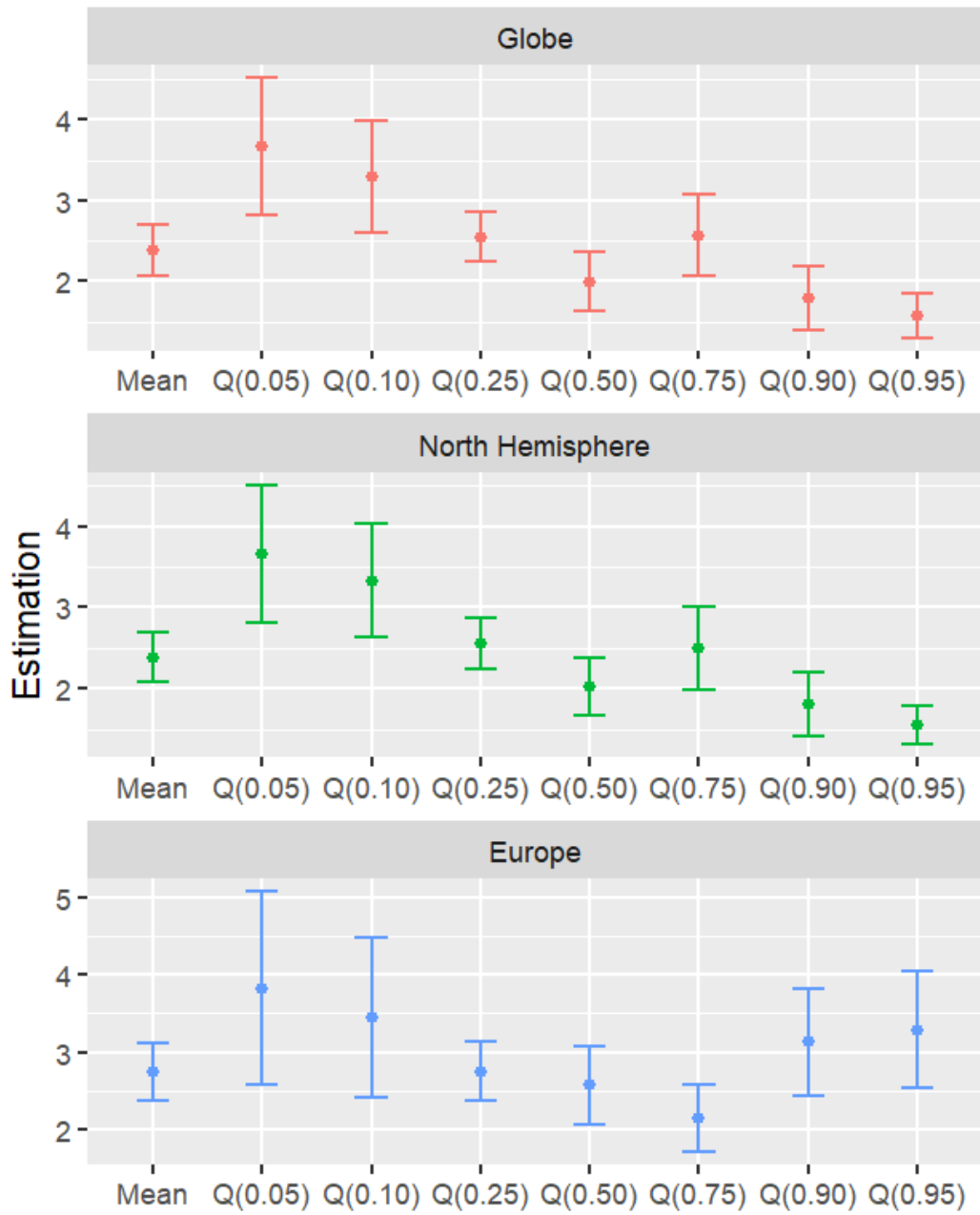


Figure D1: Climate sensitivities (expanded model)

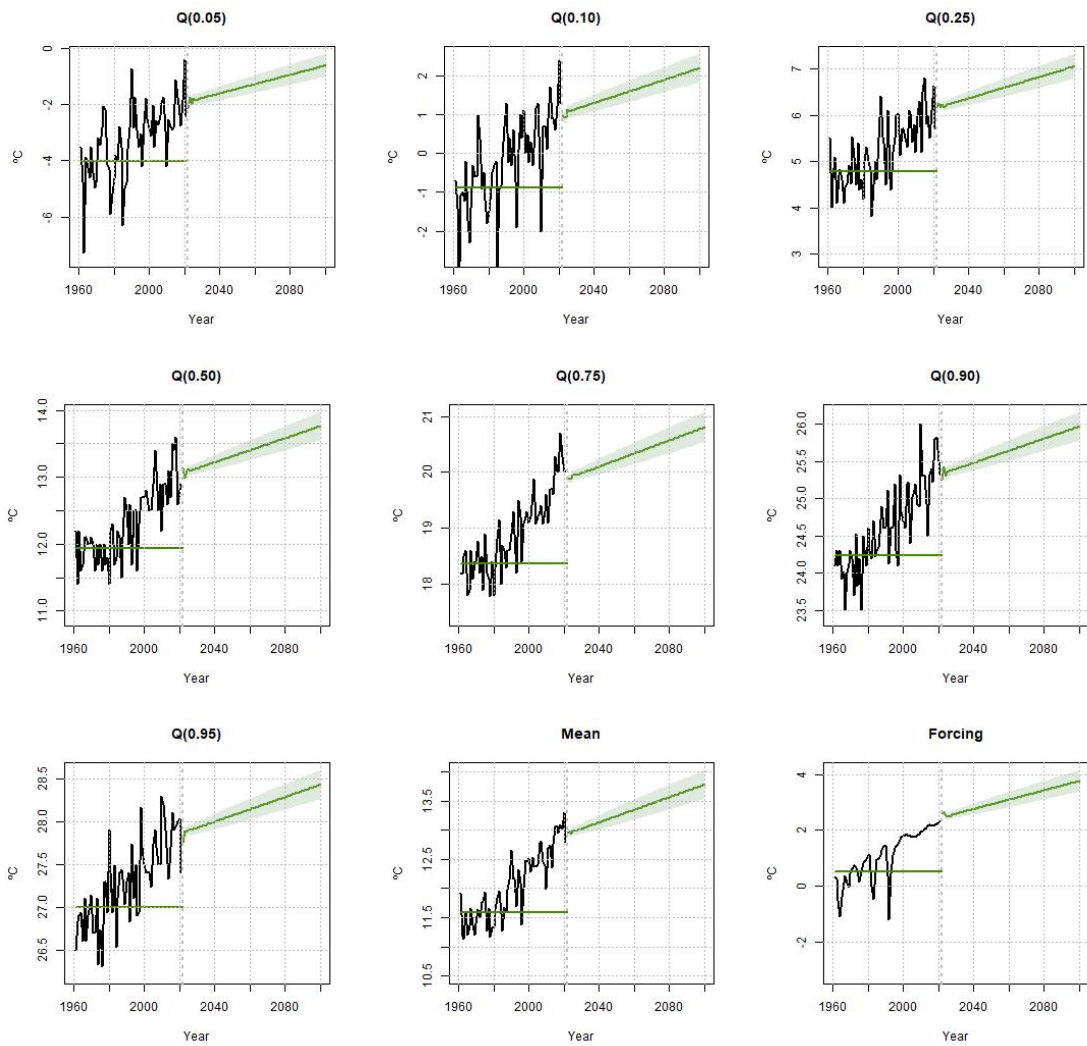


Figure D2: Forecasts including forcing dynamics (Globe, expanded model)

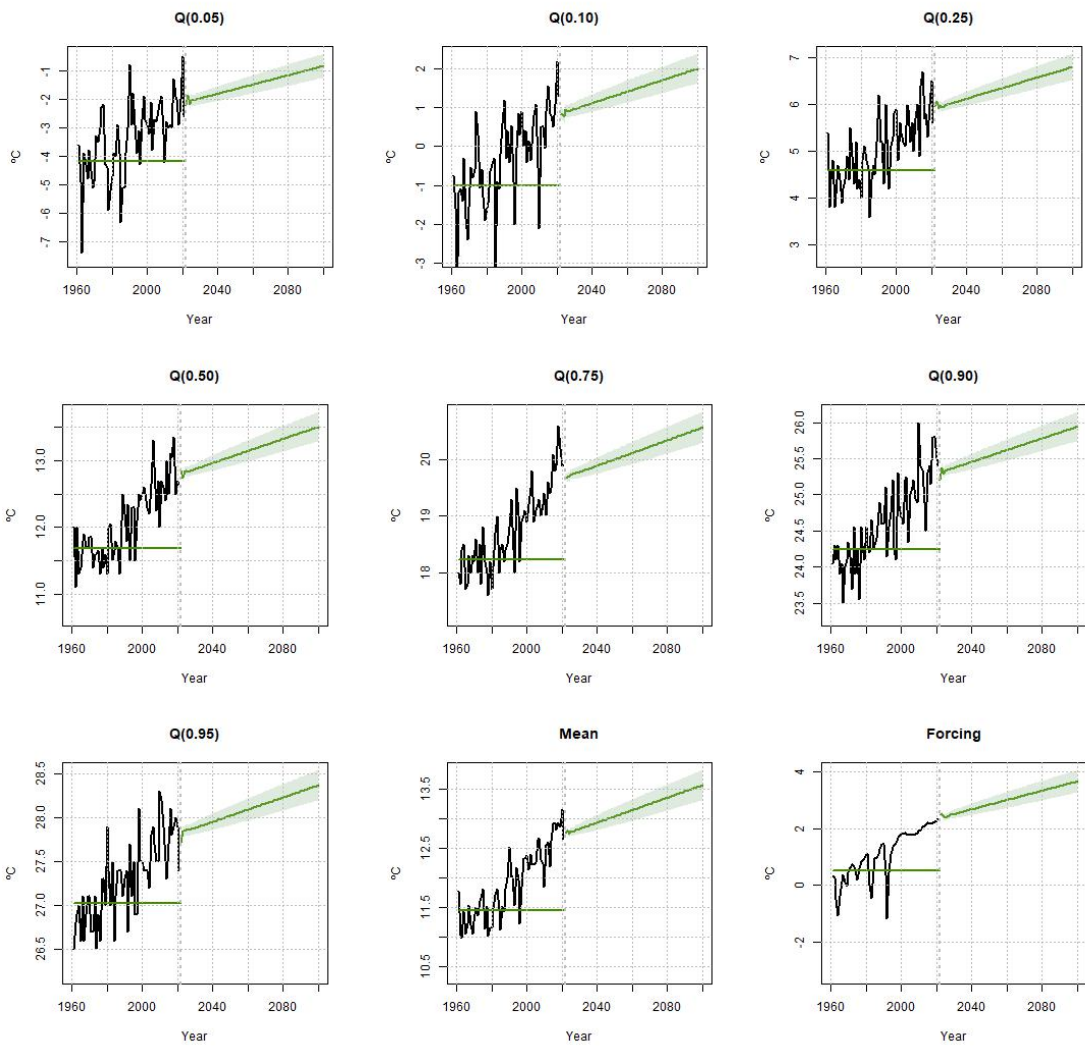


Figure D3: Forecasts including forcing dynamics (North Hemisphere, expanded model)

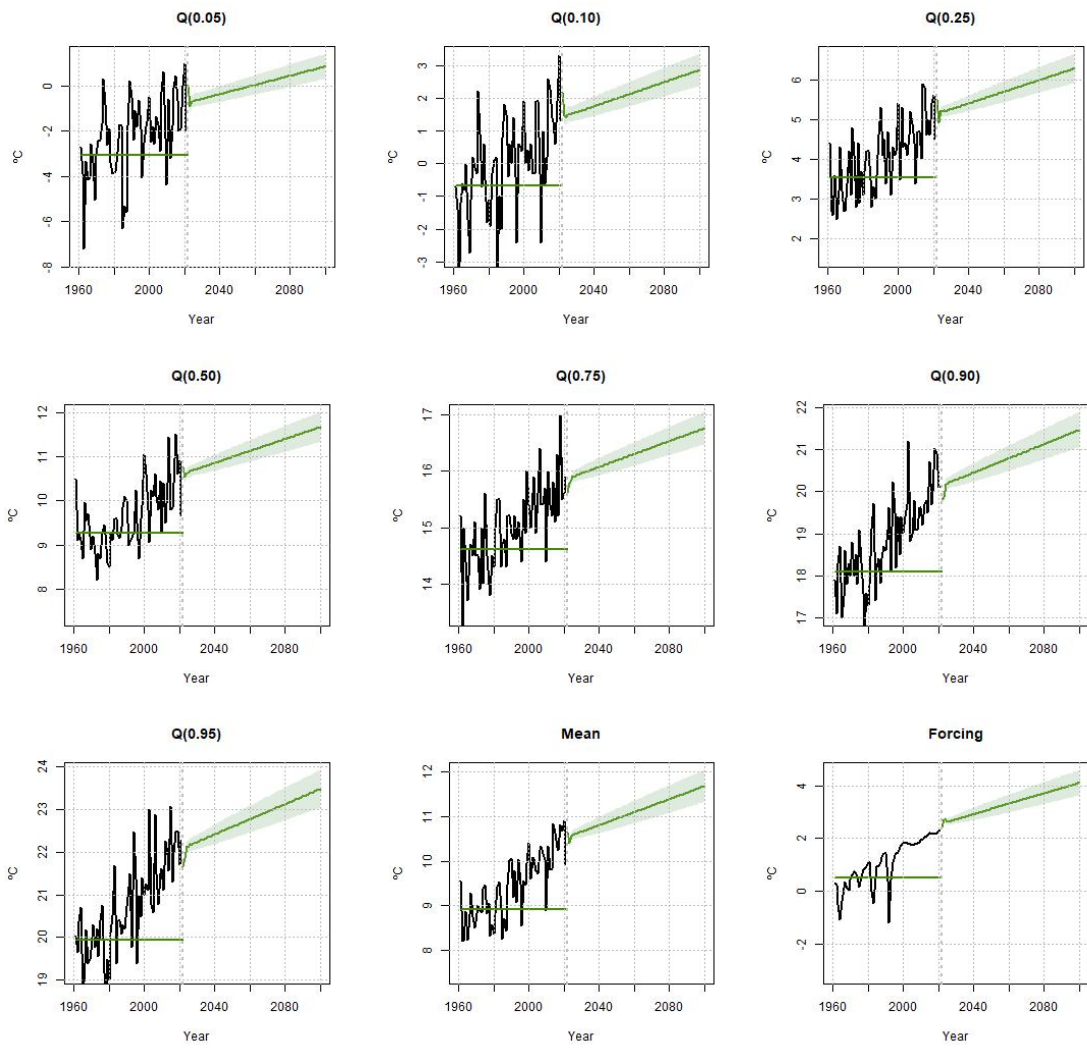


Figure D4: Forecasts including forcing dynamics (Europe, expanded model)

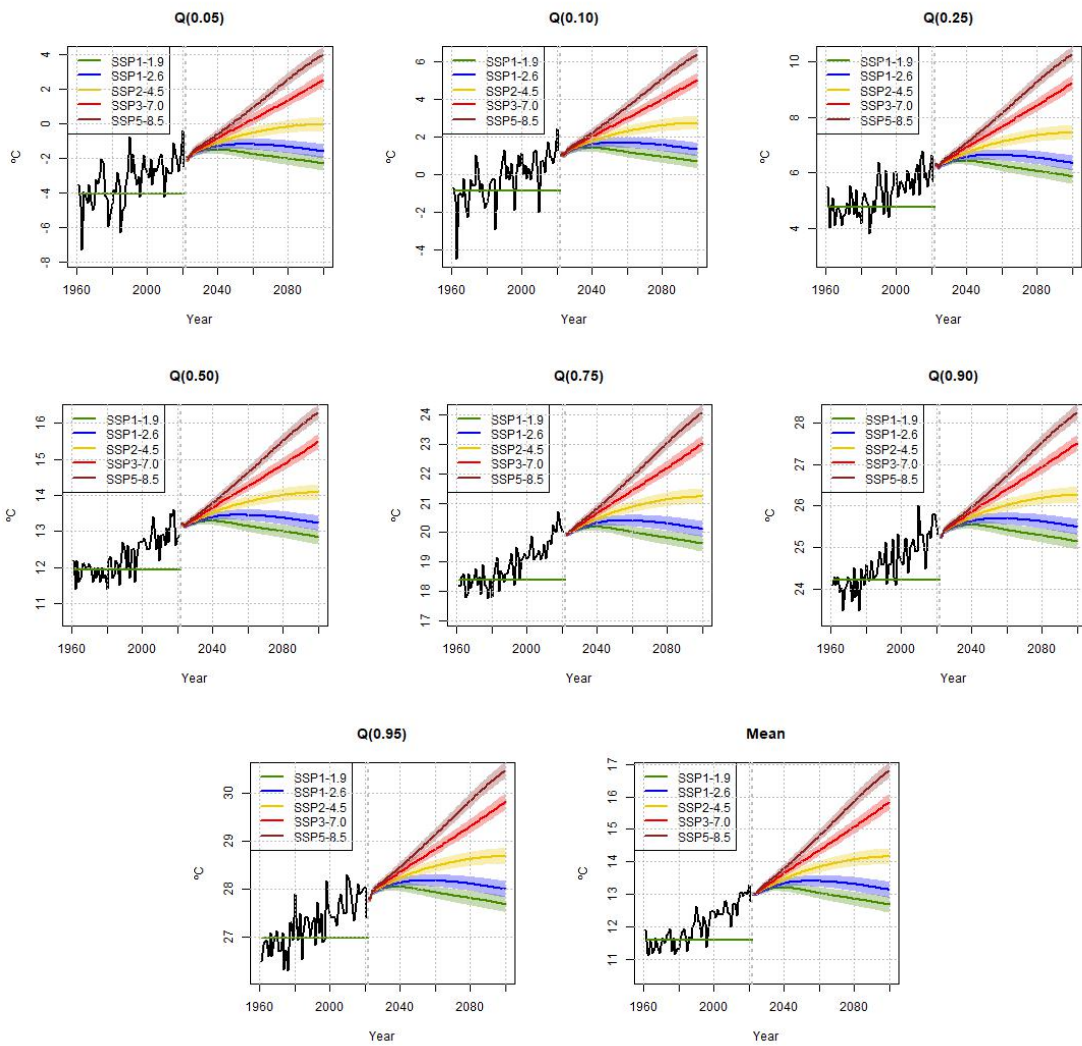


Figure D5: Long-term projections under RCP scenarios (Globe, expanded model)

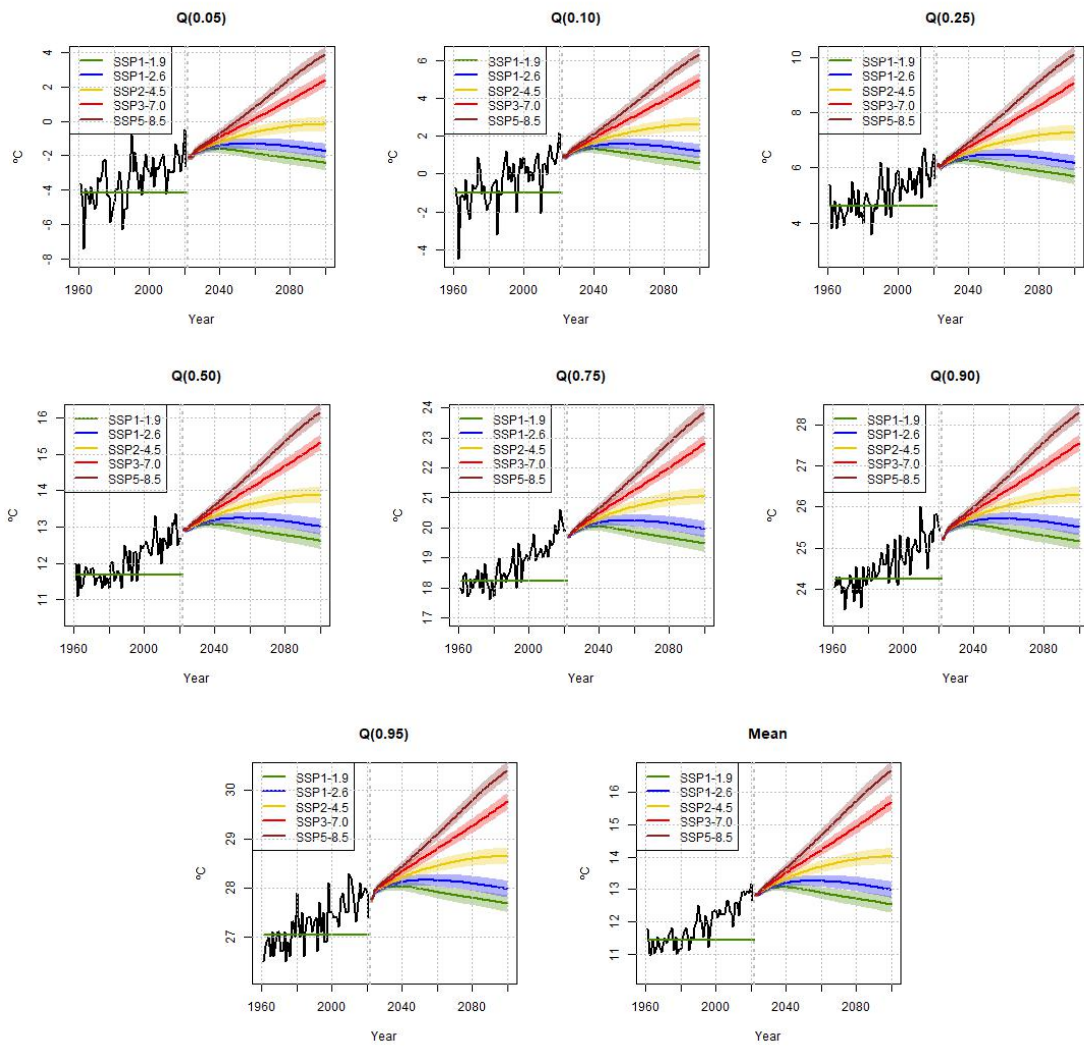


Figure D6: Long-term projections under RCP scenarios (North Hemisphere, expanded model)

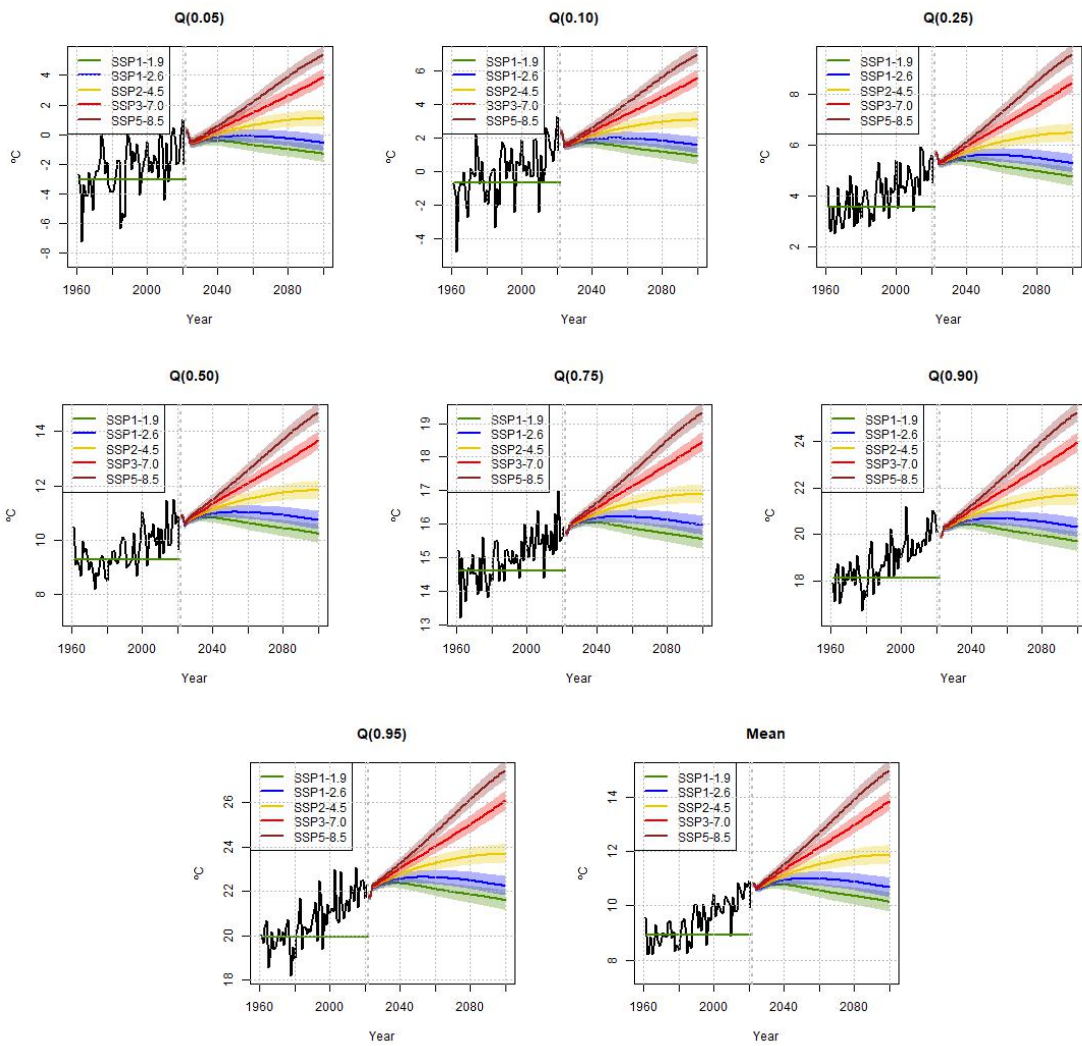


Figure D7: Long-term projections under RCP scenarios (Europe, expanded model)

Table E1: Testing for trends in distributional characteristics (1958-2021)

Characteristic	Globe		North Hemisphere		Europe		Central England	
	Test-statistic	p-value	Test-statistic	p-value	Test-statistic	p-value	Test-statistic	p-value
$Q_t(0.05)$	0.0429	0.0000	0.0439	0.0000	0.0411	0.0000	0.0269	0.0000
$Q_t(0.10)$	0.0443	0.0000	0.0467	0.0000	0.0393	0.0000	0.0266	0.0000
$Q_t(0.25)$	0.0323	0.0000	0.0341	0.0000	0.0311	0.0000	0.0218	0.0000
$Q_t(0.50)$	0.0220	0.0000	0.0238	0.0000	0.0227	0.0000	0.0124	0.0000
$Q_t(0.75)$	0.0266	0.0000	0.0289	0.0000	0.0260	0.0000	0.0154	0.0000
$Q_t(0.90)$	0.0222	0.0000	0.0237	0.0000	0.0384	0.0000	0.0193	0.0000
$Q_t(0.95)$	0.0201	0.0000	0.0220	0.0000	0.0389	0.0000	0.0222	0.0000
Mean	0.0279	0.0000	0.0296	0.0000	0.0305	0.0000	0.0195	0.0000

Notes: Annual distributional characteristics estimated using the cross-sectional temperature distribution at each year from 1959-2021. Test-statistics and p-values correspond to a significance test for the trend-slope in a regression of the distributional characteristic on a constant and a linear trend, using HAC standard-errors.

E Reduced Sample 1958 - 2021

The analysis is zoomed to the post-1958 period in order to avoid the criticism raised by [Pretis and Hendry \(2013\)](#) about the combination of proxy-based and observed historical forcing series constructed with changing methodologies. This focus on a more recent and methodologically homogeneous dataset offers the advantage of increasing the number of cross-sectional units available for computing the annual distributional characteristics of temperature. However, this comes at the expense of a reduced temporal dimension, which increases uncertainty in the estimation and testing procedures within the VECM methodology. This period is characterized by steeper trends in the temperature characteristics, as inferred from Table E1 and its comparison with the baseline analysis. The origin of this empirical fact is the detected structural breaks in aggregate and individual temperature series occurred around 1965 as explained in [Estrada et al. \(2013\)](#), [Estrada and Perron \(2017\)](#), or [Gadea et al. \(2024\)](#). The break date is consistent with the "onset of a sustained global warming" process, a period characterized by rapid increases in temperatures and radiative forcing as a consequence of the post-World War II economic expansion and the consequent acceleration in GHGs emissions.

The qualitative patterns observed in the analysis of the full sample are preserved in the reduced sample. However, important differences emerge in the magnitudes of the estimated quantities. For instance, the co-trending slopes between the distributional characteristics of temperature and F_t as shown in Table E3, are uniformly higher in the reduced sample, implying stronger climate sensitivity (CS) values. Both unconditional forecasts and conditional projections under various SSP scenarios are produced in the same way as before. The quantitative results reveal a heterogeneous response of the temperature distribution, with the magnitude of changes being more pronounced in this exercise.

Table E2: Co-trending slopes of relationships between unconditional quantiles and the average temperature (1958-2021)

Slope	Globe		North Hemisphere		Europe		Central England	
	Estimate	Cot-test	Estimate	Cot-test	Estimate	Cot-test	Estimate	Cot-test
$\beta(0.05)$	1.4903***	0.5224	1.4558***	0.5854	1.2965***	0.6705	1.2470***	0.4278
	(0.2104)		(0.2268)		(0.2079)		(0.3196)	
$\beta(0.10)$	1.5618***	0.4223	1.5462***	0.3507	1.2403***	0.2776	1.2306***	0.2012
	(0.0892)		(0.0966)		(0.1826)		(0.2306)	
$\beta(0.25)$	1.1381***	0.3930	1.1260***	0.2107	0.9921***	0.2854	1.1130***	0.9611
	(0.0518)		(0.0636)		(0.0583)		(0.0773)	
$\beta(0.50)$	0.8035***	0.3634	0.8242***	0.2346	0.7940***	0.3223	0.7402***	0.0646
	(0.0450)		(0.0518)		(0.0969)		(0.1424)	
$\beta(0.75)$	0.9754***	0.2602	0.9956***	0.3478	0.8649***	0.7285	0.8309***	0.1498
	(0.0539)		(0.0512)		(0.0559)		(0.0967)	
$\beta(0.90)$	0.8069***	0.5307	0.8225***	0.2802	1.2630***	0.6259	0.9269***	0.2916
	(0.0387)		(0.0472)		(0.0686)		(0.1572)	
$\beta(0.95)$	0.7102***	0.6301	0.7354***	0.6658	1.2940***	0.3530	1.0465***	0.1032
	(0.0403)		(0.0397)		(0.1039)		(0.2199)	

Notes: Column *Estimate* correspond to the estimated co-trending slope—of the quantile with respect to the average temperature—and its standard-error in parenthesis. *, **, *** denote significance at the 10%, 5%, and 1% levels, respectively. Column *Cot-test* reports the p-value of the test for common-trends.

Table E3: Co-trending slopes of relationships between the distributional characteristics of temperature and F_t (1958-2021)

Slope	Globe		North Hemisphere		Europe		Central England	
	Estimate	Cot-test	Estimate	Cot-test	Estimate	Cot-test	Estimate	Cot-test
$\lambda(0.05)$	1.1042*** (0.2046)	0.9188	1.1391*** (0.2299)	0.8602	1.0607*** (0.2076)	0.7922	0.6739*** (0.2267)	0.8846
$\lambda(0.10)$	1.1479*** (0.1381)	0.9292	1.2064*** (0.1477)	0.9821	1.0086*** (0.1791)	0.3538	0.6609*** (0.1754)	0.7440
$\lambda(0.25)$	0.8342*** (0.0823)	0.7447	0.8768*** (0.0925)	0.7507	0.8082*** (0.0787)	0.4678	0.5689*** (0.0892)	0.5009
$\lambda(0.50)$	0.5821*** (0.0641)	0.2659	0.6321*** (0.0761)	0.2604	0.6206*** (0.1201)	0.1775	0.3473*** (0.0903)	0.0298
$\lambda(0.75)$	0.7043*** (0.0863)	0.2571	0.7627*** (0.0861)	0.2508	0.6900*** (0.0886)	0.2090	0.4185*** (0.0885)	0.2627
$\lambda(0.90)$	0.5850*** (0.0625)	0.3058	0.6292*** (0.0739)	0.2283	1.0167*** (0.1343)	0.3884	0.4843*** (0.1155)	0.5932
$\lambda(0.95)$	0.5209*** (0.0504)	0.8337	0.5711*** (0.0534)	0.7846	1.0393*** (0.1544)	0.3318	0.5424*** (0.1472)	0.2452
$\bar{\lambda}$	0.7293*** (0.0724)	0.5452	0.7725*** (0.0781)	0.5448	0.8043*** (0.0938)	0.3097	0.5108*** (0.0817)	0.5033

Notes: Column *Estimate* correspond to the estimated co-trending slope—of the distributional characteristic with respect to the radiative forcing F_t —and its standard-error in parenthesis. *, **, *** denote significance at the 10%, 5%, and 1% levels, respectively. Column *Cot-test* reports the p-value of the test for common-trends.

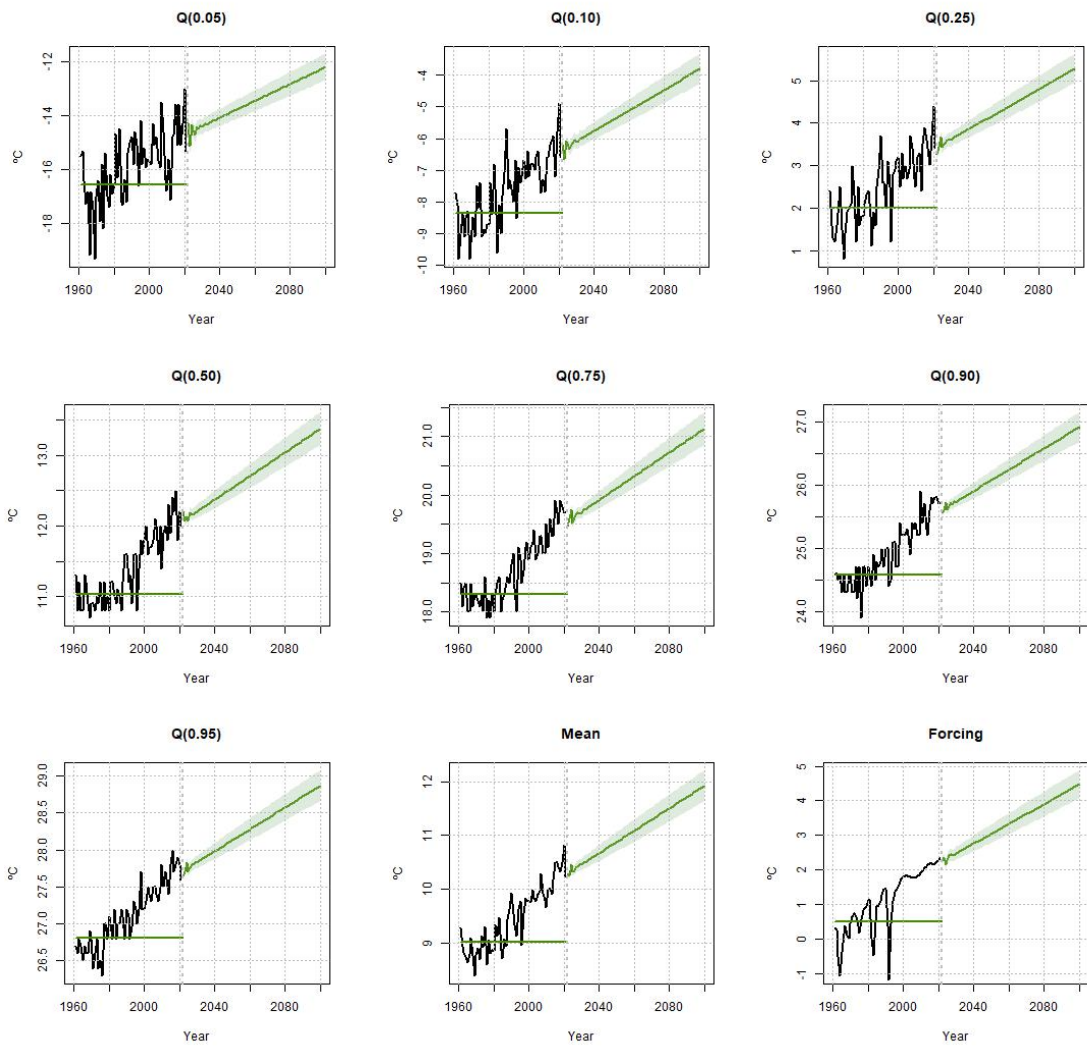


Figure E1: Forecasts including forcing dynamics (Globe, 1958-2021)

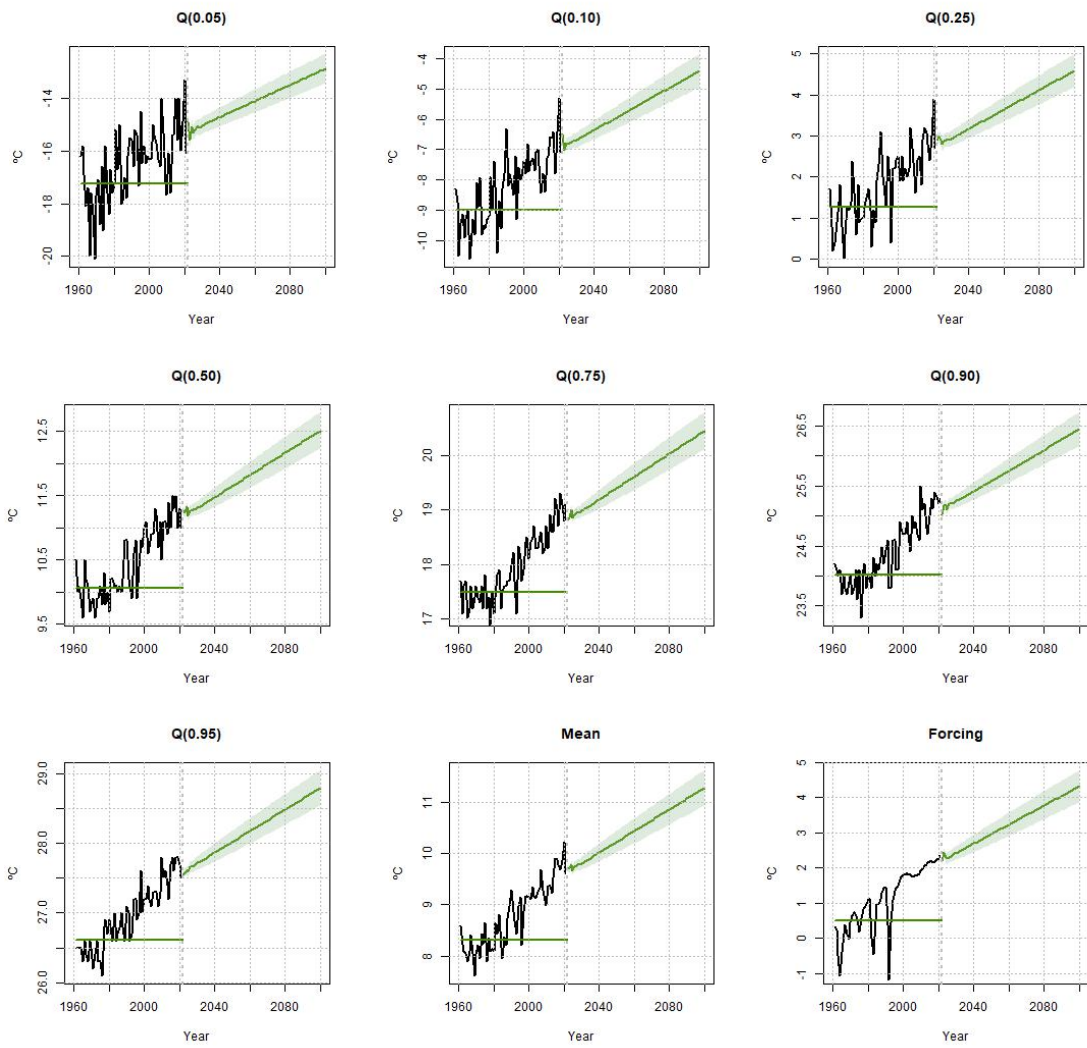


Figure E2: Forecasts including forcing dynamics (North Hemisphere, 1958-2021)

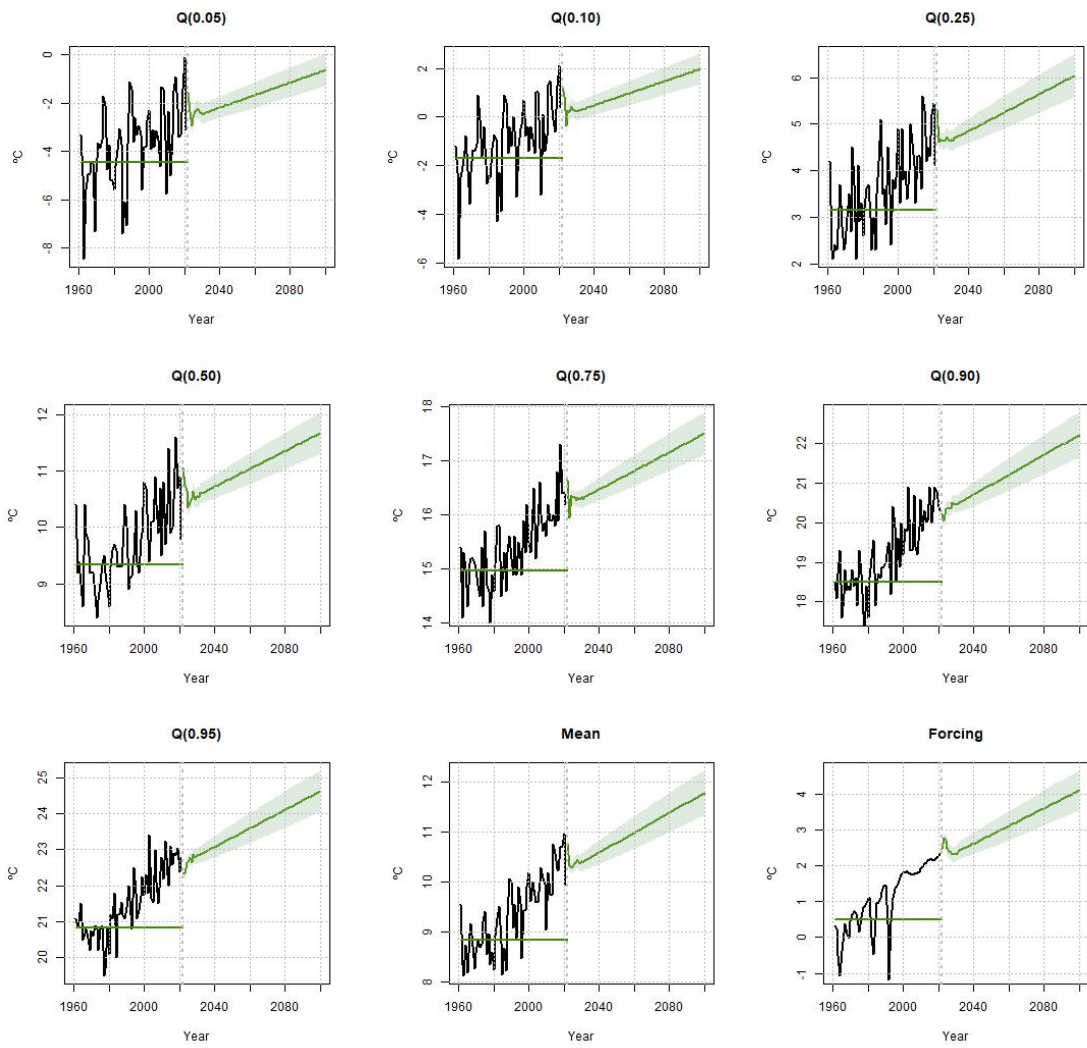


Figure E3: Forecasts including forcing dynamics (Europe, 1958-2021)

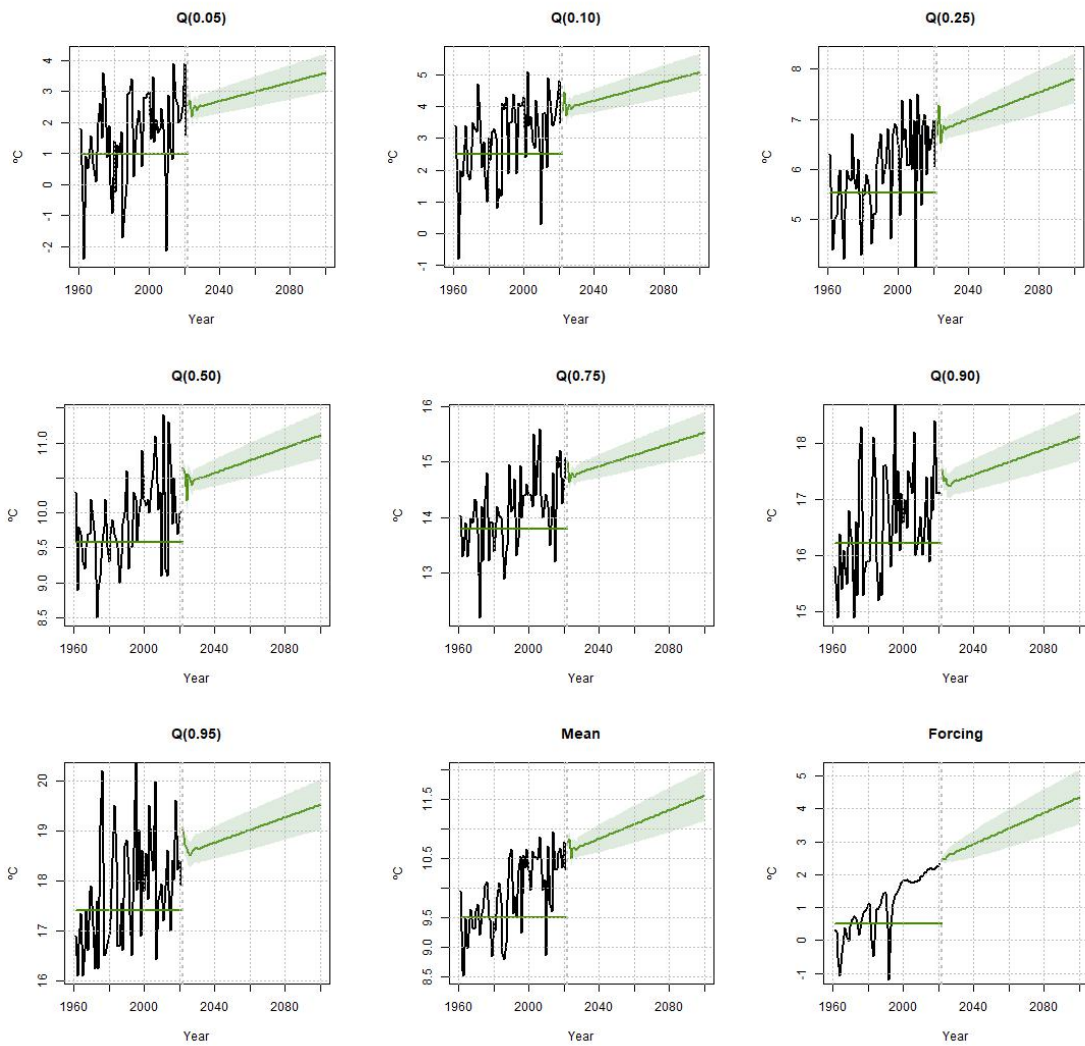


Figure E4: Forecasts including forcing dynamics (Central England, 1958-2021)

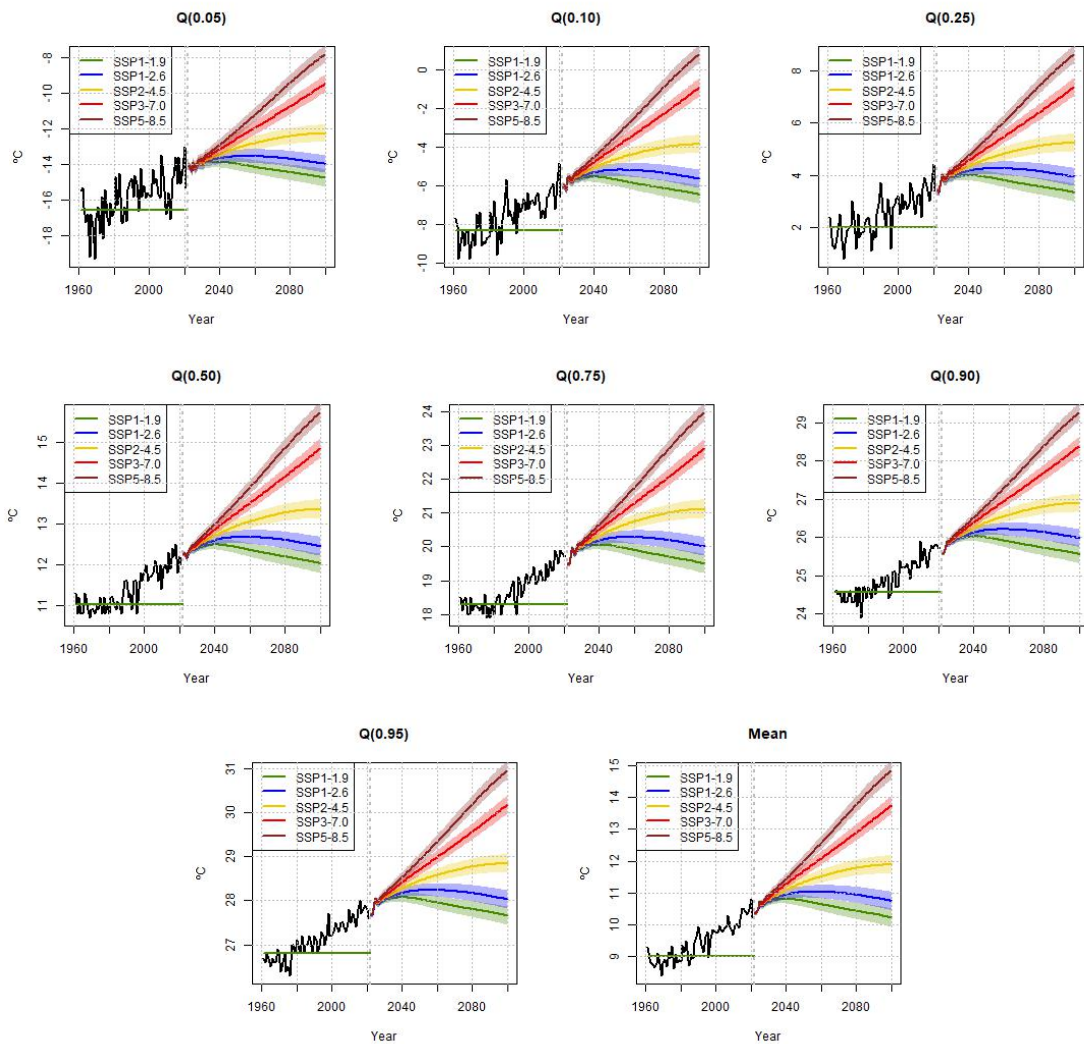


Figure E5: Long-term projections under RCP scenarios (Globe, 1958-2021)

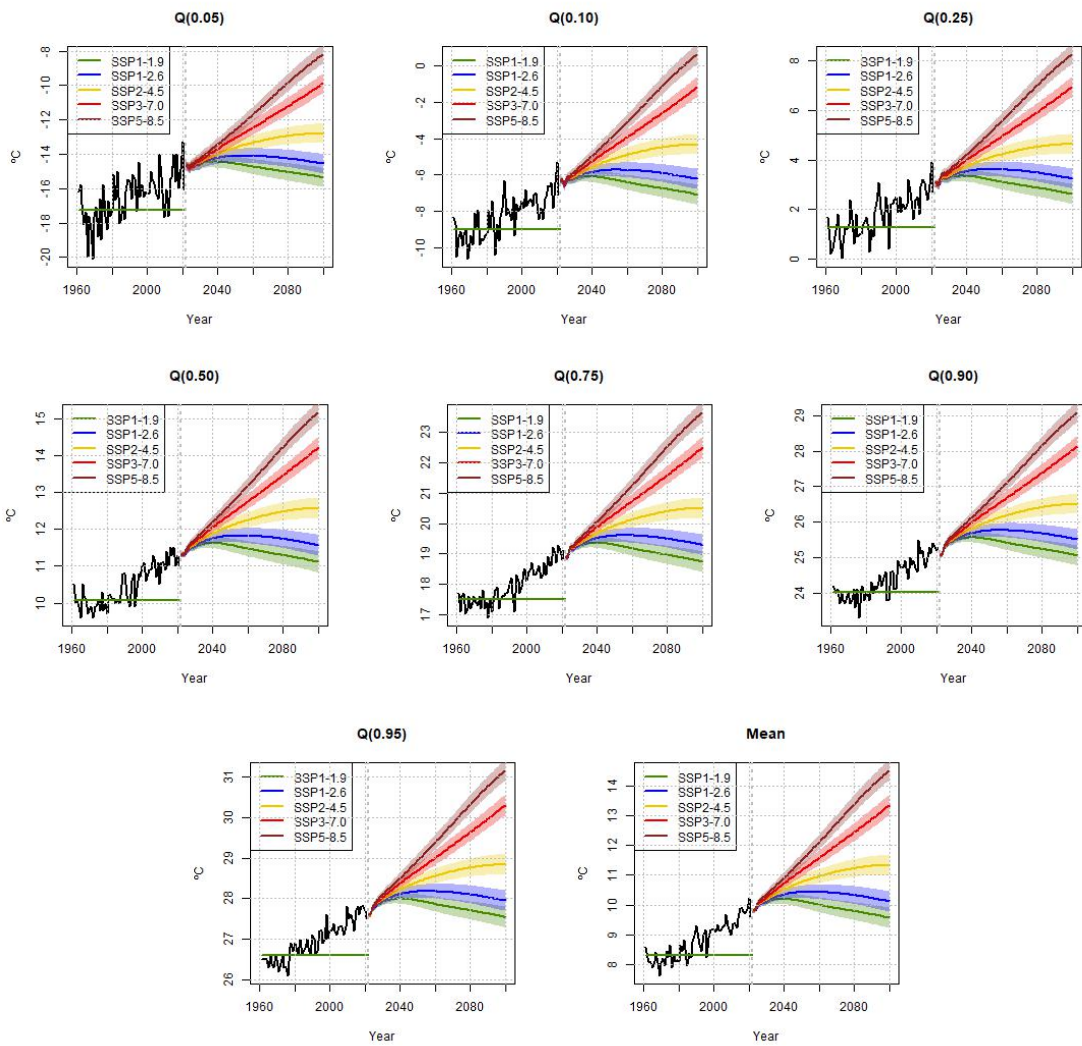


Figure E6: Long-term projections under RCP scenarios (North Hemisphere, 1958-2021)

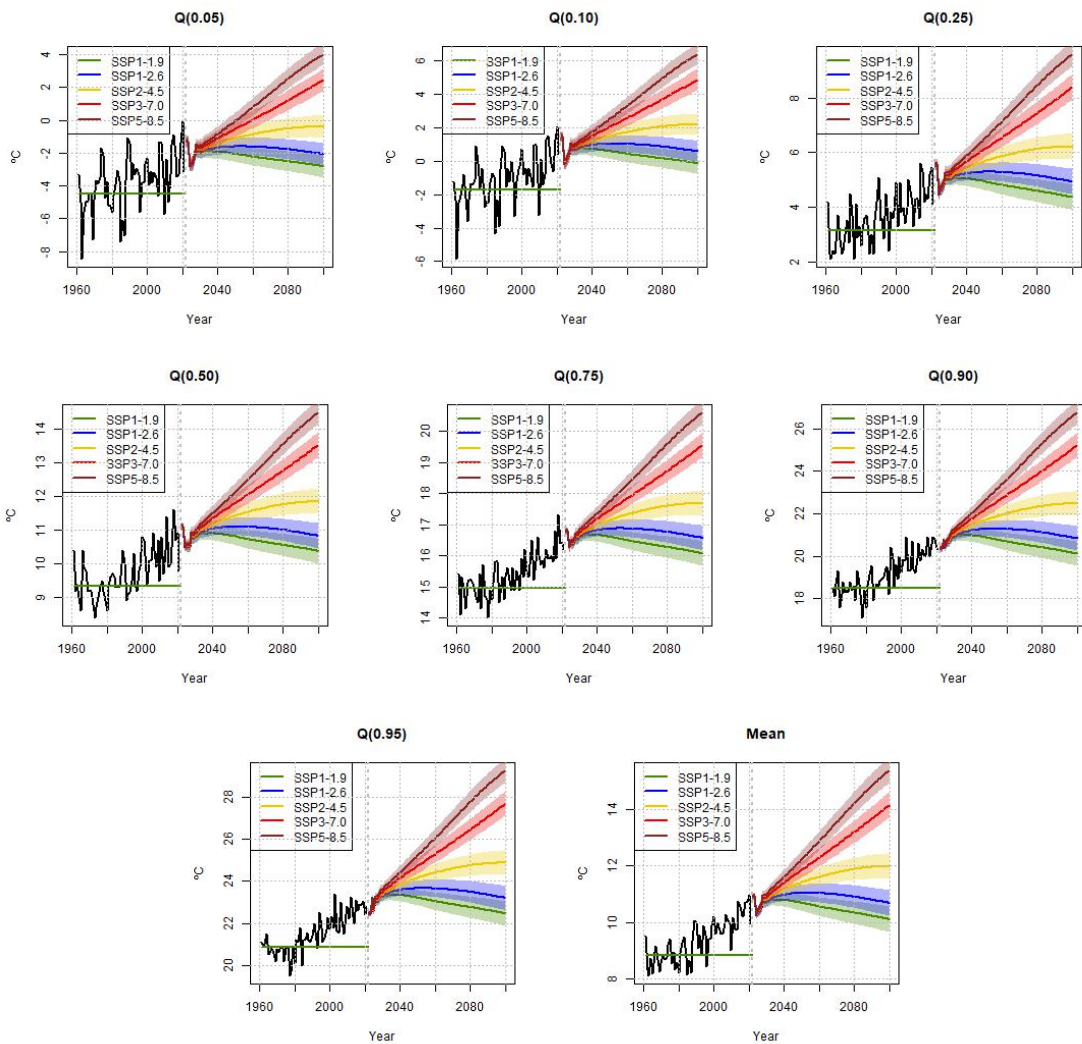


Figure E7: Long-term projections under RCP scenarios (Europe, 1958-2021)

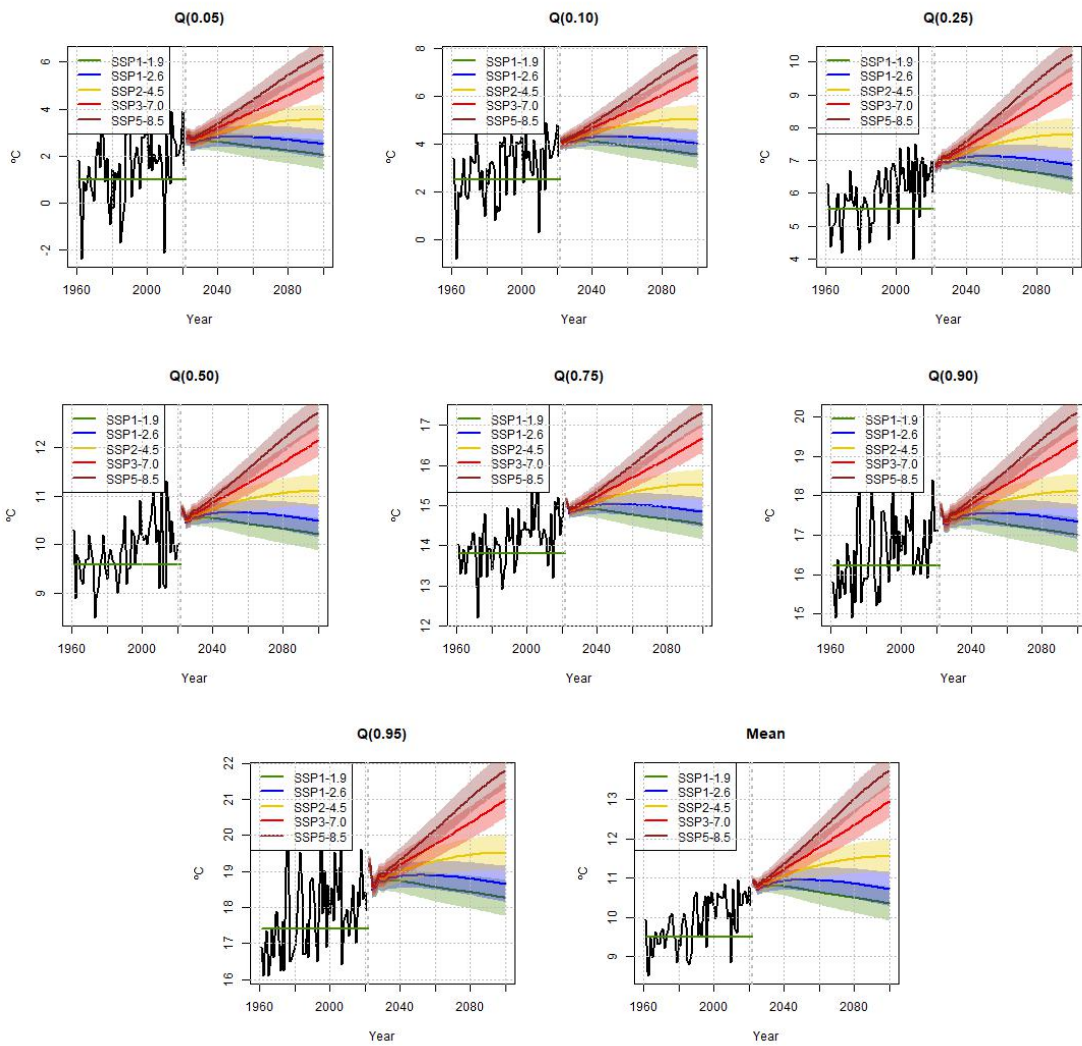


Figure E8: Long-term projections under RCP scenarios (Central England, 1958-2021)

F Macroeconomic Impact of Climate Change

This Appendix explores the use of the identified structural shocks, obtained through a Cholesky rotation of the reduced-form residuals of the unconditional-quantile VECM, to estimate the macroeconomic impact of climate change. This approach is alternative to [Bilal and Känzig \(2024\)](#). Data on constant GDP per capita for the world is sourced from the FRED database, covering the period from 1960 to 2022²⁴. I begin by considering a model for the unconditional distributional characteristics only and restricts the analysis to the Globe. Figure F1 presents the impulse-response functions of the four variables in the system, along with their respective 95% confidence bands, estimated using LPs à la ([Jordà, 2005](#)). The results are qualitatively similar to those described in Section 6.4.5, indicating the robustness of the analysis to the sample period.

I estimate the dynamic causal effects of temperature shocks using LPs. To account for serial correlation in GDP growth and temperature shocks, I include two lags of real GDP per capita and the respective shocks in the respective regression. Figure F2 shows the impulse response of world real GDP per capita to each of the identified distributional temperature shocks. The solid black lines represent the point estimates, and the shaded areas correspond to the 90% confidence bands. A shock that increases the average temperature by 0.25°C generates a permanent fall in world GDP per capita, with the peak response observed around nine years after the shock, reaching a negative value close to 1%. This value, when linearly scaled, is lower than the damage estimated by [Bilal and Känzig \(2024\)](#). The responses to other shocks are heterogeneous. While a shock to $Q_t(0.95)$ (that also increases the other distributional characteristics) reduces world GDP in the long run, a shock to $Q_t(0.50)$ actually increases it. This finding aligns well with the literature on the geographical and seasonal heterogeneity in the impacts of climate change already mentioned in this paper.

²⁴ Available at <https://fred.stlouisfed.org/series/NYGDPPCAPKDWLD>

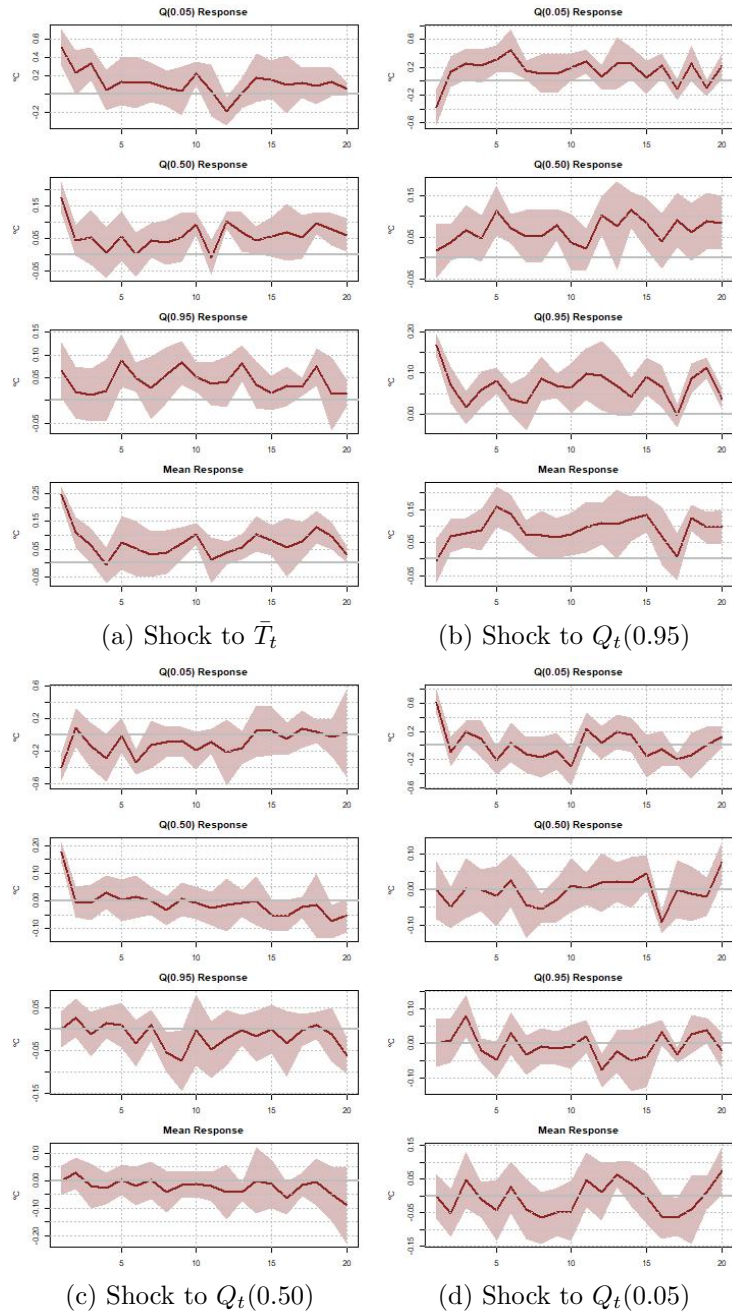


Figure F1: IRFs to identified structural shocks (Globe, 1959-2022)

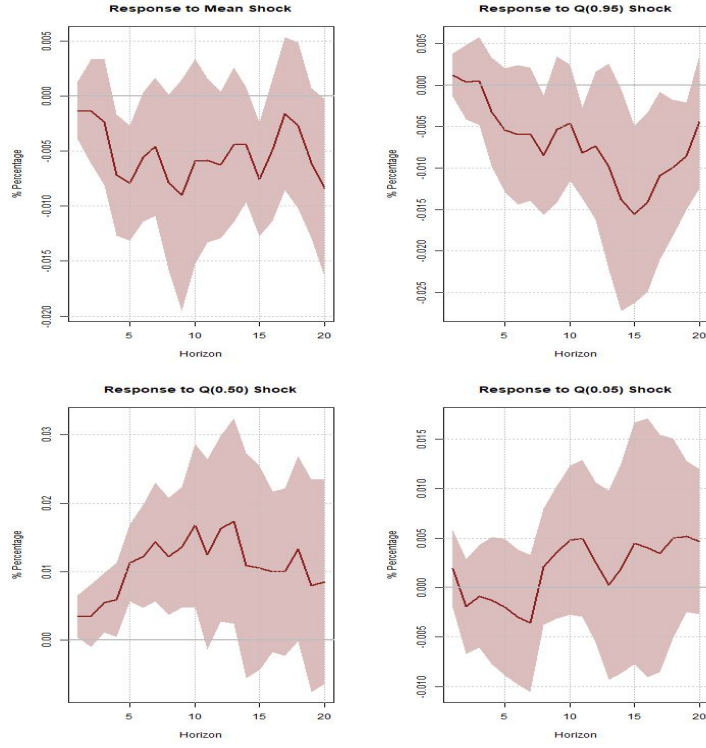


Figure F2: World GDP responses to identified structural shocks (Alternative 1)

The information set is enhanced by including radiative forcing variable in the system. Figure F3 presents the impulse responses of the endogenous variables, with radiative forcing ordered first for the Cholesky rotation of the reduced-form residuals. The results are qualitatively similar to those described in Section 6.5.7. The responses of world GDP per capita to the identified shocks are depicted in Figure F4. In this exercise, the negative effects on GDP are generated by the shocks to radiative forcing, while positive responses continue to be associated with shocks to $Q_t(0.50)$ and, to some extent, $Q_t(0.05)$. To interpret this result, it is necessary to consider that when F_t is ordered first in the vector, it implies that the reduced-form residuals of \bar{T}_t (and the other distributional characteristics) are decomposed into a common component associated with shocks to radiative forcing and an orthogonal component that does not instantaneously affect radiative forcing (Bruns et al., 2020): the responses to the forcing shocks are equivalent to the responses to the common component. An equivalent exercise, which produces the same responses, involves regressing the \bar{T}_t residuals on the F_t residuals, and then replacing the fitted values and the residuals of the previous regression in the matrix to be Cholesky-rotated. This approach clarifies the interpretation of the shocks.

The analysis of the macroeconomic impacts of climate change using the identification of struc-

tural shocks in an unconditional-quantile VECM provides promising insights that justify further research. As an alternative to [Bilal and Känzig \(2024\)](#), who identify shocks as persistent deviations from the long-run trend in global average temperature, the approach in this paper integrates elements from climate theory within a multivariate statistical model and identifies shocks based on the unexplained variability in the climate system. Moreover, this approach uses information on the entire distribution of temperature, rather than just the average, thus offering a wider amount of information for policy analysis. Other identification alternatives can be explored within this framework, including long-run or sign restrictions, statistical identification, and more. This is part of the research agenda.

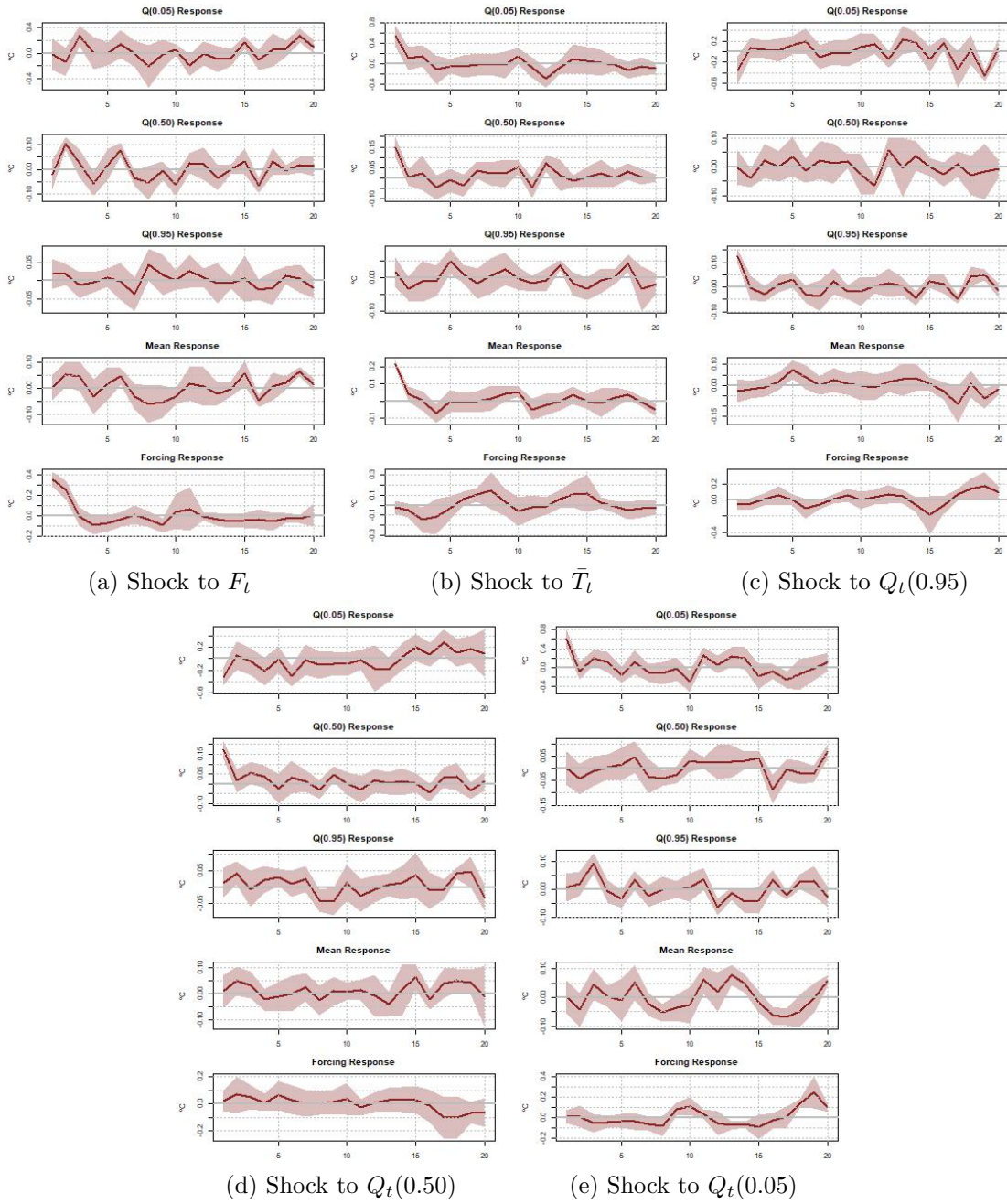


Figure F3: IRFs to identified structural shocks including forcing (Globe, 1959-2022)

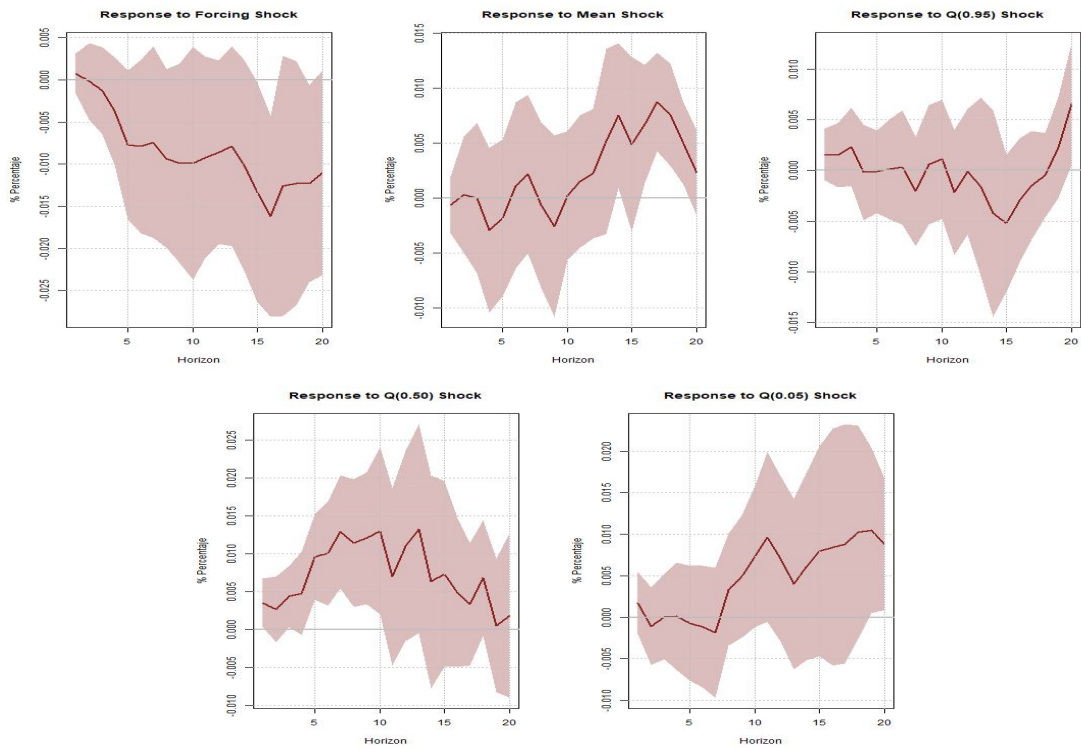


Figure F4: World GDP responses to identified structural shocks (Alternative 2)

G Including More Climate Variables

In order to obtain a more complete representation of the climate system, the information set is expanded by including additional climate variables beyond land temperature and radiative forcing. Specifically, I include ice extent, ICE_t , and sea surface temperature, SST_t . Gridded Monthly Sea Ice Extent data (in millions of Km²) for the period 1850 to 2017 is obtained from the National Snow and Ice Data Center (NSIDC)²⁵. This dataset combines historical measurements from ship observations, compilations by naval oceanographers, or analyses by national ice services, with measurements from satellite passive microwave data available from 1979 onward. Global Sea Surface Temperature Anomaly (relative to the 1961-90 average) is obtained from Our World in Data²⁶ and covers the period from 1850 to the present. The analysis is restricted to the sample from 1958 to 2017, which is the time window with the most reliable data for all variables.

In a multivariate system for $Z_t = [Q_t(0.05), Q_t(0.50), Q_t(0.95), \bar{T}_t, F_t, ICE_t, SST_t]'$, the [Guo and Shintani \(2013\)](#) procedure selects a co-trending rank of 6, implying 2 additional co-trending relationships compared to the baseline model. According to climate science theory and following [Pretis \(2020\)](#), one co-trending equation must relate the average land temperature, \bar{T}_t , and the global sea surface temperature, SST_t . The second co-trending equation must derive from the long-run relationship between the radiative forcing, F_t , and the ice extent, ICE_t , as argued by [Diebold et al. \(2023\)](#) and [Diebold and Rudebusch \(2023\)](#). Another references on the econometric forecasting of sea ice include [Coulombe and Göbel \(2021\)](#) and [Blazsek et al. \(2024\)](#). With this information, the co-trending relationships are estimated and tested following the [Chen et al. \(2022\)](#) method. The short-run dynamics of the VECM are then obtained using the two-step OLS approach.

Figures G1 and G2 present the unconditional forecasts and the long-term projections based on the SSP scenarios produced with the estimated model. In this case, I am able to obtain outputs for ICE_t and SST_t . Focusing on the results for ICE_t , notice that the negative trend is predicted to continue during the next decades, but it never reaches a zero value. Similarly, for all SSP scenarios, the long-term projections and their confidence bands are positive. As an alternative, instead of considering the annual average over the monthly observations, I include in the vector of variables the ice-extent for September, the month with the least value of ice over the year. Figure G3 shows that the ice-extent forecast only reaches a value of zero at the end of the horizon, close to the year 2100. For the SSP projections, negative values are observed only for the extreme scenarios SSP3-7.0 and SSP5-8.5 and the first negative value is obtained around 2050. This result contrast with the findings

²⁵ Available at <https://nsidc.org/data/g10010/versions/2>.

²⁶ Available at <https://ourworldindata.org/grapher/sea-surface-temperature-anomaly>.

in Diebold and Rudebusch (2022), Diebold et al. (2023), and Diebold and Rudebusch (2023), who predict a zero ice-extent value quicker in time. My results align more with the projections from climate models.

I recognize that predicting ice-extent can be a difficult task. This is a first attempt using the proposed unconditional-quantile VECM. However, more research is needed. Using my approach to complement and extend the work of Coulombe and Göbel (2021) is a promising avenue.

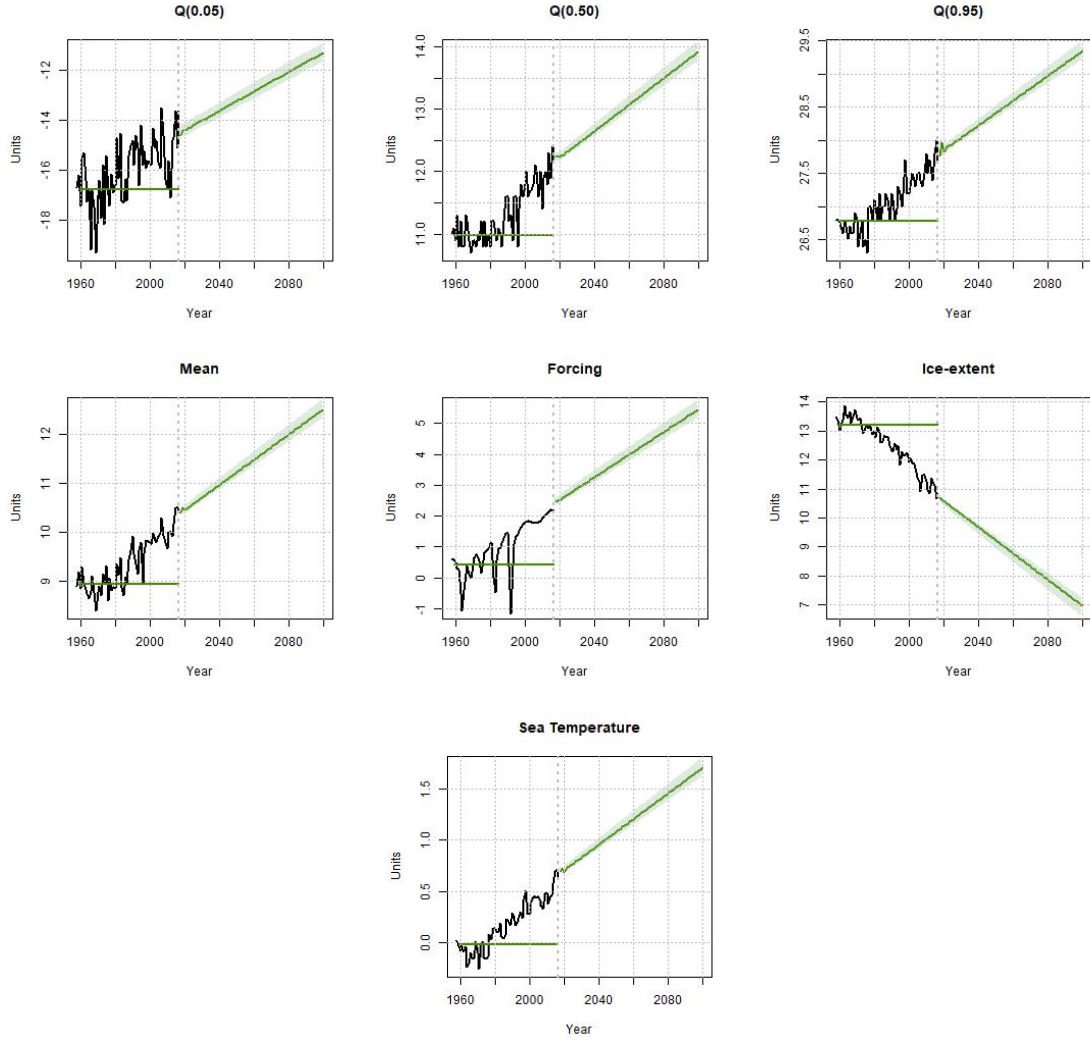


Figure G1: Forecasts including Ice extent and Sea Surface Temperature (Globe)

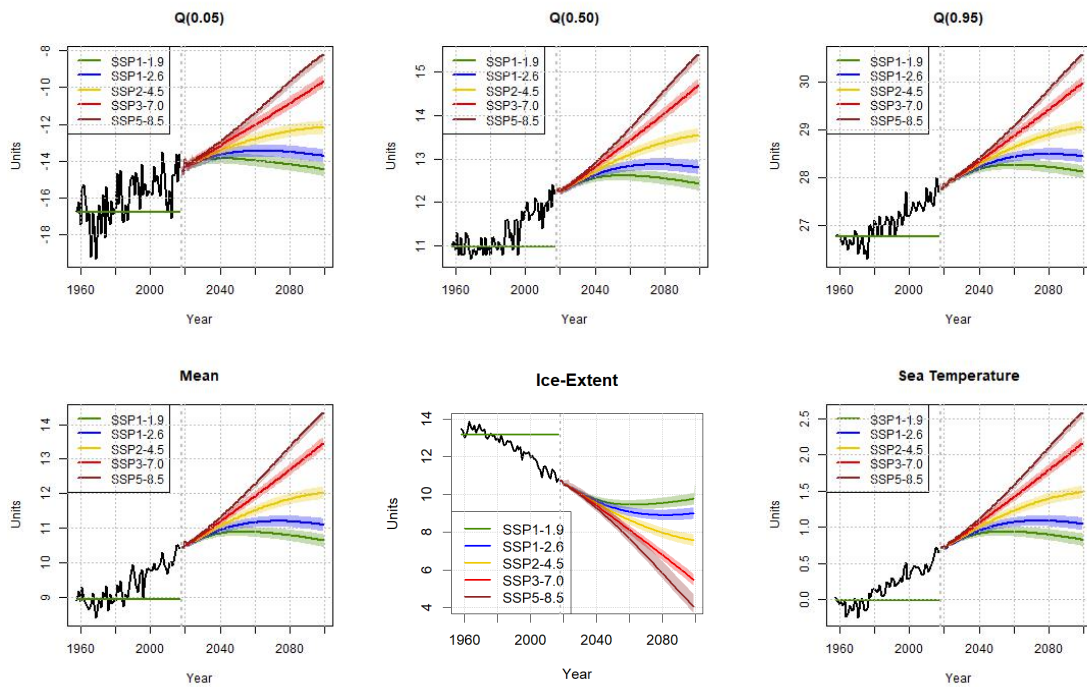


Figure G2: Long-term projections under RCP scenarios in a model including Ice extent and Sea Surface Temperature (Globe)

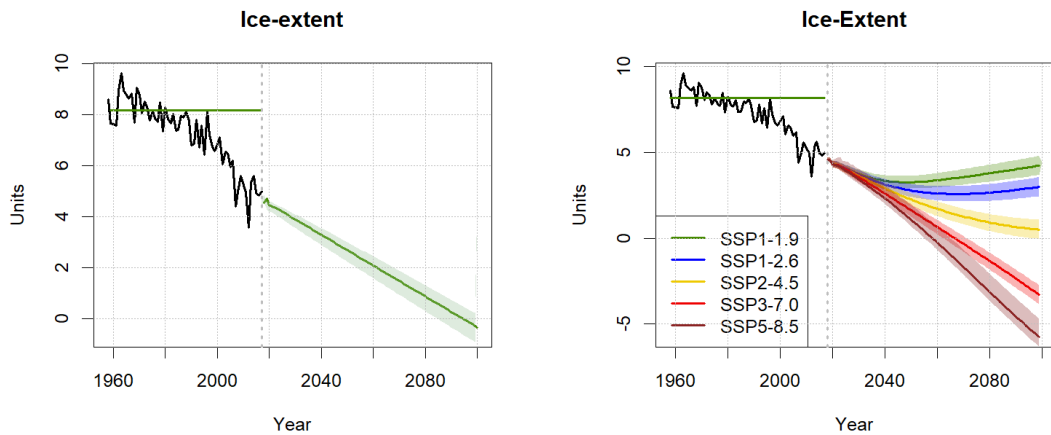


Figure G3: Forecast (left) and long-term projections under RCP scenarios (right) in a model including Ice extent in September